Addis Ababa University

Addis Ababa Institute of Technology

School of Electrical and Computer Engineering

Robust Model Reference Adaptive Controller For Trajectory Tracking Of Fixed-Wing UAV

A Thesis Submitted to School of Graduate Studies of Addis Ababa University in Partial Fulfillment of the Requirements for the Degree of Master of Science in Control Engineering

By

Tofik Kemal

Advisor

Dr. Lebsewerk Negash

September 17, 2023

Addis Ababa, Ethiopia

Addis Ababa University

Addis Ababa Institute of Technology

School of Electrical and Computer Engineering

This certification affirms that the thesis authored by Tofik Kemal, titled "Robust Model Reference Adaptive Controller for Trajectory Tracking of Fixed-Wing UAV," has been submitted to satisfy the partial requirements for the Master of Sciences degree in Control Engineering. The document meets to university regulations and attains accepted standards in terms of originality and quality.

Approved by Board of Examiners

Name	Signature	Date
Dr. Bisrat Derebssa		
(School dean)		
Dr. Lebsework Negash		
(Chairman)		
Dr. Lebsework Negash		
(Advisor)		
Dr. Dereje Shiferaw		
(External examiner)		
Mr.Getu Gabissa		
(Internal examiner)		

Declaration

I declare that the work entitled "Robust Model Reference Adaptive Controller For Trajectory Tracking Of Fixed-Wing UAV" is my original work and has not been presented for the fulfillment of any degree in this university or any other university or college and all sources and materials used for the thesis are acknowledged.

Name	Signature	Date
Tofik Kemal		

(Name of student)

This thesis has been submitted for examination with my approval as a university advisor.

Dr. Lebsework Negash

(Name of advisor)

Acknowledgement

First, I would like to express my deepest gratitude to the Almighty God for His immeasurable grace and countless blessings that have been with me from the very start of my academic journey up to this point of obtaining a master's degree. It is with immense appreciation that I acknowledge God's unwavering support, guidance, and love, which have been the pillars of my success and achievements in my journey.

Secondly, I would like to sincerely thank Dr. Lebsework Negash, Assistant Professor of Electrical Engineering, who served as my adviser and provided unwavering support during my research and MSc studies. His excitement, tolerance, depth of knowledge, and—above all—his faith in my ability were priceless. I was able to complete my research and write my thesis with his assistance.

Lastly, I would especially like to thank my family for their emotional support and encouragement throughout the successful completion of my thesis. I also want to express my gratitude to my classmates for their insightful advice during the writing of my thesis.

Tofik Kemal

Abstract

In recent years, the application of UAVs has increased. Fixed-wing Unmanned Aerial Vehicle (UAV) is an airborne vehicle that is largely used for surveillance, reconnaissance, monitoring, and data collection or to patrol an area that is not safe for a human being. This thesis addresses Robust Model Reference Adaptive Control for trajectory tracking of fixed-wing UAV. The fixed-wing UAV is under actuated system and due to this reason controlling all six degrees of freedom directly is impossible. To overcome this problem, the proposed control algorithm has two loops inner(attitude) and outer(position)loop. The outer loop provides the pitch and yaw angle reference trajectories for the inner loop. The inner loop controls attitude(roll, pitch, and yaw angle). First, fixed-wing UAV dynamic models are driven using the Newton-Euler approach, and the dynamic models are decoupled to reduce complexity. The decoupled dynamics have six second-order Single Input Multiple Output (SIMO) systems. Second, a conventional Model Reference Adaptive Control (MRAC) is designed. However, this controller causes instability in the presence of unmatched uncertainty. Third, Robust Model Reference Adaptive Control (RMRAC) is developed to prevent parameter drift in off-nominal scenarios. This thesis addresses different robust modification techniques like σ-modification, e-modification, and optimal modification techniques. These control algorithms are tested on different trajectories and a comparative analysis is made. Lyapunov direct method is used as a mathematical tool for design and stability analysis. The performance of the proposed control strategy is verified by developing simulation results in MATLAB/SIMULINK software. Finally, the developed Robust Model Reference Adaptive Controller is tested for parametric uncertainty and external disturbance. The simulation result shows that the proposed controller is able to track the desired trajectory in the presence of external disturbance(wind gust environment) and parametric variation.

Keywords: **Surveillance**, **Model Reference Adaptive Controller**, **Robust Model Reference Adaptive Controller**, **Fixed Wing UAV**

Contents

List of Figures

List of Tables

List of Abbreviations

CG	Center of Gravity
DC	Direct Current
DCM	Direction Cosine Matrix
DOF	Degree Of Freedom
FWUAV	Fixed Wing Unmanned Aerial Vehicle
GPS	Global Positioning System
HOSMC	Higher Order Sliding Mode Control
ITAE	Integral Time Absolute Error
LQR	Linear Quadratic Regulator
LTI	Linear Time Invariant
MRAC	Model Reference Adaptive Control
NASA	National Aeronautics and Space Administration
NED	North-East-Down
PID	Proportional Integral Derivative
RBF	Radial Basis Function
RMRAC	Robust Model Reference Adaptive Control
SIMO	Single Input Multiple Output
SMC	Sliding Mode control
UAV	Unmanned Aerial Vehicle

Chapter 1

Introduction

1.1 Background

In recent times, fixed-wing UAVs have found extensive use in many applications. There are different types of UAVs, such as cross-double-rotor, four-rotor, six-rotor, helicopter, and FWUAVs. They are used in different areas based on their unique characteristics. FWUAVs, distinguished by their rapid flying speed, elevated flying altitude, and flexible attitude, are particularly applied for tasks demanding high speed and altitude [1]. Fixed-wing UAV surveillance applications are very important in sectors that require control over specific areas. In recent times, FWUAVs have been utilized in numerous surveillance applications. FWUAVs are widely successful in the acquisition of aerial images. Fixed-wing UAVs' high endurance makes them proper for the utilization of surveillance.

In the early 1950s, active research in adaptive control was primarily motivated by the need to design autopilots for aircraft. In addressing the challenges of control algorithms, Whitaker and colleagues proposed Model Reference Adaptive Control (MRAC) as a solution [2]. The development of adaptive laws for various adaptive control systems utilized the sensitivity method and the Massachusetts Institute of Technology (MIT) rule. Kalman, in [3], introduced an adaptive pole placement technique based on the optimal linear quadratic problem. There were not enough stability proofs throughout this development period, and the characteristics of adaptive control were not well understood.

In 1967, National Aeronautics and Space Administration (NASA) tested an adaptive controller on one of the three X-15 hypersonic fixed-wing UAV flights [4]. Before a disastrous test flight that ended with one of these vehicles crashing, several successful flight tests were conducted. There was a decrease in interest in adaptive control as a result of this event's

occurrence and technical failure. However, stability theory, which was founded on Lyapunov theory in the 1970s, was established as the basis for model-reference adaptive control [5]. This discovery, which accompanied the application of Lyapunov stability theory with the development of enhanced model-reference adaptive control schemes, represented a major turning point in the field of adaptive control.

In the 1980s, it was pointed out that, in spite of the Lyapunov stability theory, adaptive control can show undesirable behaviors in the presence of small perturbations or unmodeled dynamics. During the mid-1980s, various redesign techniques and modifications were introduced and analyzed, giving rise to a field of study known as robust adaptive control. When a model-reference adaptive controller maintains signal boundedness in the presence of bounded disturbances and "reasonable" categories of unmodeled dynamics, it is considered as robust. It should also offer performance error bounds proportionate to the modeling error order [6].

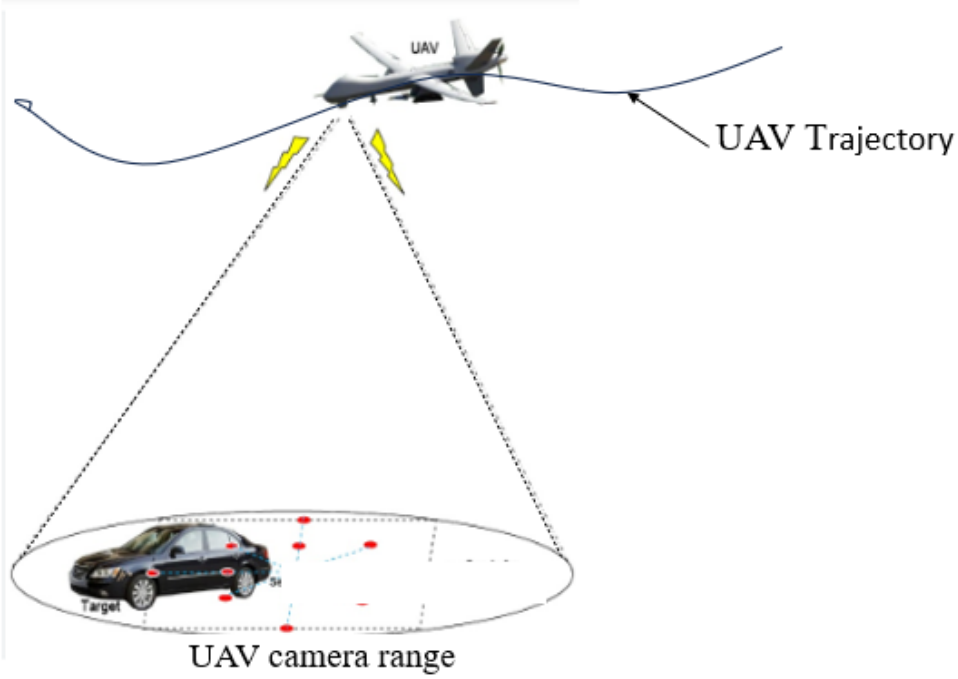

Figure 1.1: UAV aerial servillance

1.2 Statement of the problem

As a developing country, surveillance UAVs are important and necessary to assist human beings. Fixed-wing UAVs can assist human guards by patrolling work sites, capturing aerial footage, and preventing crimes with the ability to identify threats quickly and provide real-time images. This allows security staff to control the level of danger and take the appropriate response. Therefore, to assist human beings and to make efficient surveillance controlling fixed-wing UAVs is very important.

From a control perspective, it's important to note that the dynamics of fixed-wing UAVs are highly non-linear, coupled, and complex. Also, many of the fixed-wing UAV physical parameters depend on different operating conditions. For outdoor operations, this effect is significantly influenced by temperature, pressure, and many other unknown scenarios of the environment, due to this reason, uncertainty occurs during the flight period. In these cases, conventional fixed gain feedback controllers fail to ensure stabilization and conventional MRAC causes instability in the presence of unmatched uncertainty due to disturbance. Hence, Robust adaptive control techniques are designed so that controller gains can be tuned online to handle the variation and the disturbance.

1.3 Objective

1.3.1 General Objective

The main objective of this research is to design and simulate a robust model reference adaptive controller for fixed-wing UAVs.

1.3.2 Specific Objective

- To design conventional MRAC
- To design robust MRAC
- To simulate the overall system using the MATLAB/Simulink computing environment.

1.4 Contribution Of The Thesis

Fixed-wing UAVs have many useful applications for developing countries like Ethiopia. Using a surveillance UAV control over wide areas allows for regulation of access, anticipation

of incidents, remote risk assessment, and viewing of events from a safe distance. By taking appropriate action based on the information collected, a surveillance UAV can help ensure safety and security. In outdoor operation, the proposed robust model reference adaptive controllers have better performance, relative to conventional feedback controllers. Also, this thesis will be used as a document of reference for other researchers who are interested in this area.

1.5 Scope Of The Project

The scope of this research is to design, and simulate a robust MRAC for efficient stabilization and trajectory tracking in the presence of parametric uncertainty and external disturbances for fixed-wing UAVs. The design of the control system is implemented in MATLAB/Simulink environment.

1.6 Organization of The Document

The thesis includes six chapters.

1. **Chapter 2** Describe different related work, basic structure, basic force, and control surface of fixed wing UAV.
2. **Chapter 3**. Describe the flight dynamic of fixed-wing UAV, model verification of the plant, and decoupling of the model.
3. **Chapter 4**. Describe the design of a robust MRAC.
4. **Chapter 5**. Present simulation results for different trajectories.
5. **Chapter 6**. Draw a conclusion on this thesis and recommendations for future work.

Chapter 2

Overview of FWUAVs

2.1 Literature Review

The development of fixed-wing UAV control algorithms has been the subject of numerous studies. Some of them are discussed below.

2.1.1 Linear Controllers

Author in [7] proposed traditional linear PID for longitudinal control and non-linear controller for lateral control. The system was designed under a nested loop strategy, the navigation loop, and the attitude loop. Four-way-point trajectory tracking was implemented in a practical experiment to prove navigation and surveillance missions. The flight test demonstrated that the proposed controller guides FWUAV to achieve the desired three-dimensional navigation and surveillance mission.

Gain scheduled Proportional Integral Derivative (PID) was proposed by [8] for attitude control of Fixed-wing UAV. First, the dynamics of the aircraft are linearized around different operating conditions then gain scheduling is carried out by forming an interpolation between the family members of the linear closed-loop system, gain scheduling ensure smooth transition. Experimental results demonstrated that gain-scheduling PID has improved the performance of a traditional linear control system.

The author in [9] developed a Linear Quadratic Regulator (LQR) control system for surveillance FWUAV. The longitudinal and lateral dynamics were found around the trimming point. Simulation results demonstrated that LQR overcame disturbance without decreasing working performance.

2.1.2 Non-Linear controllers

Kedir Mustefa [10], designed a classical and super twisting sliding mode controller to stabilize the attitude of FWUAV. He decoupled the longitudinal and lateral dynamics to reduce the coupling effect. Finally, the comparative analysis showed that the classical sliding mode controller had a faster response with a high chartering effect, but the super-twisting sliding mode controller eliminated the chattering effect.

In [11] Feedback Linearization and Adaptive Control were used to design the attitude of FWUAVs. Feedback linearization methods with MRAC are integrated together to design the attitude control system for a FWUAV. The author in [12] combined the fuzzy adaptive method and sliding mode control was used to design attitude, altitude, and speed control systems for FWUAV. In this study, the fuzzy adaptive controller is designed to reduce the chattering effect due to sliding mode control.

Author [13] proposed an Adaptive backstepping sliding mode control method to control attitude, altitude, and speed for FWUAV. The backstepping sliding mode control method is used to reduce the nonlinear and complex dynamic model, and an adaptive law is introduced to cope the uncertainty the system. Espinoza et al. developed different nonlinear controllers to control fixed-wing UAV then compare their performances in [14]. These controllers were Backstepping, Sliding Mode control (SMC), Backstepping with Sliding Mode control, Backstepping with two Sliding Mode controls, and Backstepping with Higher Order Sliding Mode Control (HOSMC). A comparative performance analysis was done in order to show which controller has a better performance. Experimental results, in open-loop, were verified backstepping high-order sliding mode controller could reduce the chattering effect effectively.

Author [15] proposed an Adaptive Sliding Mode controller to attain the desired landing trajectory and maintain constant relative pitch and roll angles. Experimental results demonstrated that the proposed controller's effectiveness eliminates chattering effect. Author [16] proposed an extended observer based on the adaptive second-order sliding mode method for attitude and airspeed control of FWUAV. The extended observer was designed to estimate unmeasurable states of UAV and external disturbances. The experimental results demonstrated that the observer had a good tracking performance for unknown disturbances. Melkou and his team [17]proposed an adaptive second-order sliding mode method to ensure the stabilization of the attitude and altitude of FWUAV. The stability and effectiveness of the controller were also proved by experiments, and the related gain adaptation laws reduced

the tremor.

The author in [18] design adaptive sliding mode control for mass-actuated FWUAV. To reduce the effect of uncertainty, disturbance, and coupling effect adaptive sliding mode controller integrates a fuzzy system, Radial Basis Function (RBF) neural network, and sliding mode control. The experiment demonstrated the robustness of the proposed controller.

Marc L Steinberg and Anthony B Page [19] develop adaptive backstepping fight control law to maneuvering FWUAV in the situation of stabilator, rudder, and aileron failure. A genetic algorithm optimization technique was used to find optimal parameters. The simulation result showed good robustness of the proposed controller for modeling error.

Jiao Chen and his team [20] proposed robust adaptive control for nonlinear FWUAV systems with uncertainties to control longitudinal-lateral motion control of a nonlinear fixed wing UAV system. Simulation results demonstrated that the proposed robust adaptive controller was able to achieve fast adaptation without high chattering effect, and stable transient performance.

The concept of MRAC was developed in the 1950s to design the autopilot of aircraft to handle uncertainty. Much research has been conducted on the instability phenomena of standard MRAC. In 1960 NASA X-15 hypersonic vehicle was crushed due to the instability of MRAC [5]. This issue leads to robust model reference adaptive control. In the 1980s, Rohrs and colleagues Rohrs et al [21] explored the causes of instability in adaptive control arising from unmodeled dynamics. Due to this investigation, different types of robust modification strategies have been developed to ensure the robustness of MRAC. The σ modification, the e modification, and optimal control modification are well-known robust modification techniques.

From the above literature we can conclude that different authors tried to control specific states of the plant and most of the authors reduced the mathematical model of fixed-wing UAV. However, in this thesis, a fully autonomous fixed-wing UAV is designed and the mathematical model is not reduced. In this study, a robust model reference adaptive controller is proposed to control a fixed-wing UAV. This control algorithm handles the matched and unmatched uncertainties of model parameters and external disturbances. This design strategy involves position and attitude control(fully autonomous) of fixed-wing UAV. The mathematical model of fixed-wing UAVs is highly coupled and complex. Fixed-wing UAVs have a strong coupling effect it is difficult to design a controller. Therefore, it is necessary to introduce a new decoupling control method that focuses on the fixed-wing UAV control problem. Before starting controller design, it is necessary to consider the coupling effect between dif-

ferent states. Decoupling processing is mainly to extract the dominant state quantity in the control process and treat the remaining state quantity as uncertainty. The introduction of adaptive law maintains good control performance even when the parameters of the controlled system vary due to uncertainties. In this study Lyapunov direct method can be used to develop adaptation rule and stability analysis

2.2 The Basic Structure of FWUAVs

1. **Fuselage** is the body of the FWUAV, which is a long hollow tube that holds all the pieces of an airplane together. Aircraft designers typically make the fuselage hollow in order to reduce weight. Additionally, the shape of the fuselage is usually determined based on the specific mission of the aircraft.

2. **Wing** is an airfoil that, creates lift. They come in a variety of sizes and forms. Different wing designs might offer specific desired flight characteristics. By altering the shape and size of the wing we can change the amount of lift generated, balance, and stability. When designing a wing, there are several factors to consider. Both the leading and trailing edges can be straight or curved, or a combination of both. Additionally, one or both edges may be tapered to create a narrower wingtip. The shape of the wingtip can also vary and can be square, rounded, or pointed.

3. **A vertical stabilizer or tail fin** is the static part of the vertical tail of an aircraft [22]. The term is commonly used to describe the combination of a fixed surface and one or more movable rudders that are attached to it via hinges. These components play a key role in ensuring control, stability, and yaw trim (also referred to as directional stability). They constitute a part of the aircraft's empennage, specifically contributing to its stabilizers.

4. **A horizontal stabilizer** is used to keep the fixed-wing aircraft in longitudinal(vertical) balance, or trim: it applies a vertical force to make the summation of pitch moments about the center of gravity zero [23].

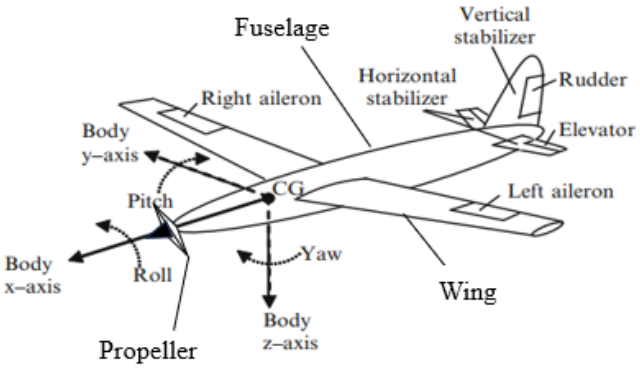

Figure 2.1: Fixed wing UAV basic structure [24]

2.3 Fixed wing UAV Basic Forces and Control input(control surface)

2.3.1 Forces

1. **Thrust** is the forward propulsive force produced by the propeller or rotor. It pushes the UAV forward and opposes the drag force. It is found on the longitudinal axis. For a fixed-wing UAV to start moving forward, the thrust force must be greater than the drug force.

2. **Drag** is created when the wing, rotor, fuselage, or other projecting items disturb the airfoil. Drag actually acts against thrust forces.

3. **Lift** is the force generated by the dynamic interaction of air with the airfoil(wing). It acts perpendicular to the lateral axis and perpendicular to the flight direction, passing via the lift's center.

4. **Weight** is the total weight of the payload, the battery, and the aircraft. The downward force of weight is what pulls the airplane down because of gravity. It acts vertically downward through the fixed-wing UAV's Center of Gravity (CG) and retard the lift force.

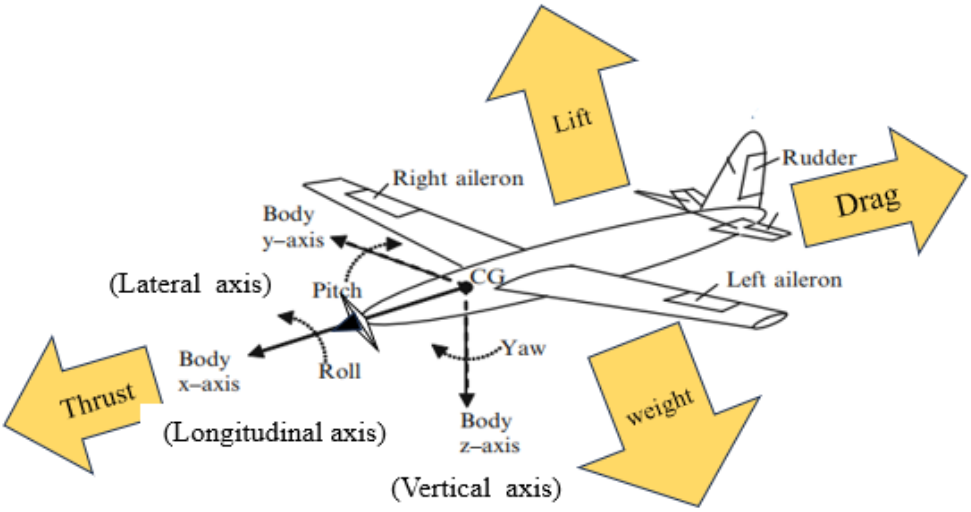

Figure 2.2: FWUAV basic forces and control surfaces

2.3.2 Control Surfaces

1. **Ailerons** travel in opposing directions and are mounted to the trailing edge of each wing, close to the wingtips. UAV roll motion is controlled by the ailerons. The left aileron goes down and the right aileron goes up when there is a positive deflection on the left aileron and a negative deflection on the right aileron. Lift on the wing is decreased with a raised aileron and increased with a lowered one. This causes the fixed-wing UAVs to roll to the right and begin to turn to the right.

2. **Elevator** is a movable component of the horizontal stabilizer, hinged in the rear of the horizontal tail. The positive deflection[1]of both elevators move down the elevator together, The negative deflection of both elevators move up the elevator together. Raised elevators increase pressure at the top and decrease pressure at the bottom of the elevator and cause the nose to pitch up. As a result, the wings fly at a higher angle of attack, producing more drag and lift. In general, elevator control the pitch motion of fixed-wing UAV

3. **Rudder** is a type of control surface that is manipulated by the autopilot command, and hinged on the trailing edge of the vertical stabilizer. The yawing motion is controlled by rudder input. When the autopilot command deflects the rudder positively pushes the tail right and causes the nose to yaw to the left and the nose yaws to the right and the tail is pushed left when the autopilot command deflects the rudder negatively.

2.4 Launch and Recovery of Fixed-Wing UAVs

For small-scale fixed-wing UAVs launch and recovery are the most critical and demanding phases of the aircraft's operation. Large-scale fixed-wing UAVs require a long runway for takeoff and landing. Catapult and parachute are used to launch and recover small-scale fixed-wing UAVs respectively as shown in the figure 2.3. A fixed-wing UAV with a mass of less than 10 kg can be launched by hand but it is important to be aware of the potential risks associated with exposure to the sharp edges of wings or propellers, as they can cause injury. It is crucial to take proper precautions and follow safety guidelines to minimize the risk of harm.

The advantage of a UAV launcher:

[1]It is simple to express the direction of the control surface by using the right-hand rule. The body frame j^b axis and the elevator hinge axis are in line. The right-hand rule for the body frame y axis implies that the elevator's trailing edge is pointing down for positive deflection and up for negative deflection.

- Save energy
- Enables the take-off of UAVs without chassis
- Eliminate the necessity of a runway.
- Enhances the safety of the operator.

In this thesis, a small-scale fixed-wing UAV is designed that uses a catapult for take-off and a parachute for recovery.

Figure 2.3: Catapult and parachute

Chapter 3

Methodology

3.1 Modelling Approach

In this section, Newton-Euler modeling approaches are used to drive the mathematical model of fixed-wing UAVs. Fixed-wing UAVs are under-actuated systems in which three control surfaces and one throttle are used to control motion in six degrees of freedom, which are three translational motions, and three rotational motions. The resulting dynamics are strongly coupled and extremely nonlinear systems due to aerodynamic factors. Thrust, drag, lift and weight are forces that act on fixed-wing UAVs in flight. In order to formulate the mathematical equations describing aerodynamic forces and moments arising from lifting surfaces, it is essential to define the control surfaces employed for maneuvering the fixed-wing UAV. These control surfaces play a crucial role in adjusting the aerodynamic forces and moments during flight. Common control surfaces on fixed-wing aircraft include the elevator, aileron, and rudder. Ailerons are responsible for controlling the roll angle (ϕ), elevators control the pitch angle (θ), and rudder input influences the yaw angle (ψ). The thrust force, generated by the power plant (rotor), propels the fixed-wing UAV forward or backward. In navigating along a specified trajectory, fixed-wing UAVs utilize their control surfaces and throttle input.

In a fixed-wing UAV system, the coordinate frame's kinematics connect the aircraft's states and transform forces and moments obtaining in various coordinate frames. A comprehensive understanding of reference frame dynamics is crucial for the design of guidance, navigation, and control systems. This chapter outlines the derivation of mathematical equations of motion using the Newtonian-Euler approach. The resulting translational and rotational equations of motion are expressed in a body coordinate frame. The principles of defining

external forces and moments acting on a generic fixed-wing UAV are presented. Given that these forces, moments, and airspeed operate in various coordinate frames, including inertial, body, stability, and wind frames, this chapter provides the conceptual framework and tools from the kinematics section to transform these forces into the body frame. Finally, the chapter introduces a decoupling technique aimed at simplifying the overall problem.

3.2 Frame Of References for UAVs

To drive the dynamics of unmanned aircraft systems, it is necessary to understand how different frames of reference are oriented relative to each other. It is important, to understand how the fixed-wing aircraft is oriented with respect to the different reference frames. This section establishes the several coordinate frames that are used to describe the fixed-wing aircraft's orientation as well as how these coordinate systems are transformed. For the following reasons, using multiple coordinate systems is required.

- While Newton's equations of motion are originally derived with respect to the inertial reference frame. However, a body frame makes it easiest to explain the motion of a fixed-wing UAV.
- The fixed-wing UAV body is subject to aerodynamic forces and moments, which can be simply described in a body reference frame.
- On-board sensors measure signals with respect to the body frame. On the other hand, position, ground speed, and course angle are measured by Global Positioning System (GPS) in reference to the inertial frame.
- Most mission specifications, including flight paths and loiter points, are specified in the inertia frame. Moreover, the inertia frame provides map information as well.

To determine the orientation of one coordinate system relative to another coordinate system there are basic operations such as rotation and and translation.

3.2.1 Rotation Matrices

Vector P is given in two orthogonal coordinate frames rotated concerning their mutual origin by angle ψ, as shown in figure 3.1

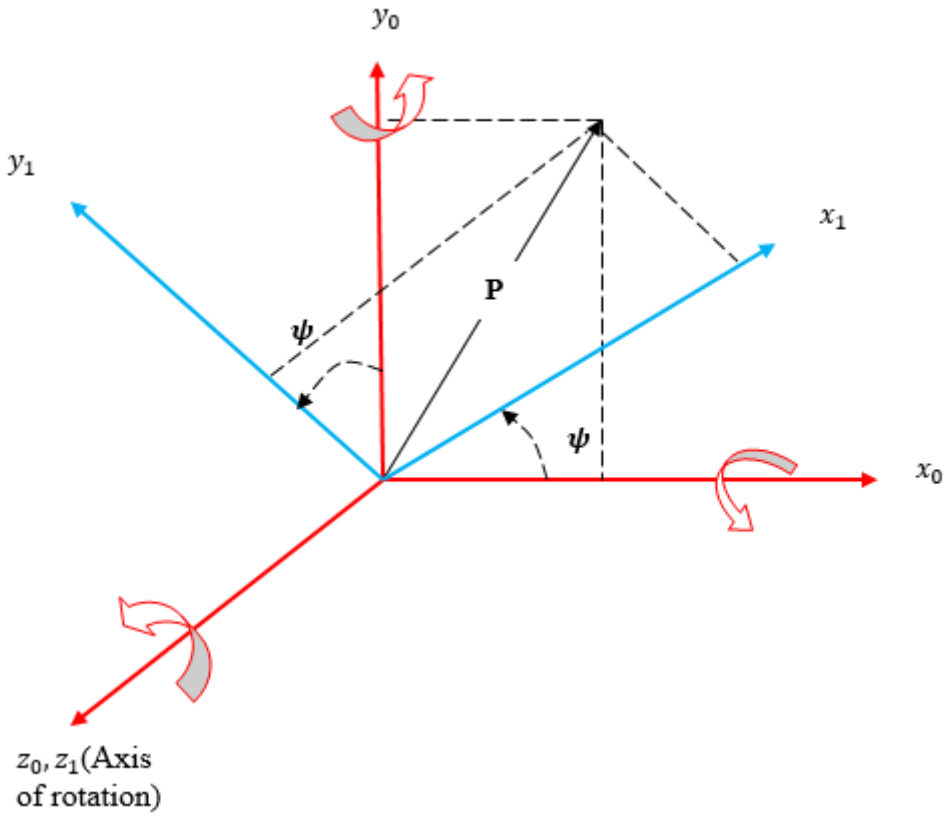

Figure 3.1: Three dimensional coordinate

By using geometric relationship we can demonstrate that vector $P = \left[x_0, y_0, z_0\right]$ can be defined as

$$\begin{aligned} x_1 &= x_0 \cos\psi + y_0 \sin\psi \\ y_1 &= -x_0 \sin\psi + y_0 \cos\psi \\ z_1 &= z_0 \end{aligned} \tag{3.1}$$

The subscripts 0 and 1 are used to refer to the coordinates of P in the original and rotated frames respectively. The resulting rotation matrix is called a Direction Cosine Matrix (DCM) matrix. It is the right-hand rotation of the original frames through angle ψ.
Rotating the coordinate system in a right-handed manner about the z-axis by an angle of ψ results in

$$R_0^1 = \begin{bmatrix} \cos(\psi) & \sin(\psi) & 0 \\ -\sin(\psi) & \cos(\psi) & 0 \\ 0 & 0 & 1 \end{bmatrix} \tag{3.2}$$

Continuing in a similar manner, a rotation of the coordinate system to the right about the

y-axis by an angle θ is obtained as

$$R_0^1 = \begin{bmatrix} \cos\theta & 0 & \sin\theta \\ 0 & 1 & 0 \\ \sin\theta & 0 & \cos\theta \end{bmatrix} \tag{3.3}$$

Continuing in a similar manner, a rotation of the coordinate system to the right about the x-axis by an angle ϕ is obtained as

$$R_0^1 = \begin{bmatrix} 1 & 0 & 0 \\ 0 & \cos\phi & \sin\phi \\ 0 & -\sin\phi & \cos\phi \end{bmatrix} \tag{3.4}$$

Properties of rotational matrices

- $(R_0^1)^{-1} = (R_0^1)^{-T} = R_1^0$
- $R_1^2 R_0^1 = R_0^2$
- $det(R_1^0) = 1$

3.2.2 The Inertia Frame F^i

An inertial frame is defined as one in which Newton's law of inertia holds. The earth coordinate is assumed to system be an inertial frame and has a flat $x - y$ plane. This coordinate frame is known as a North-East-Down (NED) frame. According to the NED convention, the unit vectors of this frame i^i, j^i, and k^i are pointed toward north, east, and down respectively.

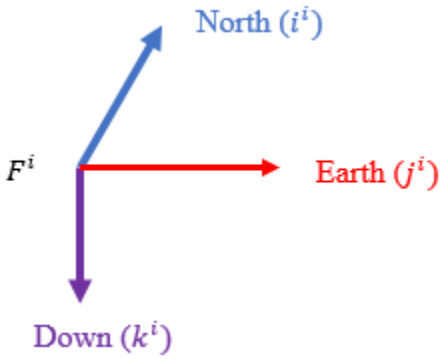

Figure 3.2: Inertia frame

3.2.3 The Vehicle Frame F^v

The vehicle frame is a representation of the inertia frame projected onto the center of mass of the fixed-wing UAV. The vehicle frame originated at the FWUAV's center of mass. The axes of the vehicle frame align with those of the inertia (earth) frame. The x^v directs north, the y^v directs east, and the z^v directs into the earth.

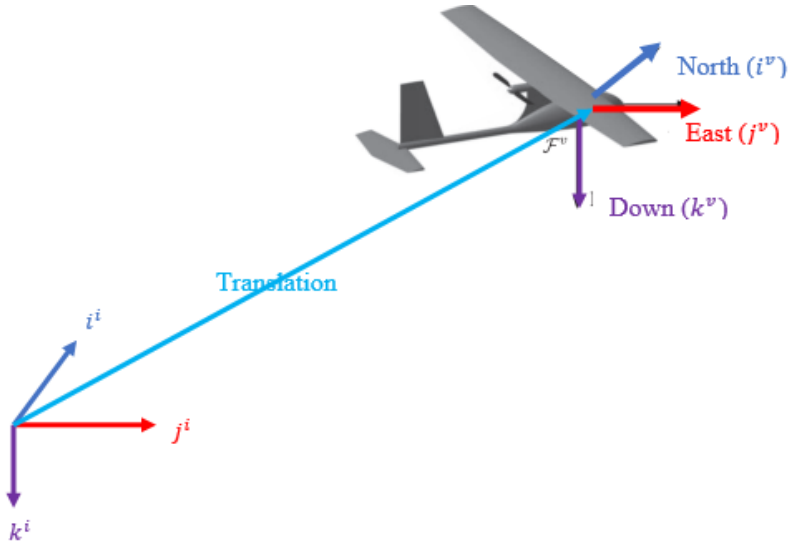

Figure 3.3: Vehicle frame

3.2.4 The Body Frame F^b

Its origin is attached to the center of the mass of the FWUAV. The roll axis i^b is aligned to the nose of the airframe, pitch axis j^b directed the right wing, and yaw axis k^b perpendicular to the other two axes forming a right-angled coordinate system and pointing out toward the earth. The x, y, and z directions of the body frame are represented by the unit vectors i^b, j^b, and k^b, respectively.

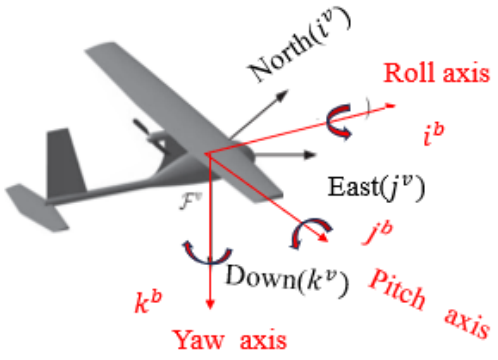

Figure 3.4: Body frame

The orientation of any given body frame relative to the inertia frame can be represented using three consecutive rotations around body frame axes. The set of the angle measure for the three rotations is called Euler angle rotation. The set of the angle measure for the three rotations is called Euler angles [25]. The transformation between coordinate frames occurs through two fundamental operations: rotation and translation. The rotation transformation from the vehicle frame to the body frame is obtained by three successive rotations according to the zyx convention. To go from the vehicle frame to the body frame introduce f^{v1} frame

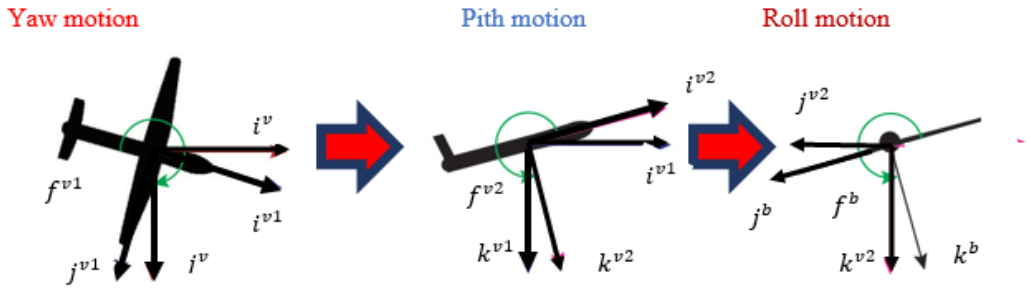

Figure 3.5: Rotating vehicle frame by Euler angle ψ,θ.ϕ

as follows:

$$P^{v1} = R_v^{v1}(\psi) * P^v \tag{3.5}$$

Here, $R_v^{v1}(\psi)$ denote the right-handed rotation matrix around the k^v axis,with yaw angle of ψ . F^{v1} has its i^{v1} axis pointing out the to the longitudinal direction from tail to head of the vehicle figure 3.5. The rotation about j^{v1} by the pitch angle θ is executed to obtain the intermediate coordinate system F^{v2}, where P^{v1} can be expressed as follows:

$$P^{v2} = R_{v1}^{v2}(\theta) * P^{v1} \tag{3.6}$$

Here is also, i^{v2} points out the longitudinal direction from tail to head of the FWUAV, but k^{v1} now points out the belly in figure3.5. Finally, the body frame F^b is achieved through the final rotation about the i^{v2} axis by the roll angle ϕ. In this configuration, i^b aligns with the longitudinal direction from tail to head of the FWUAV, j^b points towards the right wing, and k^b points out the belly in figure 3.5. The transformation from F^{v2} to F^b is:

$$P^b = R_{v2}^b(\phi) * P^{v2} \tag{3.7}$$

The corresponding rotation matrix from the inertial frame to the body frame is expressed as:

$$R_v^b(\phi,\theta,\psi) = R_{v2}^b(\phi)R_{v1}^{v2}(\theta)R_v^{v1}(\psi) = \begin{bmatrix} C_\theta C_\psi & C_\theta S_\psi & -S_\theta \\ S_\phi S_\theta C_\psi - C_\phi S_\psi & S_\phi S_\theta S_\psi + C_\phi C_\psi & S_\phi C_\theta \\ C_\phi S_\theta C_\psi + S_\phi S_\psi & C_\phi S_\theta S_\psi - S_\phi C_\psi & C_\phi C_\theta \end{bmatrix} \tag{3.8}$$

when C and S represent the cosine and sine functions, respectively. The Euler angles, denoted as ϕ, θ, and ψ, represent yaw, pitch, and roll, respectively. These angles naturally describe the orientation of the body in three dimensions relative to the inertial frame.

3.2.5 The Stability Frame F^s

To treat the aerodynamic forces, it is necessary to understand stability and wind coordinate systems. The airspeed $\boldsymbol{V_a}$ is the relative velocity between fixed-wing UAV and surrounding air. To generate sufficient lift, the FWUAV must fly at a positive angle with respect to the airspeed $\boldsymbol{V_a}$. This angle is known as the angle of attack α. The stability frame is obtained as the left-handed rotation of the body frame f^b around j^b by the angle of attack α. The importance of a left-handed rotation comes from the definition of the angle of attack. The angle of attack needs to be positive during the right-handed rotation from the stability frame to the body frame, as noted in reference [26].

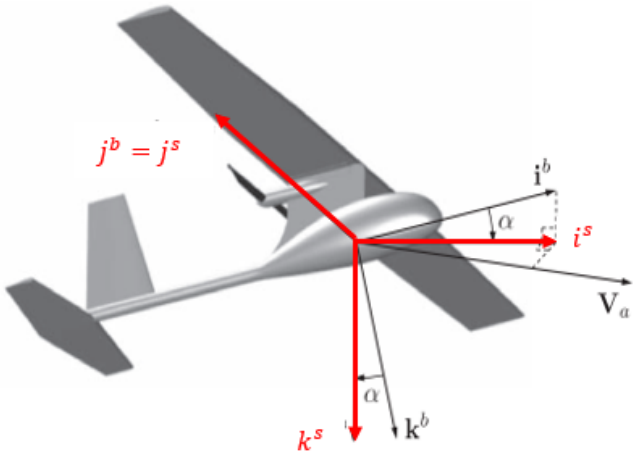

Figure 3.6: Stability frame

P^b is defined on f^b then P^s on f^s expressed as

$$P^s = R_b^s(\alpha) * P^b \tag{3.9}$$

when the left-handed rotation matrix $R_b^s(\alpha)$ is given by:

$$R_b^s(\alpha) = \begin{bmatrix} cos\alpha & 0 & sin\alpha \\ 0 & 1 & 0 \\ -sin\alpha & 0 & cos\alpha \end{bmatrix} \tag{3.10}$$

3.2.6 The Wind Reference Frame F^w

The airspeed vector $\boldsymbol{V_a}$ may also not lie in the vertical $i^b - j^b$ plane and makes a small angle to the plane called side-slip angle β. The wind frame is obtained by right-handed rotation of the stability frame by angle β around k^s axes to have i^w axes aligned with the direction of the airspeed vector, we obtain the wind frame.

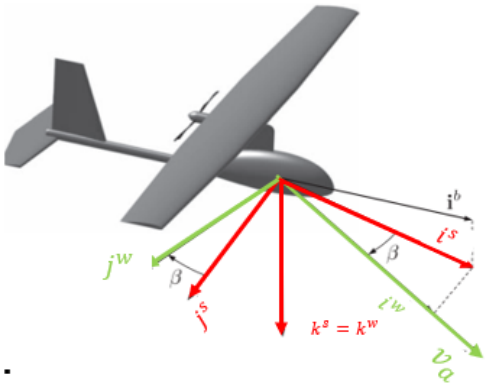

Figure 3.7: Wind frame

The transformation is given by

$$P^w = R_s^w(\beta) * P^s \tag{3.11}$$

Where

$$R_b^s(\beta) = \begin{bmatrix} cos\beta & sin\beta & 0 \\ -sin\beta & cos\beta & 0 \\ 0 & 0 & 1 \end{bmatrix} \tag{3.12}$$

Finally, the transformation from the body frame to the wind frame is given as:

$$R_b^w(\alpha,\beta) = R_s^w(\beta) * R_b^s(\alpha) = \begin{bmatrix} C_\beta C_\alpha & S_\beta & C_\beta S_\alpha \\ -S_\beta C_\alpha & C_\beta & -S_\beta S_\alpha \\ -S_\alpha & 0 & C_\alpha \end{bmatrix} \tag{3.13}$$

The transformation from the wind frame to the body frame is provided by

$$R_w^b(\alpha,\beta) = R_s^b(\alpha) * R_w^s(\beta) = \begin{bmatrix} C_\beta C_\alpha & -S_\beta & C_\alpha - S_\alpha \\ S_\beta & C_\beta & 0 \\ C_\beta S_\alpha & -S_\beta S_\alpha & C_\alpha \end{bmatrix} \tag{3.14}$$

Where C and S represent the cose and sine functions.

3.3 Airs, Wind, and Ground Speed

The wind effect on FWUAV dynamics can be calculated using the so-called wind triangle, as shown in the figure below. When we consider UAVs, the wind has a strong impact effect on the flight mechanics. Since the aerodynamic forces depend on the relative speed of the surrounding air. Therefore it is important to properly considered at the time of modeling. What follows is trying to calculate the essential expressions in developing the equations of motion of a fixed-wing UAV. The wind velocity regarding the inertial frame is denoted as V_w. Similarly, the airspeed concerning the same frame is represented as V_a and defined as V_g. Airspeed, ground, and wind speed vectors are given by equation 3.15:

$$V_a = V_g - V_w \tag{3.15}$$

In the body frame, the ground speed can be expressed as follows in terms of vector components along the (i^b; j^b; and k^b) axes:

$$V_g^b = \begin{bmatrix} u \\ v \\ w \end{bmatrix} \tag{3.16}$$

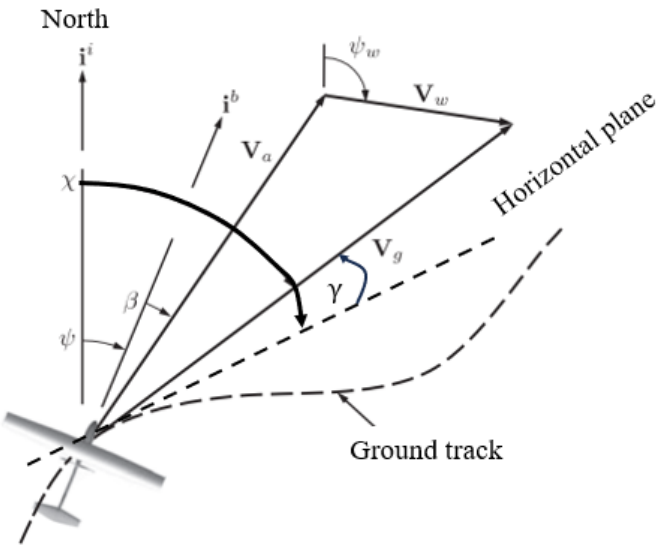

Figure 3.8: Wind triangle [27]

Also, the wind components decomposed at the body frame are given as:

$$V_w^b = \begin{bmatrix} u_w \\ v_w \\ w_w \end{bmatrix} = R_v^b(\phi, \theta, \psi) \left[V_w^i \right] \tag{3.17}$$

when

$$V_w^i = \begin{bmatrix} w_n \\ w_e \\ w_d \end{bmatrix} \tag{3.18}$$

The airspeed V_a of FWUAV component in the wind frame is expressed as

$$V_a^w = \begin{bmatrix} V_a \\ 0 \\ 0 \end{bmatrix} \tag{3.19}$$

To calculate body frame component of the the airspeed V_a vector, u_r, v_r, w_r use the rotation matrix from the wind to the body frame R_w^b is carried out:

$$V_a^b = \begin{bmatrix} u - u_w \\ v - v_w \\ w - w_w \end{bmatrix} = \begin{bmatrix} u_r \\ v_r \\ w_r \end{bmatrix} = R_w^b \begin{bmatrix} V_a \\ 0 \\ 0 \end{bmatrix} = V_a \begin{bmatrix} cos\alpha cos\beta \\ sin\beta \\ sin\alpha cos\beta \end{bmatrix} \tag{3.20}$$

From the above equation3.20 solve for V_a,α, and β as follow:

$$V_a = \sqrt{u_r^2 + v_r^2 + w_r^2} \tag{3.21}$$

$$\alpha = tan^{-1}(w_r/v_r) \tag{3.22}$$

$$\beta = sin^{-1}(v_r/\sqrt{u_r^2 + v_r^2 + w_r^2}) \tag{3.23}$$

These equations 3.20, 3.22 and 3.23 are very important for the development of dynamics and kinematics of FWUAV. In the preceding section, we introduced concepts such as reference frames, ground velocity, wind velocity, and the airspeed vector. Now, let's see the essential definitions of angles relevant to the guidance and navigation of FWUAVs. Those angles are course angle χ and the flight path angle γ

- Flight path angle γ refers to the angle between the flight path of an aircraft and the local horizontal reference plane (such as the Earth's surface).
- Course angle χ is described as the angle between true north and the ground velocity which is projected onto the horizontal plane.

The relationship between flight-path angle, angle of attack, and the pitch angle are expressed as

$$\gamma = \theta - \alpha \tag{3.24}$$

If wind is not considered, there are basic simplifications result. When V_w=0 , then that v_a=v_g, u=u_r, v=v_r, w=w_r, ψ=χ and β=0. In this thesis work, the wind effect is neglected. However, the performance of the proposed controller is verified by a wind gust environment.

3.4 Kinematics and Flight Dynamics

Finding the best mathematical model is the first step in developing control techniques for FWUAVs. As we know an airborne FWUAV has six Degree Of Freedom (DOF) of a rigid body - three for translation and three for rotation. The equations of motion for the Fixed-Wing Unmanned Aerial Vehicle (FWUAV) involve twelve state variables. Three represent translational position, three represent translational velocity, three correspond to angular positions, and the remaining three pertain to angular velocity. These variables collectively describe both the translational and rotational motion of the UAV. The state variables are

Name	Description
x	Position (i^i)
y	Position (j^i)
z	Position (k^i)
u	Linear velocity (i^b)
v	Linear velocity (j^b)
w	Linear velocity (k^b)
ϕ	Roll angle
θ	Pitch angle
ψ	Yaw angle
p	Roll rate
q	Pitch rate
r	Yaw rate

Table 3.1: State variables for FWUAVs

given in table 3.1. The kinematics focus on the relationship between positions and velocities and dynamics describes relations between forces, moments, and momentum.

3.4.1 Modelling Assumption

- The fixed-wing UAV is modeled as a rigid body in space
- The FWUAV has a symmetrical structure
- The center of gravity (CG) of the fixed-wing UAV coincides with the origin of the body coordinate system
- The mass of fixed-wing UAV is assumed to be constant during motion

3.4.2 Kinematics

The FWUAV transnational velocity is commonly expressed in terms of body coordinate frame. The ground velocity of UAV is defined on the i^b,j^b, and k^b axes, the component velocity in the body frame are u, v, and w respectively.In fact, an inertial reference frame is typically used to measure and express the FWUAV's translational position. Thus the

relation between translational velocity and position needs rotation and differentiation

$$\begin{bmatrix} \dot{x} \\ \dot{y} \\ \dot{z} \end{bmatrix} = R_b^v(\phi,\theta,\psi) \begin{bmatrix} u \\ v \\ w \end{bmatrix} = \begin{bmatrix} C_\theta C_\psi & S_\psi S_\theta C_\psi - C_\phi S_\psi & C_\phi S_\theta C_\psi + S_\phi S_\psi \\ C_\theta S_\psi & S_\psi S_\theta S_\phi + C_\phi C_\psi & C_\psi S_\theta S_\psi - S_\psi C_\psi \\ -S_\theta & S_\phi C_\theta & C_\phi C_\theta \end{bmatrix} \begin{bmatrix} u \\ v \\ w \end{bmatrix} \tag{3.25}$$

Deriving the relationship between angular positions (roll, pitch, yaw - represented by ϕ[1], θ[2] , ψ)[3] and angular velocities (p, q, r) in a fixed-wing UAV is intricate due to the consideration of roll, pitch, and yaw angles in relation to their respective intermediate frames, as shown in the figure 3.5. As we know, the Euler angles are obtained relative to intermediate frames of reference, angular rates (p, q, r) are not equals to derivatives of the angular position (ϕ, θ, ψ). The angular rates in the body frame of a system can be represented by the derivatives of the Euler angles, given that the appropriate rotational transformations are established as:

$$\begin{bmatrix} p \\ q \\ r \end{bmatrix} = \begin{bmatrix} \dot{\phi} \\ 0 \\ 0 \end{bmatrix} + R_{v2}^b(\phi) \begin{bmatrix} 0 \\ \dot{\theta} \\ 0 \end{bmatrix} + R_{v2}^b(\phi) R_{v1}^{v2}(\theta) \begin{bmatrix} 0 \\ 0 \\ \dot{\psi} \end{bmatrix} \tag{3.26}$$

Which is equal to:

$$\begin{bmatrix} p \\ q \\ r \end{bmatrix} = \begin{bmatrix} 1 & 0 & -sin\theta \\ 0 & cos\phi & sin\phi cos\theta \\ 0 & -sin\phi & cos\phi cos\theta \end{bmatrix} \begin{bmatrix} \dot{\phi} \\ \dot{\theta} \\ \dot{\psi} \end{bmatrix} \tag{3.27}$$

Inverting equation 3.27 yields

$$\begin{bmatrix} \dot{\phi} \\ \dot{\theta} \\ \dot{\psi} \end{bmatrix} = \begin{bmatrix} 1 & tan\theta sin\phi & cos\phi tan\theta \\ 0 & cos\phi & -sin\phi \\ 0 & sin\phi/cos\theta & cos\psi/cos\theta \end{bmatrix} \begin{bmatrix} p \\ q \\ r \end{bmatrix} \tag{3.28}$$

[1]Positive bank angle, when aircraft right wing down
[2]Positive pitch angle, when aircraft nose up
[3]Positive yaw angle, when clockwise rotation of the aircraft nose from the true north direction

Equation 3.28 reveals that the Euler angles representing the attitude exhibit a singularity at $\theta = \pm\pi/2$ degrees, leading to an undefined yaw angle at these points—commonly referred to as gimbal lock. However, for FWUAVs, gimbal lock does not occur during normal flight, as the pitch angle remains below $\pi/2$. The rotational constraints are defined as follows: roll ($-\pi < \phi < \pi$), pitch ($-\pi/2 < \theta < \pi/2$), and yaw ($-\pi < \psi < \pi$). These Euler angles provide an instantaneous orientation of the aircraft's body-fixed coordinate system relative to the inertial frame of reference.

3.4.3 Rigid-Body Dynamics

To derive the dynamic equations of motion, Newton's second law is employed. Forces and moments are typically expressed in the inertial frame, although they can also be described using components associated with other frames, such as the body frame. In this analysis, we consider the flat earth model, particularly suitable for small FWUAVs.

3.4.3.1 Translational Motion

Apply Newton's second law on a body passing through translational motion can be given as:

$$m(\frac{\mathrm{dV_g}}{\mathrm{d}t})^i = \sum_k {F_k}^i \tag{3.29}$$

V_g is the linear velocity of the body in the inertial frame, m is the time-invariant mass of the FWUAV, d/dt is the time derivative in the inertial frame and F_k is the $k-th$ external force sum of all external forces applied to the UAV. External forces are included by aerodynamic, gravitational, and propulsive forces [27]. The superscript i indicates that the time derivative is held on the inertial frame. According to the vector differentiation rule the velocity of the inertial frame can be written concerning the derivative in the body frame:

$$(\frac{\mathrm{dV_g}}{\mathrm{d}t})^i = \frac{\mathrm{dV_g^b}}{\mathrm{d}t_b} + w_{b/i}^b \times V_g^b \tag{3.30}$$

Where $w_{b/i}^b$ is the angular velocity of the UAV concerning the inertial frame. From equation 3.29 and 3.30 we can get another statement of Newton's second law with differentiation applied in the body frame:

$$m(\frac{\mathrm{dV_g^b}}{\mathrm{d}t_b} + w_{b/i}^b \times V_g^b) = \sum_k F^b \tag{3.31}$$

When $V_g^b = \begin{bmatrix} u \\ v \\ w \end{bmatrix}$,$w_{b/i}^b = \begin{bmatrix} p \\ q \\ r, \end{bmatrix}$,$\sum_k F^b = \begin{bmatrix} \sum(f_{xa} + f_{xp} + f_{xg} = F_x) \\ \sum(f_{ya} + f_{yp} + f_{yg} = F_y) \\ \sum(f_{za} + f_{zp} + f_{zg} = F_z) \end{bmatrix}$,$\frac{\mathrm{dV_g^b}}{\mathrm{dt_b}} = \begin{bmatrix} \dot{u} \\ \dot{v} \\ \dot{w} \end{bmatrix}$

By computing the cross product in equation 3.31 we can obtain the following expressions.

$$\begin{bmatrix} \dot{u} \\ \dot{v} \\ \dot{w} \end{bmatrix} = \begin{bmatrix} rv - qw \\ pw - ru \\ qu - pu \end{bmatrix} + 1/m \begin{bmatrix} F_x \\ F_y \\ F_z \end{bmatrix} \tag{3.32}$$

3.4.3.2 Rotational Motion

In the case of rotational motion Newton's Law is stated as:

$$(\frac{\mathrm{d}\mathbf{h}}{\mathrm{d}t})^i = \sum_k \mathbf{m}_k^i \tag{3.33}$$

When $\mathbf{h}$ represents the angular momentum in vector form and $\mathbf{m}$ denotes the $k-th$ accumulation of torques, the provided equation sums moments around the center of mass of the UAV. The expansion of the derivative of angular momentum in the inertial frame can be performed using the vector derivative principle, as follows [28].

$$(\frac{\mathrm{d}\mathbf{h}}{\mathrm{d}t_b})^i = (\frac{\mathrm{d}\mathbf{h}}{\mathrm{d}t_b})^b + w_{b/i}^b \times h = \sum_k \mathbf{m}^b \tag{3.34}$$

In the context of a rigid body, angular momentum is expressed as the product of the inertia tensor$J$ and the angular velocity vector: i.e $h^b = J * w_{b/i}^b$, when J is the inertia tensor, given as:

$$J = \begin{bmatrix} \int(y^2+z^2)dm & -\int(xy)dm & -\int(xz)dm \\ -\int(xy)dm & \int(x^2+z^2)dm & -\int(yz)dm \\ -\int(xz)dm & -\int(yz)dm & \int(x^2+y^2)dm \end{bmatrix} = \begin{bmatrix} J_{xx} & -J_{xy} & -Jxz \\ -J_{xy} & J_{yy} & -Jyz \\ -J_{xz} & -J_{yz} & Jzz \end{bmatrix} \tag{3.35}$$

The moments of inertia are the diagonal terms of J, while the products of inertia are the off-diagonal terms [29]. FWUAVs are commonly symmetric about the plane spanned by i^b

and k^b, and so, $J_{xy} = J_{yz} = 0$. Since J is determined in the body frame, its derivative in the similar frame is clearly $(\frac{\mathrm{d}}{\mathrm{d}t}J)^b = 0$ [30]. Equation 3.34 then becomes:

$$J(\frac{\mathrm{d}}{\mathrm{d}t}w_{b/i})^b + (w_{b/i})^b \times J(w_{b/i})^b = \sum_k \mathbf{m}^b \tag{3.36}$$

multiply both sides by J^-1

$$\dot{w}^b_{b/i} = J^{-1}(-w^b_{b/i} \times (Jw^b_{b/i}) + \sum_k \mathbf{m}^b) \tag{3.37}$$

Under the assumption that the rigid body is symmetric i.e. $(J_{xy} = J_{yz} = 0)$ the inverse of the inertia matrix is determined as follows:

$$J^{-1} = \begin{bmatrix} J_{zz}/\Gamma & 0 & J_{xz}/\Gamma \\ 0 & 1/J_{yy} & 0 \\ J_{xz}/\Gamma & 0 & J_{xx}/\Gamma \end{bmatrix} \tag{3.38}$$

when $\Gamma = J_{xx}J_{zz} - J^2_{xz}$. By letting $w^b_{b/i}$=$\begin{bmatrix} p & q & r \end{bmatrix}^T$ be the angular rates and the summation of the moment be $\sum_k \mathbf{m}^b$= $\begin{bmatrix} \mathcal{L} & \mathcal{M} & \mathcal{N} \end{bmatrix}^T$
Where $\mathcal{L}$, $\mathcal{M}$, and $\mathcal{N}$ roll moment, pitch moment, and yaw moment respectively. Finally, the rotational dynamics can be written as:

$$\dot{w}^b_{b/i} = \begin{bmatrix} \dot{p} \\ \dot{q} \\ \dot{r} \end{bmatrix} = \begin{bmatrix} \Gamma_1 pq - \Gamma_2 pr \\ \Gamma_5 pr - \Gamma_6(p^2 - r^2) \\ \Gamma_7 pq - \Gamma_1 qr \end{bmatrix} + \begin{bmatrix} \Gamma_3\mathcal{L} + \Gamma_4\mathcal{N} \\ 1/J_{yy}\mathcal{M} \\ \Gamma_4\mathcal{L} + \Gamma_8\mathcal{N} \end{bmatrix} \tag{3.39}$$

Where

$$\Gamma_1 = \frac{J_{xz}(J_{xx} - Jyy + J_{zz})}{\Gamma}$$
$$\Gamma_2 = \frac{J_{zz}(J_{zz} - J_{yy}) + J_{xz}^2}{\Gamma}$$
$$\Gamma_3 = \frac{J_{zz}}{\Gamma}$$
$$\Gamma_4 = \frac{J_{xz}}{\Gamma}$$
$$\Gamma_5 = \frac{J_{zz} - J_{xx}}{J_{yy}}$$
$$\Gamma_6 = \frac{J_{xz}}{J_{yy}}$$
$$\Gamma_7 = \frac{(J_{xx} - J_{yy})J_{xx} + J_{xz}^2}{\Gamma}$$
$$\Gamma_8 = \frac{J_{xx}}{\Gamma}$$

The six-degree of freedom, a 12-state model for FWUAV is dynamics and kinematics are enlisted as follows.

$$
\begin{cases}
\begin{bmatrix} \dot{x} \\ \dot{y} \\ \dot{z} \end{bmatrix} = \begin{bmatrix} C_\theta C_\psi & S_\phi S_\theta C_\psi - C_\phi S_\psi & C_\phi S_\theta C_\psi + S_\phi S_\psi \\ C_\theta S_\psi & S_\phi S_\theta S_\psi + C_\phi C_\psi & C_\phi S_\theta S_\psi - S_\phi C_\psi \\ -S_\theta & S_\phi C_\theta & C_\phi C_\theta \end{bmatrix} \begin{bmatrix} u \\ v \\ w \end{bmatrix} \\
\begin{bmatrix} \dot{u} \\ \dot{v} \\ \dot{w} \end{bmatrix} = \begin{bmatrix} rv - qw \\ pw - ru \\ qu - pu \end{bmatrix} + 1/m \begin{bmatrix} F_x \\ F_y \\ F_z \end{bmatrix} \\
\begin{bmatrix} \dot{\phi} \\ \dot{\theta} \\ \dot{\psi} \end{bmatrix} = \begin{bmatrix} 1 & tan\theta sin\phi & cos\phi tan\theta \\ 0 & cos\phi & -sin\phi \\ 0 & sin\phi/cos\theta & cos\psi/cos\theta \end{bmatrix} \begin{bmatrix} p \\ q \\ r \end{bmatrix} \\
\begin{bmatrix} \dot{p} \\ \dot{q} \\ \dot{r} \end{bmatrix} = \begin{bmatrix} \Gamma_1 pq - \Gamma_2 pr \\ \Gamma_5 pr - \Gamma_6 (p^2 - r^2) \\ \Gamma_7 pq - \Gamma_1 qr \end{bmatrix} + \begin{bmatrix} \Gamma_3 \mathcal{L} + \Gamma_4 \mathcal{N} \\ 1/J_{yy} \mathcal{M} \\ \Gamma_4 \mathcal{L} + \Gamma_8 \mathcal{N} \end{bmatrix}
\end{cases}
$$

The UAV's dynamics are shown by equations 3.25, 3.28, 3.32, and 3.39. Because the forces and moments exerted externally have not yet been described, the equations are incomplete. The actions of gravity, propulsion, and aerodynamics interaction result in external forces and moments. The next section will drive forces and moments because of gravity, aerodynamics, and propulsion.

3.5 External Forces and Moments

The primary goal of this section is to determine the forces and moments acting on a FWUAV. These forces and moments predominantly arise from three key factors: gravity, aerodynamics, and propulsion [31]. The sum of the whole exerted forces and moments are:

$$F = F_p + F_g + F_a \tag{3.40}$$

$$M = M_p + M_a \tag{3.41}$$

The subscript g indicates the gravity effect, a indicates the aerodynamic effect and p indicates the propulsion effect.

3.5.1 Gravitational Forces

The gravitational field's effect on a UAV can be defined as a mass-proportional force acting in the k^i direction on the center of mass. The gravitational force is expressed as follows in the vehicle frame F^v:

$$F_g^v = \begin{bmatrix} 0 \\ 0 \\ mg \end{bmatrix}$$

But all the force must be expressed in the body frame axis. Then we have to transform the gravitational force into its body reference frame as:

$$F_g^b = R_v^b \begin{bmatrix} 0 \\ 0 \\ mg \end{bmatrix} = \begin{bmatrix} -mgsin\theta \\ mgcos\theta sin\phi \\ mgcos\theta cos\phi \end{bmatrix} \tag{3.42}$$

Because gravitational force is on the UAV's center of mass, zero moments are generated by gravity.

3.5.2 Aerodynamics Force and Moments

Control Surfaces

The control surfaces are listed below, we are going to drive the equation of force and moment exerted on the body. Figure 3.9 introduces the standard configuration of FWUAVs control surfaces when the aileron deflection input is indicated by δ_a, the elevator deflection input is δ_e, the rudder deflection with δ_r . The aileron deflection can be written as:

$$\delta_a = \frac{1}{2}(\delta_{al} - \delta_{ar}) \tag{3.43}$$

when δ_{al} and δ_{ar} are the left and right deflection of aileron respectively. Each deflection is expressed in radians except the throttle deflection which is by %. The direction of the surface deflection is indicated by a right-hand rule to the joint axis of the control surface. A positive δ_a may produce a a positive rolling moment along i^b with respect to the convention.

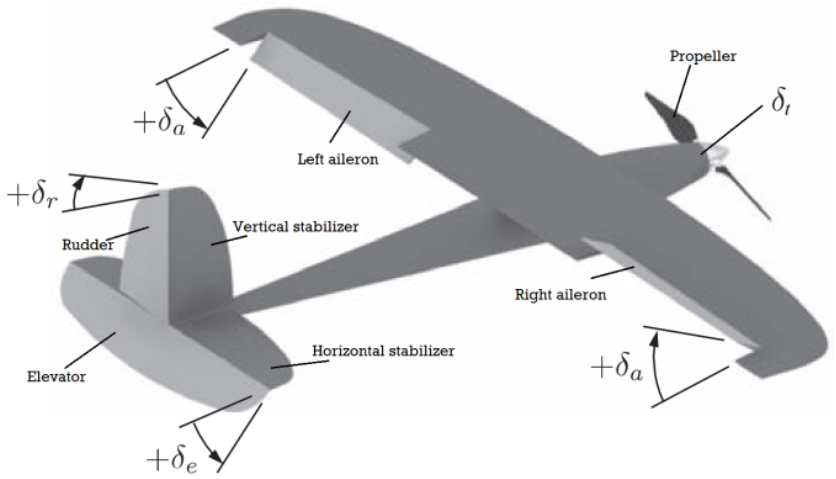

Figure 3.9: Standard aircraft control surfaces, and the propeller [27]

The movement of a Fixed-Wing Unmanned Aerial Vehicle (FWUAV) can be divided into two interrelated motion modes, providing a more straightforward representation conducive to the application of control techniques. These modes are longitudinal motion and lateral-directional motion, as highlighted in [24].

For small-scale FWUAVs, there are other configurations. For instant v tail configuration as shown in figure 3.10. The control surface is called ruddervator. The deflection of the right ruddervators is represented by δ_{rr}, and the deflection of the right ruddervators is represented by δ_{rr} the deflection of the left ruddervators is represented by δ_{rl}. The difference of right and left ruddervators has the same effect as a rudder, producing torque around k^b. The sum of right and left ruddervators has the same effect as elevators, producing torque around j^b

Mathematically we can express

$$\delta_e = \delta_{rl} + \delta_{rr} \tag{3.44}$$

$$\delta_r = \delta_{rl} - \delta_{rr} \tag{3.45}$$

Using the above relation, we can express the forces and torques equation in terms of standard rudder-elevator notation.

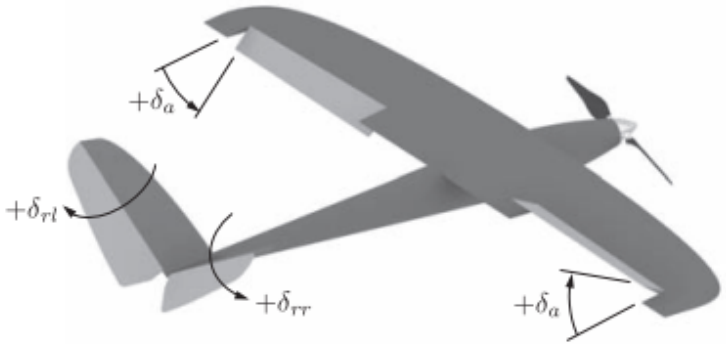

Figure 3.10: v-tail aircraft [27]

3.5.2.1 Longitudinal Aerodynamics

The forces and moments responsible for creating motion in the $(i^b; k^b)$ plane include the lift force, drag force, and pitch moment. The influence of the angle of attack α, pitch rate q, and elevator deflection δ_e significantly affects the lift, drag forces, and pitching moment, as stated in [29].

$$F_{lift} = \frac{1}{2}\rho {V_a}^2 S C_L(\alpha, q, \delta_e) \tag{3.46}$$

$$F_{drag} = \frac{1}{2}\rho {V_a}^2 S C_D(\alpha, q, \delta_e) \tag{3.47}$$

$$\mathcal{M} = \frac{1}{2}\rho {V_a}^2 S c C_M(\alpha, q, \delta_e) \tag{3.48}$$

When considering ρ as air density, S as the planform area of the single wing, and c as the main chord of the wing, with V_a representing the airspeed, and C_L, C_D, C_M as non-dimensional coefficients depend on α, q, δ_e, their aerodynamic coefficient relationship can be approximated using a first-order Taylor series, expressed as:

$$C_L(\alpha, q, \delta_e) = C_{L_0} + \frac{\partial C_L}{\partial \alpha}\alpha + \frac{\partial C_L}{\partial q}q + \frac{\partial C_L}{\partial \delta_e}\delta_e \tag{3.49}$$

When $\alpha = q = \delta_e = 0$, the C_L value is represented by the coefficient C_{L0}. It is clear that this dimensionless linear approximation's partial derivatives are easily calculable. Given that C_L, together with the angles α and δ_e (both given in radians), are dimensionless, $\frac{\partial C_L}{\partial q}$ is the main component needed to render the system non-dimensional. Since q has units in rad/s, $c/(2V_a)$ is a common factor to utilize. As a result, we can write equation 3.49 like this:

$$C_L(\alpha, q, \delta_e) = C_{L_O} + C_{L_\alpha}\alpha + C_{L_q}\frac{c}{2V_a}q + C_{L_{\delta_e}}\delta_e \tag{3.50}$$

Where $C_{L_\alpha} = \frac{\partial C_L}{\partial \alpha}$, $C_{L_q} = \frac{\partial C_L}{\frac{\partial qc}{2V_a}}$, $C_{L\delta_e} = \frac{\partial C_L}{\partial \delta_e}$. Similarly, we calculate the aerodynamic drag force and pitching moment using linear approximations as follows:

$$C_D(\alpha, q, \delta_e) = C_{Do} + C_{D\alpha}\alpha + C_{Dq}\frac{c}{2V_a}q + C_{D\delta_e}\delta_e \tag{3.51}$$

$$C_M(\alpha, q, \delta_e) = C_{M_o} + C_{M\alpha}\alpha + C_{M_q}\frac{c}{2V_a}q + C_{M_{\delta_e}}\delta_e \tag{3.52}$$

The lift force and drag force are described in the stability frame 3.11. To describe them onto the body frame, the following equation holds true:

$$\begin{bmatrix} f_x \\ 0 \\ f_z \end{bmatrix} = R_s^b(\alpha) \begin{bmatrix} -F_{drag} \\ 0 \\ -F_{lift} \end{bmatrix} \tag{3.53}$$

Where

$$R_s^b(\alpha) = \begin{bmatrix} cos\alpha & 0 & -sin\alpha \\ 0 & 1 & 0 \\ sin\alpha & 0 & cos\alpha \end{bmatrix}$$

The negative sign indicates the NED convention of the body frame.

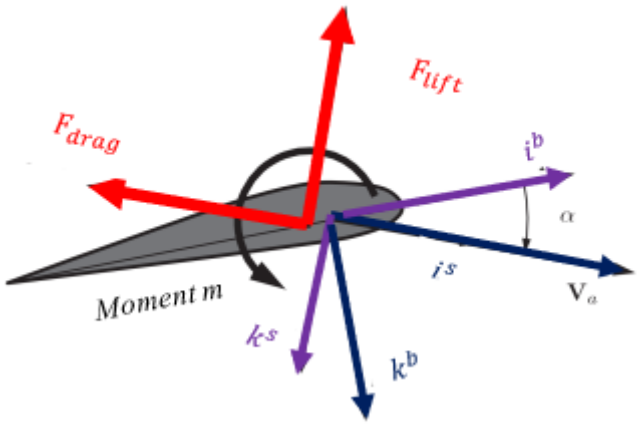

Figure 3.11: Lift and drag forces at the positive directions of the angle of attack

3.5.2.2 Lateral Aerodynamics

The lateral aerodynamic force and moment directly affect the lateral direction along j^b, and also the rolling and yawing moments. They are affected by β, p, r, δ_a, and δ_r as shown in the next expressions:

$$f_y = \frac{1}{2}\rho V_a^2 S C_Y(\beta, p, r, \delta_a, \delta_r) \tag{3.54}$$

$$\mathcal{L} = \frac{1}{2}\rho V_a^2 S b C_l(\beta, p, r, \delta_a, \delta_r) \tag{3.55}$$

$$\mathcal{N} = \frac{1}{2}\rho V_a^2 S b C_n(\beta, p, r, \delta_a, \delta_r) \tag{3.56}$$

When b represents the wing span. By following a similar way to longitudinal aerodynamics, the coefficient of lateral aerodynamics first-order Taylor serious expansion will be expressed as follows:

$$C_Y(\beta, p, r, \delta_a, \delta_r) = C_{Y_o} + C_{Y_\beta}\beta + C_{Y_p}\frac{b}{2V_a}p + C_{Y_r}\frac{b}{2V_a}r + C_{Y_{\delta_a}}\delta_a + C_{Y_{\delta_r}}\delta_r \tag{3.57}$$

$$C_l(\beta, p, r, \delta_a, \delta_r) = C_{l_o} + C_{l_\beta}\beta + C_{l_p}\frac{b}{2V_a}p + C_{l_r}\frac{b}{2V_a}r + C_{l_{\delta_a}}\delta_a + C_{l_{\delta_r}}\delta_r \tag{3.58}$$

$$C_n(\beta, p, r, \delta_a, \delta_r) = C_{n_o} + C_{n_\beta}\beta + C_{n_p}\frac{b}{2V_a}p + C_{n_r}\frac{b}{2V_a}r + C_{n_{\delta_a}}\delta_a + C_{n_{\delta_r}}\delta_r \tag{3.59}$$

This section is generalized with two statements: the first one is that C_{Y_o}, C_{l_o}, and C_{n_o} are zero for aircraft symmetric about $(i^b; k^b)$. Then the other statement is, the coefficients connected to α, β, p, q, and r are referred to as stability derivatives, and those connected to δ_a, δ_e, and δ_r as control derivatives.

3.5.3 Propulsion Force and Moments

There are numerous propeller models in various literature, but the Bernoulli principle may be used to compute the propeller's thrust, providing a clear model that is useful for FWUAV propeller modeling. It is stated as [27]:

$$F_p = S_{prop}\Delta P \tag{3.60}$$

When S_{prop} is the area covered by the propeller and $\Delta P = P_{out} - P_{in}$ where P_{in} is pressure before the propeller and P_{out} is pressure after the propeller. By the principle of Bernoulli

input and output pressure can be expressed as:

$$P_{in} = P_o + \frac{1}{2}\rho V_a^2 \tag{3.61}$$

$$P_{out} = P_o + \frac{1}{2}\rho V_{out}^2 \tag{3.62}$$

when V_{out} is the air velocity at the way out of the propeller. Neglecting transients in the motor, there exists a linear correlation between the pulse-width-modulation command δ_t and the velocity of the propeller. The propeller generates a way out air speed of

$$V_{out} = k_{motor}\delta_t$$

The thrust generated by the motor is:

$$F_{xp} = S_{prop}C_{prop}(P_{out} - P_{in})$$

$$= \frac{1}{2}\rho S_{prop}C_{prop}[(k_{motor}\delta_t)^2 - V_a^2]$$

Then

$$f_p = \frac{1}{2}\rho S_{prop}C_{prop}\begin{bmatrix}(k_{motor}\delta_t)^2 - V_a^2\\ 0\\ 0\end{bmatrix} \tag{3.63}$$

Typically, FWUAVs are designed with thrust applied directly along the i^b body-axis of the aircraft, resulting in no generation of moments about the center of mass.

The thrust force applied to the air passing through the propeller by the rotating UAV propeller advances the air's motion and exerts force on the UAV. The propeller is subject to equal and opposing forces from the air. These forces provide a torque to be felt by the UAV about the propeller axis. The torque that the motor applies to the propeller causes the propeller to provide an equal and opposite torque to the motor that is mounted to the UAV body. The torque generated is proportional to the square of the propeller's angular velocity and is directed in the opposite direction of rotation.

$$T_p = -k_{Tp}(k_\Omega\delta_t)^2 \tag{3.64}$$

When $\Omega = k_\Omega \delta_t$ is propeller speed and k_{Tp} experimentally determined constant [27]. Then the moment generated due to the propulsion is given by:

$$m_p = \begin{bmatrix} -k_{Tp}(k_\Omega \delta_t)^2 \\ 0 \\ 0 \end{bmatrix} \tag{3.65}$$

Generally, the propeller torque has little influence. In the opposite direction of the propeller rotation, the propeller thrust produces a rolling motion. A minor aileron deflection can be applied to successfully negate this effect.

3.5.4 Model Verification

As we know the equations of motion of FWUAV are a fairly complicated set of 12 nonlinear, coupled, first-order, ordinary differential equations. Because of highly coupling nature of FWUAV's dynamics, it is difficult to show how specific input affects their corresponding output(state). Therefore to overcome this problem verifying the model at specific operating conditions (trim point) is necessary. Find the trim point at steady-state flight, the dynamic is decoupled to longitudinal and lateral motion. Then the trim point values are used as an initial value at steady-state flight. Finally, the dynamics are decoupled into longitudinal and lateral motion at steady-state flight. Longitudinal motion components are forward speed u, vertical speed w, pitch angle ϕ, angle of attack α, elevator input δ_e and altitude h. Lateral motion, which includes rudder input δ_r, aileron input δ_a, lateral axis speed v, lateral position y, side sleep angle β, roll angle ϕ, and heading angle ψ. While there is coupling between longitudinal and lateral motion, it is sufficiently small at steady-state flight. The model is trimmed at a steady-state climbing phase with an initial speed of 25 m/s and $10m$ initial height. MATLAB/SIMULINK software is used to find the trim points and verify the model.

Flight Dynamics

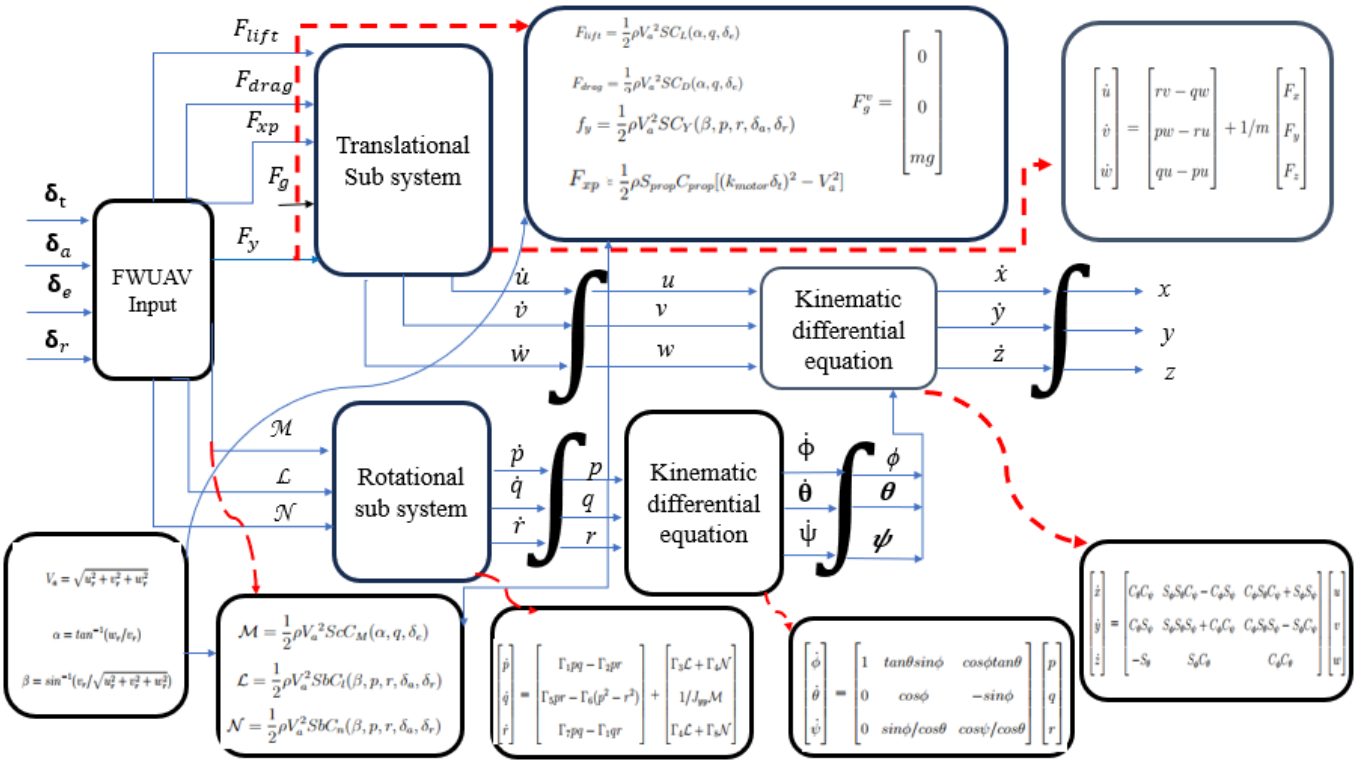

Figure 3.12: FWUAV flight dynamics

3.5.5 Elevator Input kick

A constant -5.7 degree (-0.1 radians) elevator kick was introduced at t=10 *seconds* with no deflection on the aileron and rudder while keeping the throttle input at 33.5% and initial forward velocity 25 m/s for a duration of 40 *seconds*. The elevator kick creates motion along the longitudinal axis. From figure3.13 there is motion along the longitudinal axis alone and the longitudinal axis states change its value when the kick-off starts, there is no motion along lateral-directional motion. From figure 3.13 we can analyze that the forward velocity u, the vertical transnational speed w, pitch angle theta θ, position x and position z change their value after 10 *seconds*, but there is no change in lateral-directional states like roll angle ϕ, yaw angle ψ, vertical speed v and position y. From figure 3.14 we analyze that after kick-off the angle of attack changed its previous value, but the side sleep angle was found at zero value the reason behind here is there is no motion along the lateral direction, and in modeling part we assume that the wind speed is zero.

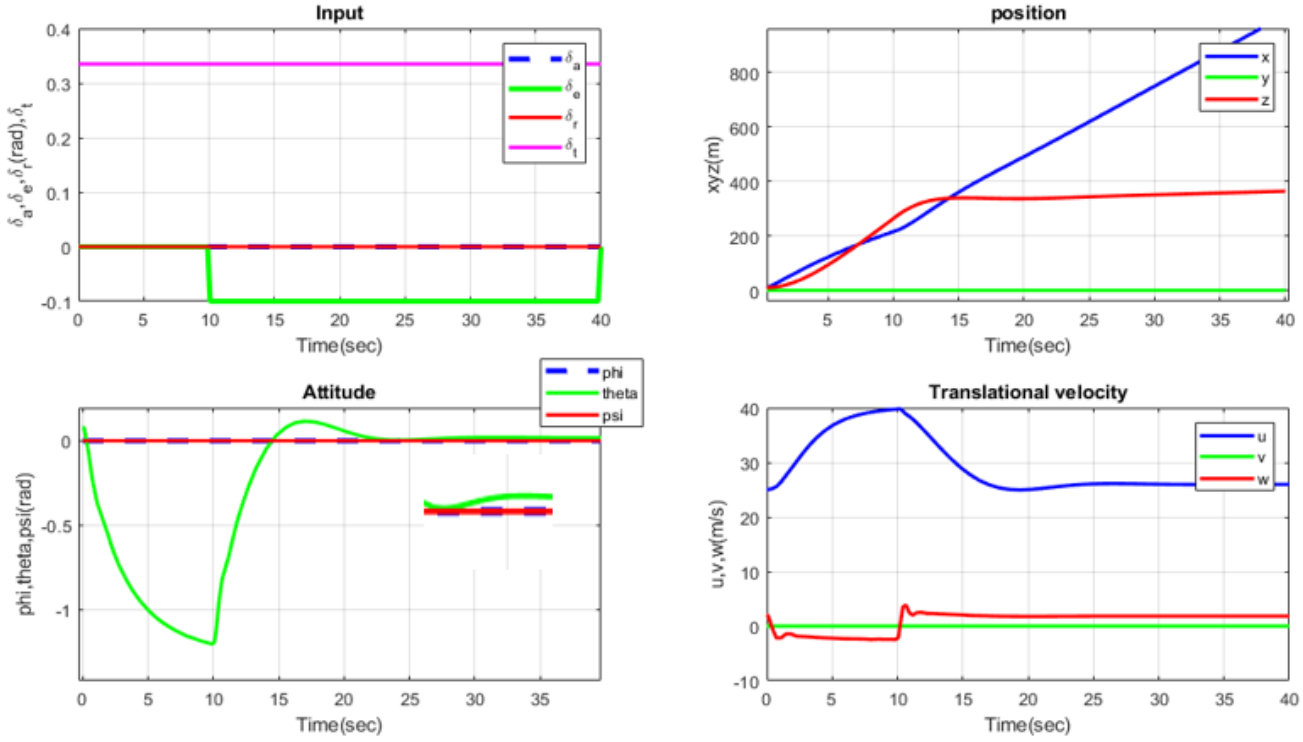

Figure 3.13: Model verification for elevator kick

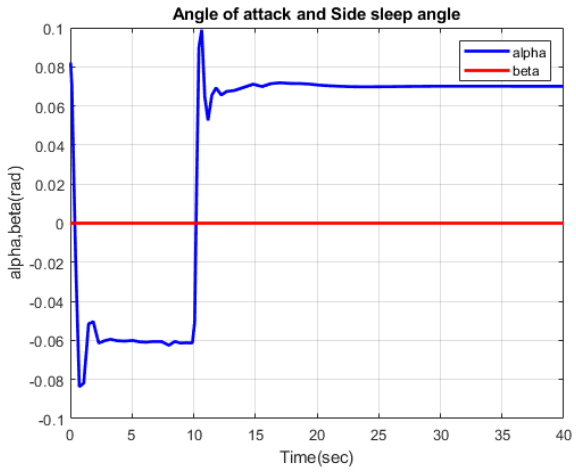

Figure 3.14: Model verification for elevator kick

3.5.6 Rudder Input kick

A constant -11.4 degree (-0.2 radians) rudder kick was introduced from t=10 *seconds* with no deflection on the aileron and elevator while keeping the throttle input at 33.5 % and initial forward velocity 25 m/s for a duration of 40 *seconds*. As we know rudder deflection affects the lateral-direction motion fixed-wing UAV changes its flight direction, but there is a sufficiently small coupling effect that may affect longitudinal motion. From figure 3.15 we analyze that the rudder kick generates lateral motion along y position change its previous value and also the yaw angle ψ and roll angle ϕ change their initial value after 10 *seconds*

but the longitudinal axis state z and pith angle θ attain their previous value after kick-off. Because of the small coupling effect, there is a small change in vertical speed w After kick-off,

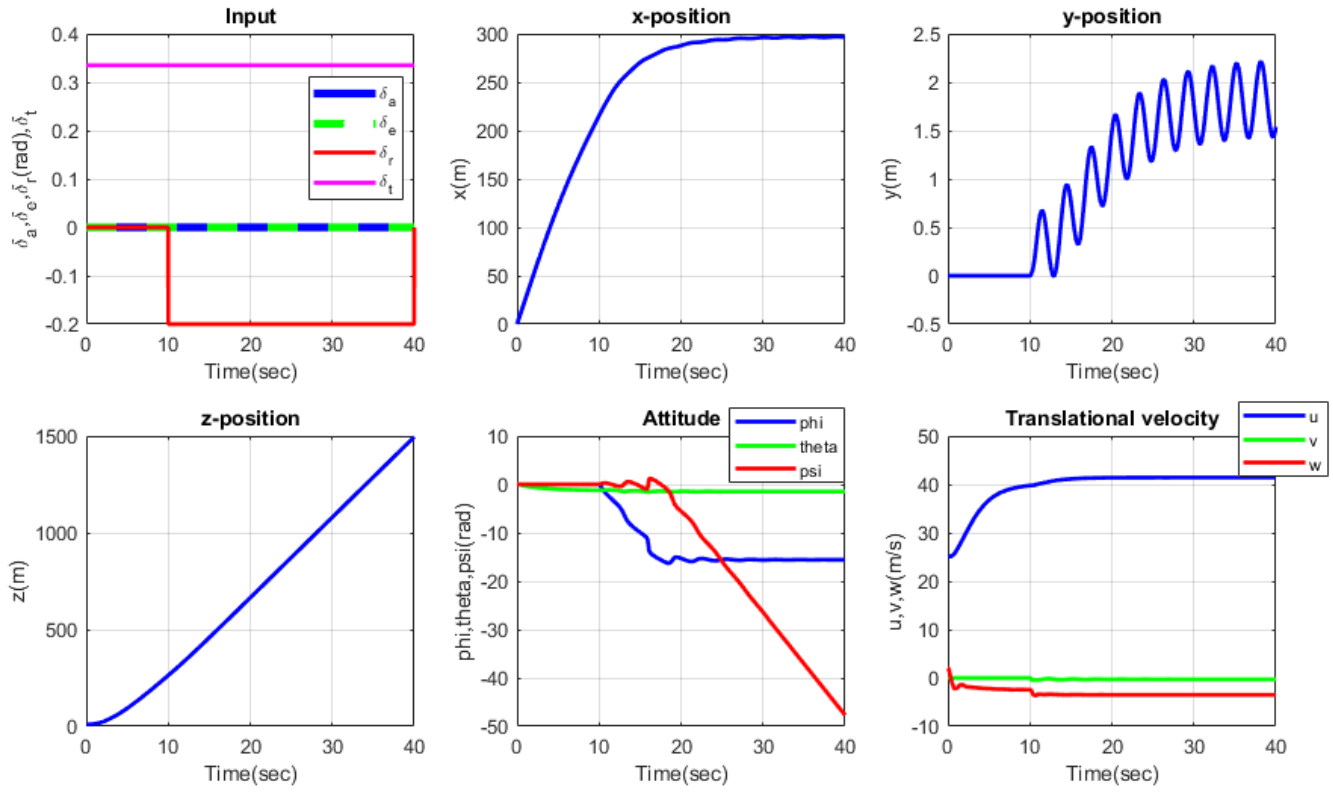

Figure 3.15: Model verification for rudder-kick

the side-sleep angle changes the initial value as shown in the figure3.16. We know that the side-sleep angle β is affected by rudder input. Also, there are very small coupling effects between longitudinal and lateral motion the rudder input affects the angle of attack α has small changes.

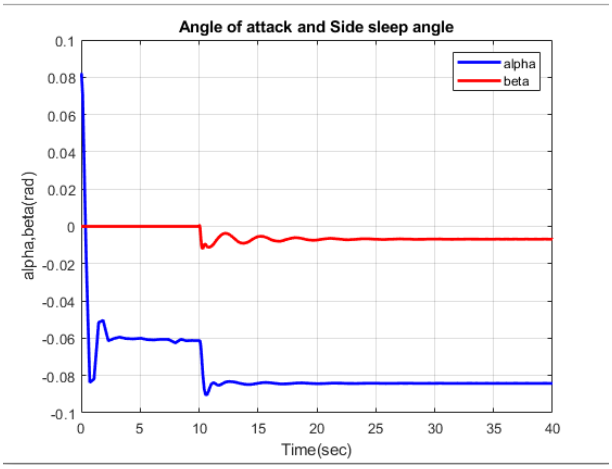

Figure 3.16: Model verification for rudder-kick

3.5.7 Aileron Input kick

A constant -11.4 degree (-0.2 radians) rudder kick was introduced from t=10 *seconds* with no deflection on the aileron and elevator while keeping the throttle input at 33.5% and initial forward velocity 25 m/sec for a duration of 40 *seconds*. The lateral plane is mainly affected by aileron and rudder input in this case we ignore the rudder and elevator input and trigger the aileron input. From figure 3.17 we conclude that the aileron kick affects the lateral motion states.

From figure 3.18 after 10 *seconds* the side sleep angle changes its value to 0.06 *rad* because the aileron input affects the lateral motion but due to the small coupling effect between longitudinal and later motion the angle of attack has also a small change after 10 *seconds*.

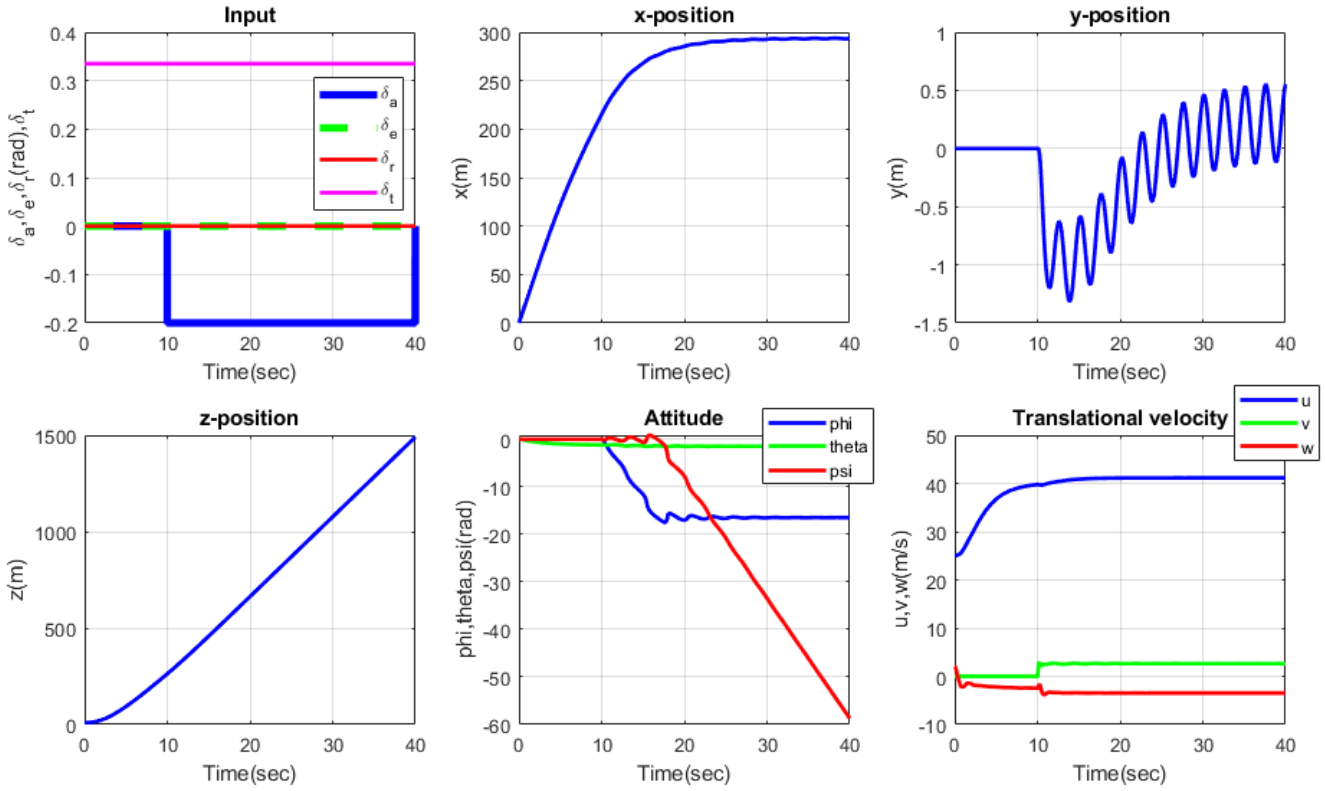

Figure 3.17: Model verification for aileron input

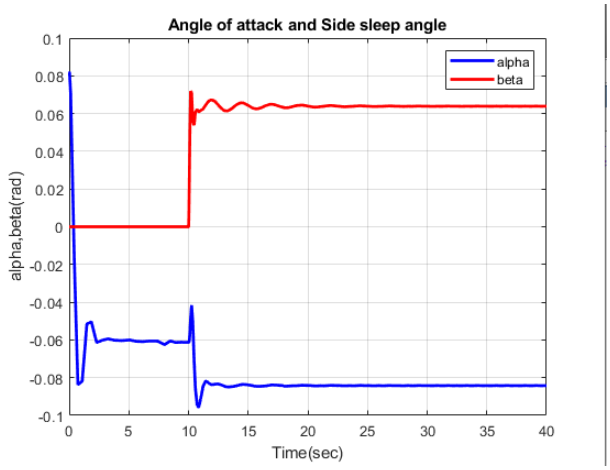

Figure 3.18: Angle of attack and side sleep angle for aileron input

3.6 Decoupling

The primary goal of this thesis is to control the inertial position (x, y, z), and attitude (ϕ, θ, ψ) of FWUAVS. Due to the complex and highly coupled nature of their mathematical models, simplifying the control process is crucial. To achieve this, it is essential to decouple the mathematical models before designing controllers. The decoupling process involves identifying the dominant state variable in the control process and treating the remaining control variables as uncertainties.

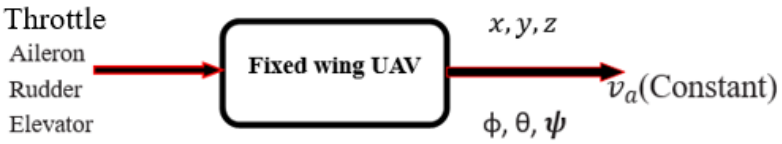

Figure 3.19: control input and controlled state

3.6.1 12-state non-linear equations of motion

$$\begin{aligned}\dot{x} = \; & (cos(\theta)cos(\psi))u + (sin(\phi)sin(\theta)cos(\psi) + cos(\phi)sin(\psi))v \\ & +(cos(\phi)sin(\theta)cos(\psi) + sin(\phi)sin(\psi))w\end{aligned} \tag{3.66}$$

$$\begin{aligned}\dot{y} = \; & (cos(\theta)sin(\psi))u + (sin(\phi)sin(\theta)sin(\psi) + cos(\phi)cos(\psi))v \\ & +(cos(\phi)sin(\theta)sin(\psi) - sin(\phi)cos(\psi))w\end{aligned} \tag{3.67}$$

$$\dot{z} = \quad sin(\theta)u - sin(\phi)cos(\theta)v - cos(\phi)cos(\theta)w \tag{3.68}$$

$$\begin{aligned}\dot{u} = \quad rv - qw - gsin(\theta) + \frac{\rho v_a^2 s}{2m}\left[c_x(\alpha) + c_{x_q}(\alpha)\frac{c}{2v_a}q + c_{x_{\delta e}}(\alpha)\delta_e\right] \\ +\frac{1}{2}\rho S_{prop}C_{prop}((k_{motor}\delta_t)^2 - V_a^2)\end{aligned} \tag{3.69}$$

$$\begin{aligned}\dot{v} = \quad pw - ru - gcos(\theta)sin(\phi) + \frac{\rho v_a^2 s}{2m}\Bigg[C_{y_o} + C_{y_\beta} + c_{Y_p}\frac{b}{2v_a}p + c_{Y_r}\frac{b}{2v_a}r \\ +C_{y_{\delta a}}\delta_a + C_{y_{\delta a}}\delta_a + C_{y_{\delta r}}\delta_r\Bigg]\end{aligned} \tag{3.70}$$

$$\dot{w} = \quad qu - pv + gcos(\theta)cos(\phi) + \frac{\rho v_a^2 s}{2m}\left[C_z(\alpha) + C_{z_q}(\alpha)\frac{c}{2v_a}q + C_{z_\delta e}\delta e\right] \tag{3.71}$$

$$\dot{\phi} = p + qsin(\phi)tan(\theta) + rcos(\phi)tan(\theta) \tag{3.72}$$

$$\dot{\theta} = qcos(\phi) - rsin(\phi) \tag{3.73}$$

$$\dot{\psi} = qsin(\phi)sec(\theta) + rcos(\phi)sec(\theta) \tag{3.74}$$

$$\dot{p} = \Gamma_1 pq - \Gamma_2 qr + \frac{1}{2}\rho v_a^2 sb\left[C_{p_0} + C_{p_\beta}\beta + C_{p_p}\frac{b}{2v_a}p + C_{p_r}\frac{b}{2v_a}r + C_{p_{\delta a}}\delta a + C_{p_{\delta r}}\delta r\right] \tag{3.75}$$

$$\dot{q} = \Gamma_5 pr - \Gamma_6(p^2 - r^2) + \frac{1}{2j_y}\rho v_a^2 sc\left[C_{m_0} + C_{m_\alpha}\alpha + C_{m_q}\frac{c}{2v_a}q + c_{m_{\delta e}}\delta e\right] \tag{3.76}$$

$$\dot{r} = \Gamma_7 pq - \Gamma_1 qr + \frac{1}{2j_y}\rho v_a^2 sb\left[C_{r_0} + C_{r_\beta}\beta + C_{r_p}\frac{b}{2v_a}p + C_{r_r}\frac{b}{2v_a}r + C_{r_{\delta a}}\delta_a + C_{r_{\delta r}}\right] \tag{3.77}$$

3.6.2 Decoupling the state

Roll angle(ϕ)

θ and ϕ will be very small. The dominant state that influence $\dot{\phi}$ is the roll rate p

$$\dot{\phi} = p + qsin(\phi)tan(\theta) + rcos(\phi)tan(\theta) \tag{3.78}$$

$$\dot{\phi} = p + d_{\phi 1} \tag{3.79}$$

and considering $d_{\phi 1}$ as a disturbance and differentiate equation 3.79 then substitute 3.75

$$d_{\phi 1} = qsin(\phi)tan(\theta) + rcos(\phi)tan(\theta) \tag{3.80}$$

$$\ddot{\phi} = \Gamma_1 pq - \Gamma_2 pr + \frac{1}{2}\rho v_a^2 sb\left[C_{p_0} + C_{p_\beta}\beta + C_{p_p}\frac{b}{2v_a}p + C_{p_r}\frac{b}{2v_a} + C_{p_{\delta a}}\delta a + C_{p_{\delta r}}\delta r\right] + d_{\dot{\phi}1} \tag{3.81}$$

$$= \Gamma_1 pq - \Gamma_2 qr + \frac{1}{2}\rho v_a^2 sb\left[C_{p_0} + C_{p_\beta}\beta + C_{p_p}\frac{b}{2v_a}(\dot{\phi} - d_{\phi 1}) + C_{p_r}\frac{b}{2v_a}r + C_{p_{\delta a}}\delta a + C_{p_{\delta r}}\delta r\right] + d_{\dot{\phi}1} \tag{3.82}$$

$$\ddot{\phi} = \frac{1}{2}\rho v_a^2 sbC_{p_p}\frac{b}{2v_a}\dot{\phi} + \frac{1}{2}\rho v_a^2 sbC_{p_{\delta a}}\delta a + \left\{\Gamma_1 pq - \Gamma_2 pr + \frac{1}{2}\rho v_a^2 sb\left[C_{p0} + C_{p_\beta}\beta + C_{p_p}\frac{b}{2v_a}d_{\phi 1} + C_{p_r}\frac{b}{2v_a}r + C_{p_{\delta r}}\delta r\right] + d_{\dot{\phi}1}\right\} \tag{3.83}$$

$$\ddot{\phi} = a_{\phi 1}\phi + a_{\phi 2}\delta a + d_{\phi 2} \tag{3.84}$$

Pitch angle(θ)

The influence of angle ϕ and $\cos\phi - 1$ on the system can be thought of as the disturbance because angle ϕ has a small value during normal flight. The value of q in this case is the main factor affecting a change in θ.

$$\dot{\theta} = q + (cos(\phi) - 1)q - sin(\phi)r = q + d_{\theta 1} \tag{3.85}$$

where $d_{\theta 1}$ assumed to be a disturbance

Take the derivative of equation 3.85 of both sides with respect to time and substitute equation3.76.

$$\ddot{\theta} = \dot{q} + \dot{d_{\theta 1}} = \Gamma_5 pr - \Gamma_6(p^2 - r^2) + \frac{1}{2J_y}\rho v_a^2 sc\left[C_{mo} + C_{m\alpha}\alpha + C_{mq}\frac{c}{2v_a}q + C_{m\delta e}\delta e\right] + \dot{d_{\theta 1}} \tag{3.86}$$

$\alpha = \theta - \gamma$ where γ is climbing angle and α is angle of attack

$$= \Gamma_5 pr - \Gamma_6(p^2 - r^2) + \frac{1}{2J_y}\rho v_a^2 sc\left[C_{mo} + C_{m\alpha}(\theta - \gamma) + C_{mq}\frac{c}{2v_a}(\dot{\theta - d_{\theta 1}}) + C_{m\delta e}\delta e\right] + \dot{d_{\theta 1}} \tag{3.87}$$

$$= \frac{1}{2J_y}\rho v_a^2 scC_{mq}\frac{c}{2v_a}\dot{\theta} + \frac{1}{2J_y}\rho v_a^2 scC_{m\alpha}\theta + \frac{1}{2J_y}\rho v_a^2 scC_{m\delta e}\delta e + \left\{\Gamma_5 pr - \Gamma_6(p^2 - r^2) + \frac{1}{2J_y}\rho v_a^2 sc\left[C_{m0} - C_{m\alpha}\gamma + C_{mq}\frac{c}{2v_a}(-d_\theta)\right] + \dot{d_{\phi 1}}\right\} \tag{3.88}$$

$$\ddot{\theta} = a_{\theta 1}\dot{\theta} + a_{\theta 2}\theta + a_{\theta 3}\delta e + d_{\theta 2} \tag{3.89}$$

yaw angle(ψ)

When a UAV is flying, the values of ψ and θ are very small. The value of ψ is mainly affected by r.

$\sin(\phi)\approx 0$, $\sec(\theta)\approx 1$,$\cos(\phi)\approx 1$

$$\dot{\psi} = qsin(\phi)sec(\theta) + rcos(\phi)sec(\theta) \tag{3.90}$$

$$\dot{\psi} = r + d_{\psi 1} \tag{3.91}$$

where $d_{\psi 1}$ the disturbance to the

Take the derivative of equation 3.91 with respect to time and substitute equation 3.77

$$\ddot{\psi} = \dot{r} + \dot{d_{\psi 1}} \tag{3.92}$$

$$= \Gamma_7 pq - \Gamma_1 qr + \frac{1}{2}\rho v_a^2 sb\left[C_{r_0} + C_{r_\beta}\beta + C_{r_p}\frac{b}{2v_a}p + C_{r_r}\frac{b}{2v_a}r + C_{r_{\delta a}}\delta a + C_{r_{\delta r}}\delta r\right] + \dot{d_{\psi 1}} \tag{3.93}$$

$$= \Gamma_7 pq - \Gamma_1 qr + \frac{1}{2}\rho v_a^2 sb\left[C_{r_0} + C_{r\beta}\beta + C_{r_p}\frac{b}{2v_a}p + C_{r_r}\frac{b}{2v_a}(\dot{\psi} - r) + C_{r_{\delta a}}\delta a + C_{r_{\delta r}}\delta r\right] + \dot{d_{\psi 1}} \tag{3.94}$$

$$= \frac{1}{2}\rho v_a^2 sbC_{r_r}\frac{b}{2v_a}\dot{\psi} + \frac{1}{2}\rho v_a^2 sbC_{r_{\delta r}}\delta r + \left\{\Gamma_7 pq - \Gamma_1 qr + \frac{1}{2}\rho v_a^2 sb\left[C_{r0} + C_{r_\beta}\beta + C_{r_p}\frac{b}{2v_a}p + C_{r_r}\frac{b}{2v_a}(-r) + C_{r_{\delta a}}\delta a\right] + \dot{d_{\psi 1}}\right\}$$

$$\ddot{\psi} = a_{\psi 1}\dot{\psi} + a_{\psi 2}\delta r + d_{\psi 2} \tag{3.95}$$

$$\dot{V_e} = \begin{bmatrix} \ddot{x} \\ \ddot{y} \\ \ddot{z} \end{bmatrix} \tag{3.96}$$

$$m\begin{bmatrix} \ddot{x} \\ \ddot{y} \\ \ddot{z} \end{bmatrix} = \begin{bmatrix} C_\theta C_\psi & S_\phi S_\theta C_\psi - C_\phi S_\psi & C_\phi S_\theta C_\psi + S_\phi S_\psi \\ C_\theta S_\psi & S_\phi S_\theta S_\psi + C_\phi C_\psi & C_\phi S_\theta S_\psi - S_\phi C_\psi \\ -S_\theta & S_\phi C_\theta & C_\phi C_\theta \end{bmatrix}\begin{bmatrix} fp \\ 0 \\ 0 \end{bmatrix} + \begin{bmatrix} 0 \\ 0 \\ mg \end{bmatrix} + \begin{bmatrix} d_x \\ d_y \\ d_z \end{bmatrix} \tag{3.97}$$

$$\begin{bmatrix} d_x \\ d_y \\ d_z \end{bmatrix} = R_b^i f_a^b = R_b^i \begin{bmatrix} f_{ax}^b \\ f_{ay}^b \\ f_{az}^b \end{bmatrix} \tag{3.98}$$

Consider the inertial frame component of aerodynamic force as an uncertainty

After rearranging equation 3.97 yields

$$\ddot{x} = c\theta c\psi \frac{f_p}{m} + \frac{d_x}{m} \tag{3.99}$$

$$\ddot{y} = c\theta s\psi \frac{f_p}{m} + \frac{d_y}{m} \tag{3.100}$$

$$\ddot{z} = -s\theta \frac{f_p}{m} + \frac{d_z}{m} + g \tag{3.101}$$

The six-state decoupled second order equation of motion of fixed-wing UAV

$$\begin{cases} \ddot{\phi} = a_{\phi 1}\phi + a_{\phi 2}\delta a + d_{\phi 2} \\ \ddot{\theta} = a_{\theta 1}\dot{\theta} + a_{\theta 2}\theta + a_{\theta 3}\delta e + d_{\theta 2} \\ \ddot{\psi} = a_{\psi 1}\dot{\psi} + a_{\psi 2}\delta r + d_{\psi 2} \\ \ddot{x} = c\theta c\psi \frac{f_p}{m} + \frac{d_x}{m} \\ \ddot{y} = c\theta s\psi \frac{f_p}{m} + \frac{d_y}{m} \\ \ddot{z} = -s\theta \frac{f_p}{m} + \frac{d_z}{m} + g \end{cases}$$

In the above equation $d_{\phi 2}$, $d_{\theta 2}$, $d_{\psi 2}$, $\frac{d_x}{m}$, $\frac{d_y}{m}$ and $\frac{d_z}{m} + g$ are considered as the uncertainty.

3.6.3 State space representation

$$\ddot{x} = cos(\theta)cos(\psi)\frac{f_p}{m} + \frac{d_x}{m} = U_x + \frac{d_x}{m} \quad where \quad U_x = cos(\theta)cos(\psi)\frac{f_p}{m} \tag{3.102}$$

$$\begin{cases} x_1 = x, x_2 = \dot{x} \\ \dot{x_1} = x_2 \\ \dot{x_2} = U_x + \frac{d_x}{m} \end{cases} \tag{3.103}$$

$$\ddot{y} = cos(\theta)sin(\psi)\frac{f_p}{m} + \frac{d_y}{m} = U_y + \frac{d_y}{m} \quad where \quad U_y = cos(\theta)sin(\psi)\frac{f_p}{m} \tag{3.104}$$

$$\begin{cases} x_3 = y, x_4 = \dot{y} \\ \dot{x_3} = x_4 \\ \dot{x_4} = U_y + \frac{d_y}{m} \end{cases} \tag{3.105}$$

$$\ddot{z} = -sin(\theta)\frac{f_p}{m} + \frac{d_z}{m} + g = U_z + \frac{d_z}{m} + g \quad where \quad U_z = -sin(\theta)\frac{f_p}{m} + g \tag{3.106}$$

$$\begin{cases} x_5 &= z, x_6 = \dot{z} \\ \dot{x_5} &= x_6 \\ \dot{x_6} &= U_z + \frac{d_z}{m} \end{cases} \tag{3.107}$$

$$\ddot{\phi} = a_{\phi 1}\dot{\phi} + a_{\phi 2}\delta_a + d_{\phi 2} \tag{3.108}$$

$$\begin{cases} x_7 = \phi, x_8 = \dot{\phi} \\ \dot{x_7} = x_8 \\ \dot{x_8} = a_{\phi 1}x_8 + a_{\phi 2}\delta_a + d_{\phi 2} \end{cases} \tag{3.109}$$

$$\ddot{\theta} = a_{\theta 1}\dot{\theta} + a_{\theta 2}\theta + a_{\theta 3}\delta_e + d_{\theta 2} \tag{3.110}$$

$$\begin{cases} x_9 = \theta, x_{10} = \dot{\theta} \\ \dot{x_9} = x_{10} \\ \dot{x_{10}} = a_{\theta 1}x_{10} + a_{\theta 2}x_9 + a_{\theta 3}\delta_e + d_{\theta 2} \end{cases} \tag{3.111}$$

$$\ddot{\psi} = a_{\psi 1}\dot{\psi} + a_{\psi 2}\delta_r + d_{\psi 2} \tag{3.112}$$

$$\begin{cases} x_{11} = \psi, x_{12} = \dot{\psi} \\ \dot{x_{11}} = x_{12} \\ \dot{x_{12}} = a_{\phi 1}x_{12} + a_{\phi 2}\delta_r + d_{\phi 2} \end{cases} \tag{3.113}$$

3.7 Actuator Dynamics

In fixed-wing UAVs, the control surfaces are controlled by the motors. The dynamics of Direct Current (DC) brushless servo motors are modeled as a second-order system [32].

$$\frac{\theta(s)}{v(s)} = \frac{k_a k_t}{Js^2} \tag{3.114}$$

where v is the input voltage, k_a and k_l are motor constants, θ is the motor position in this case θ represents the deflection surface δ_a or δ_e or δ_r. However, in practice, we can assume that the dynamics of the motor are relatively fast compared to the dynamics of fixed-wing UAV [33].

Chapter 4

Robust MRAC Design

4.1 Overview

Conventional feedback controllers are poor in handling variations in plant dynamics, imposed non-linearity, and changes in environmental conditions. Modelling errors are also another source of uncertainty. There is a difference between robust and adaptive control algorithms. A robust controller is designed to function under the assumption of worst-case conditions. This controller may use excessive actions to maintain the process. On the contrary, an adaptive controller aims to dynamically estimate process uncertainty in real-time and subsequently generate a control input to predict, counteract, or minimize any undesired deviation from the specified closed-loop plant behavior [34]. Hence, they are designed to learn system uncertainties and counteract their effects online, which leads to the gradual enhancement of the system response during operation.

The development of adaptive control dates back to 1950, there was an extensive research interest in developing advanced autopilots for aircraft that operated over a wide range of flight conditions [35]. Throughout the years, several research have been made on adaptive controllers to ensure acceptable performance of the problem of control of non-linear systems with various uncertainties. Fixed-wing UAVs suffer from parametric and non-parametric uncertainty. Its parameters may be partially known or time-varying. The capability of adaptive controllers to ensure reference tracking in the presence of matched uncertainties makes them an ideal candidate for control systems like aerial vehicles. One area that poses unique challenges for overall stabilizing controllers is the outdoor operation of aerial vehicles. The main goal of adaptive control is to estimate adaptive parameters online and compute a control law in response to variations in the environment and internal parameters.

Elements of MRAC System

1. **Uncertain Plant**

   Adaptive control is applicable to both linear and nonlinear plants that encounter various types of uncertainty, such as unstructured, structured, or unmodeled dynamics.

2. **Reference Model**

   A reference model is employed to define the desired behavior of the closed-loop adaptive control system to an input command. Mostly, a reference model is given in terms of a Linear Time Invariant (LTI) model, but a nonlinear model is also used to formulate a reference model, although it has complexity. To select the reference model we use time domain performance specifications like settling time and overshoot. The selected reference model must be stable.

3. **An adaptation (update) law**

   An adaptive law is a mathematical formulation involving constants, gains, states, and errors. It dictates how adaptive parameters should be adjusted to minimize tracking errors effectively. In standard MRAC, the updated law is expressed as a function of the tracking errors between the reference model state and the plant state.

4. **Controller**

   A fixed-gain controller is designed to ensure overall system performance and stability for a certain plant, serving as a baseline controller. This controller may function as a baseline either fully adaptive or augmented with an adaptive controller, as described in [36].

The objective of the model reference adaptive controller is to make the plant output follow the desired behavior of the reference model. The reference model chosen is based on the second-order performance specification. The poles of the reference model must have a negative eigenvalue to ensure stability. There are two MRAC strategies direct method and indirect method.

Direct adaptive control

Direct adaptive control involves the direct adjustment of a feedback control system within a control system to eliminate uncertainties, enabling the restoration of control system performance in the presence of reasonable system uncertainty [36].

Mathematically direct adaptive controller is given as

$u = k_x(t)x + k_r(t)r$

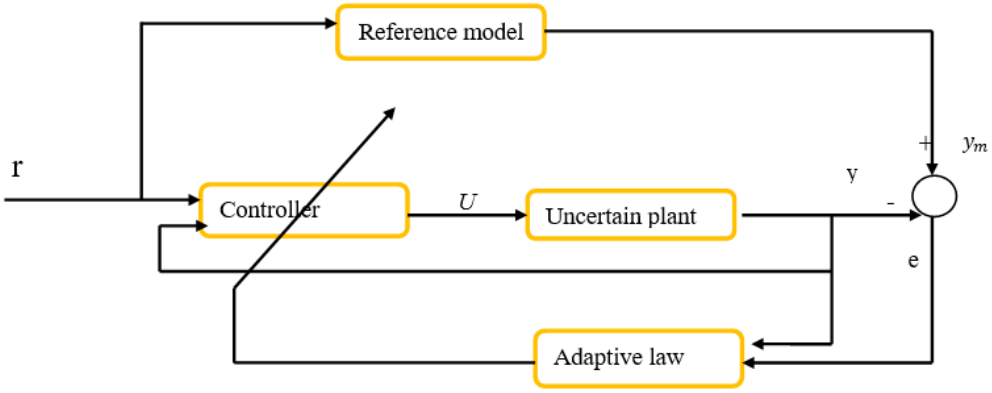

Figure 4.1: Direct MRAC

Indirect adaptive control

In contrast to direct adaptive control, an indirect adaptive controller adjusts the control gains through an indirect approach to attain the same goal, which may be expressed as

$u = k_x(p(t))x + k_r(p(t))r$

Here, the system parameters $p(t)$ are continuously estimated online to facilitate the updating of control gains.

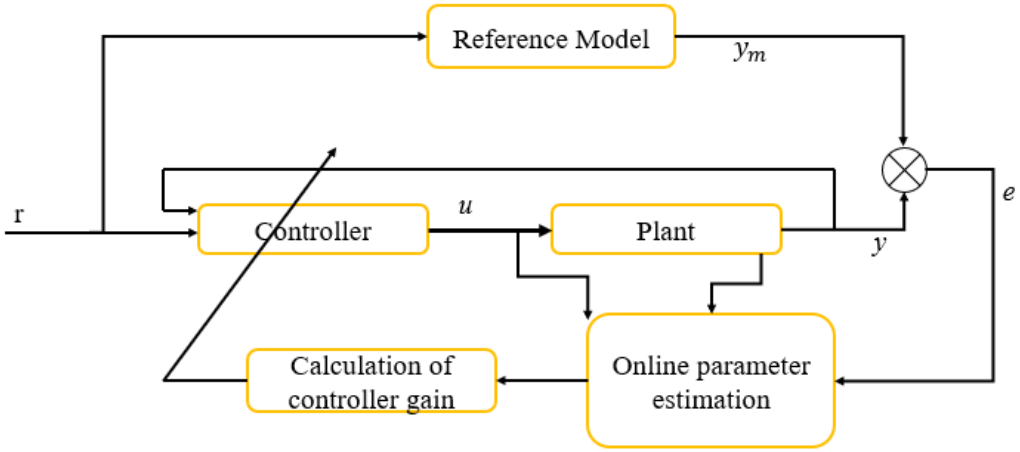

Figure 4.2: Indirect MRAC

4.2 Controller Architecture

Fixed-wing UAVs has six degrees of freedom, which are three rotational and three translational motion. However, the system has four control inputs due to the under-actuated nature of fixed-wing UAV, the control design is to be explicit. The virtual control concept is a common type of control strategy used for controlling under-actuated systems.

The overall control system is designed as the outer(position) and inner(attitude) loop. First, the state feedback model reference adaptive controller is designed for position control. Indirect control x, y, and z positions are achieved through the implementation of the outer loop. The controller inputs of the outer loop namely, U_x,U_y and U_z are provided to determine the desired pitch angle (θ_r) and yaw angle (ψ_r). Second, the inner loop MRACs are designed to track the command input angles θ_r, ψ_r and ϕ_r. The appropriate ϕ_r is set for given trajectories.

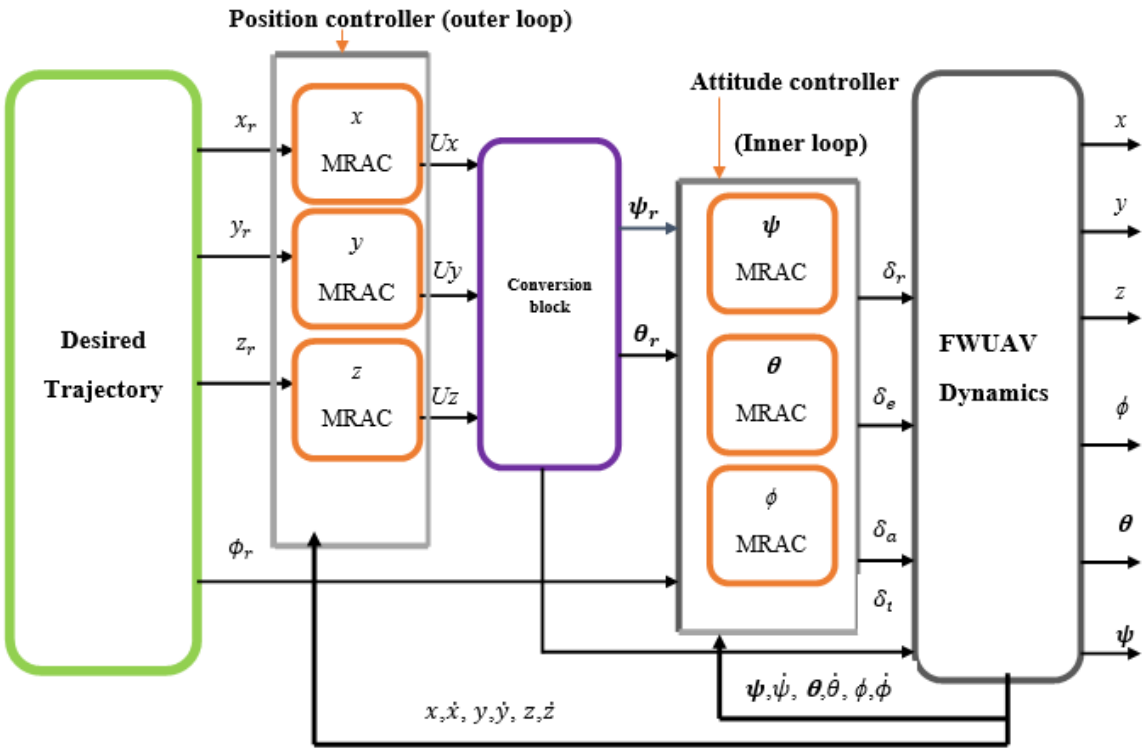

Figure 4.3: Controller Architecture

4.3 Conventional Direct MRAC Design

To design MRAC mathematical tools are used like MIT rule and Lyapunov direct method to develop adaptation rule. To derive adaptation laws using the MIT rule, a cost function is initially defined based on the error. The adaptation laws are then derived by setting

the time derivative of the controller parameters to be the negative of the cost function's gradient. However, the MIT rule is a commonly used and simple method for designing MRAC controllers that typically yield satisfactory results during performance evaluations. It is highly sensitive to changes in the reference input amplitude and cannot ensure global stability within the MRAC system. On the other hand, the Lyapunov direct method is a well-known method that can be applied to ensure the overall stability in the MRAC system [37]. It is based on establishing some positive definite or Lyapunov candidate function of tracking and estimation errors, first, and then adaptation laws are derived in a way that makes the gradient of the candidate Lyapunov function negative. In this way, the candidate Lyapunov function will decrease as time goes forward and derived adaptation laws give bounded asymptotic convergence of control parameters so that the controller can assure global stability of the overall system.

Before starting the design of position MRAC specify the desired behavior of 3D position (x, y,z) in terms of reference model. In this work, similar second-order reference models are chosen for x, y, and z positions. In the MRAC technique, the reference model represents system behavior; and adaptive law forces the plant response to act like the reference model. The error between the plant output and the reference model output is used to adjust the adaptive controller parameters. Direct MRAC system has two loops as shown in the figure 4.1. The inner loop, which consists of a plant and nominal non-adaptive controller, is used to track the set point and stabilize the system in a nominal case. The outer loop consists of an adaptive controller that adjusts controller parameters in such a way that driving reference model response tracking error toward zero. The adjustment mechanism is used to adjust parameters in the control law online by searching parameters that make plant response similar to a reference model. So, it should be designed to guarantee the stability of the control system as well as the convergence of tracking error toward zero [38]. In this thesis fully adaptive controller is designed for both position and attitude.

According to the controller architecture in the figure 4.3 the outer loop controller provides the desired orientation. Hence, for a desired trajectory, the attitude controllers have to make the FWUAV track a desired attitude command. U_x,U_y, and U_z are considered as virtual control, and the relationship between the virtual control input, Euler angle, and propulsion force is given in equation 3.102, 3.104 and 3.106. The desired pitch angle θ_r, the desired yaw

angle ψ_r, and propulsion forces are given by.

$$\theta_r = \arctan(\frac{\cos(\psi_r) * (g - U_z)}{U_x}) \tag{4.1}$$

$$\psi_r = \arctan(\frac{U_y}{U_x}) \tag{4.2}$$

$$f_p = m * \sqrt{U_x^2 + U_y^2 + (U_z - g)^2} \tag{4.3}$$

From equation 3.63 drives the throttle input δ_t, it is a pulse-width-modulation voltage ratio command.

$$\delta_t = \sqrt{\frac{\frac{2fp}{\rho S_{prop} C_{prop}} + V_a^2}{k_{motor}^2}} \tag{4.4}$$

4.3.1 Design Conventional Direct MRAC For Both Position and Attitude

Plant dynamics with matched parametric and unmatched uncertainty are given as

$$\dot{x} = Ax(t) + B(u(t) + \Theta^{*T}\phi(x)) + d(t) \tag{4.5}$$

(A, B) is controllable $x(t) \in \mathbb{R}^n$ is a state vector, A is system matrix $A \in \mathbb{R}^n \mathrm{x} \mathbb{R}^n$, B is input matrix $B \in \mathbb{R}^n \mathrm{x} \mathbb{R}^m$, $U(t) \in \mathbb{R}^m$is a control input, $\Theta^* \in \mathbb{R}^p \mathrm{x} \mathbb{R}^n$ is parametric uncertain matrix, $\phi(x)$ is a known bounded regressor function. The term $\Theta^{*T}\phi(x)$ is a parametric uncertainty, and $d(t)$ is unmatched uncertainty due to disturbance, and it is bounded, but in this work, $d(t)$ represent some part of dynamics and considered as uncertainty [39]. When the adaptation is perfect, the control input can eliminate the parametric uncertainty when it is matched. In this thesis $\phi(x) = x$, when x is the state of the plant ϕ or θ or ψ. The

parametric uncertain matrix and regressor function are expressed as

$$\Theta^* = \begin{bmatrix} \Theta_1 & \Theta_2 & \Theta_3 .... \Theta_p \end{bmatrix}^T \quad \phi(x) = \begin{bmatrix} \phi_1(x) \\ \phi_2(x) \\ \phi_3(x) \\ . \\ \phi_p(x) \end{bmatrix}$$

The reference model which is designed based on the desired performance specification for second order system is given by

$$\dot{x_m} = A_m x_m(t) + B_m r(t) \tag{4.6}$$

Where $x_m(t)$ is a uniformly bounded model reference signal, $r(t)$ is a piecewise continuous bounded reference command signal and A_m is Hurwitz
Then the ideal controller in nominal case

$$u^* = k_x^{*T} x + k_r^* r - \Theta^{*T} \phi(x) \tag{4.7}$$

Where u^* is ideal control input k_x^*, k_r^* and Θ^{*T} are final constant estimated values of controller gains when the plant model output is perfectly track the reference model response. Then substitute equation 4.7 in to 4.5 and compare with 4.6
Model matching condition

$$A + B k_x^{*T} = A_m$$

$$B k_r^* = B_m$$

The design of the full-state feedback adaptive controller is formulated as follows:

$$u_{ad} = k_x(t)^T x(t) + k_r(t) r(t) - \Theta(t)^T \phi(x) \tag{4.8}$$

Here, $k_x(t) \in \mathbb{R}^2$,$k_r(t) \in \mathbb{R}^1$, and $\Theta(t) \in \mathbb{R}^2$ are parameters to be estimated on-line in this case u_{ad} represent u_x or u_y or u_z or δ_a or δ_e or δ_r

Estimation error are given by

$$\hat{k_x} = k_x(t) - k_x^*, \hat{k_r} = k_r(t) - k_r^*, \hat{\Theta} = \Theta(t) - \Theta^* \tag{4.9}$$

Substitute equation 4.8 into the plant model 4.5 and $d(t)$ is neglected. Then the closed-loop dynamics are given by

$$\dot{x} = (A + Bk_x^{*T} + B\hat{k_x}^T)x + (Bk_r^* + B\hat{k_r})r - B\hat{\Theta}^T\phi(x) \tag{4.10}$$

Now compute the closed-loop tracking error and differentiate the error dynamics

$$\dot{e(t)} = \dot{x_m(t)} - \dot{x(t)} = A_m e - B\hat{k_x}^T x - B\hat{k_r} r + B\hat{\Theta}^T\phi(x) \tag{4.11}$$

Now to drive the adaptive law use the Lyapunov direct method and choose the Lyapunov candidate function, it is a positive definite function

$$V(e, \hat{k_x}, \hat{k_r}, \hat{\Theta}) = e^T pe + trace(\hat{k_x}^T\Gamma_x^{-1}\hat{K}_x + \hat{k_r}^T\Gamma_r^{-1}\hat{K}_r + \hat{\Theta}^T\Gamma_\Theta^{-1}\hat{\Theta}) \tag{4.12}$$

Where $\Gamma_x = \Gamma_x^T > 0 \in \mathbb{R}^2 x \mathbb{R}^2$, $\Gamma_r = \Gamma_r^T > 0 \in \mathbb{R}^1 x \mathbb{R}^1$, $\Gamma_\Theta = \Gamma_\Theta^T > 0 \in \mathbb{R}^2 x \mathbb{R}^2$ are known as the adaptation rates matrix for x, r and Θ respectively.

A Lyapunov function $V(e, \hat{k_x}, \hat{k_r}, \hat{\Theta})$ satisfies the following conditions.

- $V(e, \hat{k_x}, \hat{k_r}, \hat{\Theta})>0$
- $V(e, \dot{\hat{k_x}}, \hat{k_r}, \hat{\Theta})\leq 0$

For Hurwitz/asymptotically stable A_m

$$PA_m + A_m^T P = -Q \tag{4.13}$$

Where $P = P^T > 0$ and $Q = Q^T > 0$, the time derivative of V is evaluated along 4.11 trajectory.

$$\begin{aligned}
\dot{V} &= \dot{e^T} Pe + e^T \dot{e} + 2tr(\hat{k_x}^T \Gamma_x^{-1} \dot{\hat{K}}_x + \hat{k_r}^T \Gamma_r^{-1} \dot{\hat{K}}_r + \hat{\Theta}^T \Gamma_\Theta^{-1} \dot{\hat{\Theta}}) \\
&= (A_m e - B\hat{k_x}^T x - B\hat{k_r} r + B\hat{\Theta}^T \phi(x))^T Pe \\
&+ e^T P(A_m e - B\hat{k_x}^T x - B\hat{k_r} r + B\hat{\Theta}^T \phi(x)) \\
&+ 2tr(\hat{k_x}^T \Gamma_x^{-1} \dot{\hat{K}}_x + \hat{k_r}^T \Gamma_r^{-1} \dot{\hat{K}}_r + \hat{\Theta}^T \Gamma_\Theta^{-1} \dot{\hat{\Theta}})
\end{aligned} \tag{4.14}$$

Substitute equation 4.13 into 4.14 yields

$$\begin{aligned}
\dot{V} = -e^T Qe &+ \left[-2e^T PB\hat{k_x^T} x + 2tr(\hat{k_x}^T \Gamma_x^{-1} \dot{\hat{K}}_x) \right] \\
&+ \left[-2e^T PB\hat{k_r^T} r + 2tr(\hat{k_r}^T \Gamma_r^{-1} \dot{\hat{K}}_r) \right] \\
&+ \left[2e^T PB\hat{\Theta^T} \phi(x) + 2tr(\hat{\Theta}^T \Gamma_\Theta^{-1} \dot{\hat{\Theta}}) \right]
\end{aligned} \tag{4.15}$$

Using vector trace identity

$$\begin{aligned}
e^T PB\hat{k_x^T} x &= tr(\hat{k_x^T} x e^T PB) \\
e^T PB\hat{k_r^T} r &= tr(\hat{k_r^T} r e^T PB) \\
e^T PB\hat{\Theta^T} \phi(x) &= tr(\hat{\Theta^T} \phi(x) e^T PB)
\end{aligned} \tag{4.16}$$

Substitute equation 4.16 into 4.15 yields

$$\dot{V} = -e^T Q e + 2tr(\hat{k_x^T}\left[\Gamma_x^{-1}\dot{\hat{K}}_x - xe^T PB\right]) + 2tr(\hat{k_r^T}\left[\Gamma_r^{-1}\dot{\hat{K}}_r - re^T PB\right]) + 2tr(\hat{\Theta^T}\left[\Gamma_\Theta^{-1}\dot{\hat{\Theta}} + \phi(x)e^T PB\right]) \tag{4.17}$$

$\dot{V} = -e^T Q e\dot{V} \leq 0$(globally negative semi-definite). If the adaptive laws are selected as

$$\begin{aligned} \dot{k_x} = \dot{\hat{k_x}} &= \Gamma_x x(t) e^T PB \\ \dot{k_r} = \dot{\hat{k_r}} &= \Gamma_r r(t) e^T PB \\ \dot{\Theta} = \dot{\hat{\Theta}} &= -\Gamma_\Theta \phi(x) e^T PB \end{aligned} \tag{4.18}$$

The error $e(t)$ and the error in adaptive parameter estimation errors $\hat{k_x}$, $\hat{k_r}$ and $\hat{\Theta}$ are uniformly bounded and so are the adaptive parameter estimates $k_x(t)$, $k_r(t)$ and $\Theta(t)$. Since A_m has negative poles and $r(t)$ is bounded, then $x_m(t)$ and $\dot{x_m}(t)$ bounded. Therefore the system state $x(t)$ and $\dot{x(t)}$ are uniformly bounded, and the control input signal in 4.8 is bounded [24]. The adaptive law4.8 utilizes the capability of the system state x to globally asymptotically track the state x_m of the reference model 4.6 ensuring that all signals remain uniformly bounded over time.

Remarks on MRAC

- Direct MRAC 4.8 and 4.6 functions using online measured signals in the system.
- Ensuring that over time, every signal in the closed-loop system stays continuously bounded.
- The reference model state x_m is tracked asymptotically by the plant state x.
- There is no guarantee that the adaptive estimated parameters $\hat{k_x}$, $\hat{k_r}$, and $\hat{\Theta}$ will converge to their real ideal values, k_x^*, k_r^*, and Θ^*, or that they will converge to ideal values in any manner. Just that these signals continue to be uniformly bounded in time is known [40].

4.3.1.1 Selection Reference Model

The reference model should chosen by considering two basic requirements. The first one is, that it should reflect performance specifications in the control tasks in terms of transient

response like settling time, rise time, and maximum overshoot. The second one is, that the reference model should reflect the order, and relative degree of the plant model [38]. Since the reference model sets the desired performance of the closed-loop system for a reference input, it must be chosen properly by checking all the above criteria, which is the basic process in the selection of a reference model for the MRAC system. By considering the above requirement, a reference model is designed as follows
The reference model transfer function is given by

$$x_m = \frac{w_n^2}{s^2 + 2\zeta w_n s + w_n^2} r \tag{4.19}$$

w_n the undamped natural frequency of a second-order system refers to the oscillation frequency of the system in the absence of damping. ζ the damping ratio of a second-order system quantifies the system's resistance to changes in the output, indicating the degree of dampening. w_n and ζ can be determined from second-order specification settling time and overshoot

- **Settling time** is the duration it takes for the response curve to reach and consistently remain within a specified range around the final value, specified by absolute percentage of the final value (usually 2%)

$$t_s = \frac{4}{\zeta w_n} \tag{4.20}$$

- **Maximum Overshoot** represents the highest peak value of the response curve, measured from unity.

$$\%M.O = e^{\frac{-\zeta\pi}{\sqrt{1-\zeta^2}}} \tag{4.21}$$

Position Reference model

The plant's response needs to be fast with little overshoot in order to follow the trajectory accurately. So the position response should converge its final value with 5 *seconds* (settling time) and 5% overshoot, from this specification the computed value of w_n=1.16 and ζ=0.69. The state space model of the reference model is given at 4.6

$$A_m = \begin{bmatrix} 0 & 1 \\ -w_n^2 & -2\zeta w_n \end{bmatrix} = \begin{bmatrix} 0 & 1 \\ -1.3456 & -1.6008 \end{bmatrix} \tag{4.22}$$

$$B_m = \begin{bmatrix} 0 \\ \\ w_n^2 \end{bmatrix} = \begin{bmatrix} 0 \\ \\ 1.3456 \end{bmatrix} \tag{4.23}$$

Now take the second order state space equation of 3.103,3.105 and 3.107 and ignore unmatched uncertainty term, the system matrix A and input matrix B for x, y, and z are expressed as follow

$$A = \begin{bmatrix} 0 & 1 \\ \\ 0 & 0 \end{bmatrix}, B = \begin{bmatrix} 0 \\ \\ 1 \end{bmatrix} \tag{4.24}$$

The input and system matrix for x, y, and z positions are similar

Let's take arbitrary positive definite matrix Q and solve for P from equation4.13

$$Q = \begin{bmatrix} 10 & 0 \\ \\ 0 & 10 \end{bmatrix}, P = \begin{bmatrix} 1.27 & 0.36 \\ \\ 0.36 & 0.5375 \end{bmatrix} \tag{4.25}$$

Attitude Reference Model

In a nested control approach, it is crucial to consider the system's speed or response time. This speed is responsible for determining the system's ability to respond to changing input commands or controlled parameters. To ensure overall closed-loop stability in the nested control architecture, the response time of the inner loop must be faster than that of the outer loop. In cases where servo or tracking systems are involved, the inner loop's response time should be faster than the outer loop's.

Desired Performance specification

Settling time (t_s)<2 *seconds*

$\%M.O$=0

From the above specification compute w_n=2 and ζ=1

$$A_m = \begin{bmatrix} 0 & 1 \\ \\ -w_n^2 & -2\zeta w_n \end{bmatrix} = \begin{bmatrix} 0 & 1 \\ \\ -4 & -4 \end{bmatrix} \tag{4.26}$$

$$B_m = \begin{bmatrix} 0 \\ \\ w_n^2 \end{bmatrix} = \begin{bmatrix} 0 \\ \\ 4 \end{bmatrix} \tag{4.27}$$

Now take the second order position dynamics given by equation 3.109, 3.111 and 3.113 and ignore unmatched uncertainty term, the system matrix A and input matrix B of ϕ,θ,ψ attitude state space are given as follow

Roll angle system and the input matrix

$$A_\phi = \begin{bmatrix} 0 & 1 \\ \\ 0 & a_{\phi 1} \end{bmatrix}, B_\phi = \begin{bmatrix} 0 \\ \\ a_{\phi 2} \end{bmatrix} \tag{4.28}$$

Pitch angle system and input matrix

$$A_\theta = \begin{bmatrix} 0 & 1 \\ \\ a_{\theta 2} & a_{\theta 1} \end{bmatrix}, B_\theta = \begin{bmatrix} 0 \\ \\ a_{\theta 2} \end{bmatrix} \tag{4.29}$$

Yaw angle system and the input matrix

$$A_\psi = \begin{bmatrix} 0 & 1 \\ \\ 0 & a_{\psi 1} \end{bmatrix}, B_\psi = \begin{bmatrix} 0 \\ \\ a_{\psi 2} \end{bmatrix} \tag{4.30}$$

Let's take arbitrary positive definite matrix Q and solve for P from equation4.13

$$Q = \begin{bmatrix} 10 & 0 \\ \\ 0 & 10 \end{bmatrix}, P = \begin{bmatrix} 90/8 & 10/8 \\ \\ 10/8 & 50/32 \end{bmatrix}$$

4.3.2 Uncertainty

It is clear there is a pure kinematic relationship in the equation describing the position of fixed-wing UAVs. Hence there is no parametric uncertainty that appears in position equation 3.99, 3.100, and 3.101. On the other hand, the attitude propagation equation presented in equation 3.109, 3.111, and 3.113 suffer from two main types of uncertainties listed below

- The inertia tensors, which are mostly responsible for the parametric uncertainty in the rotational subsystem, can be represented as a diagonal matrix of I_x, I_y, and I_z.

- The aerodynamic coefficients of forces and moments

4.4 Robust MRAC Design In The Presence of Dynamics($d(t)$)

- **Parameter Drift** is a consequence when an adaptive parameter diverges when the time elapsed in the presence of unmatched uncertainty due disturbance [5] and parameter drift is the result of the lack of a mathematical guarantee of convergence of adaptive parameters. It leads to instability and sudden failure of the system

Consider the plant model given below

$$\dot{x} = Ax(t) + B(u(t) + \Theta^{*T}\phi(x)) + d(t) \tag{4.31}$$

(A, B) is controllable $x(t) \in \mathbb{R}^2$ is a state vector, A is system matrix $A \in \mathbb{R}^2 \mathrm{x} \mathbb{R}^2$, B is input matrix $B \in \mathbb{R}^2 \mathrm{x} \mathbb{R}^1$, $U(t) \in \mathbb{R}^2$is a control input, $\Theta^* \in \mathbb{R}^1$ is parametric uncertain matrix, $\phi(x))$ is a known bounded regressor function.
Assume the system is operating in the presence of uncertainty due to disturbance $d(t) \in (R)^1$

$$||d(t)|| \leq \bar{d} \tag{4.32}$$

Constant upper bound $\bar{d} \geq 0$, and the error dynamics are given as

$$\dot{e(t)} = \dot{x_m(t)} - \dot{x(t)} = A_m e - B\hat{k_x}^T x - B\hat{k_r} r + B\hat{\Theta}^T \phi(x) - d(t) \tag{4.33}$$

A radially unbounded quadratic Lyapunov function candidate is selected in the familiar form

$$V(e, \hat{k_x}, \hat{k_r}, \hat{\Theta}) = e^T pe + trace(\hat{k_x}^T \Gamma_x^{-1} \hat{K_x} + \hat{k_r}^T \Gamma_r^{-1} \hat{K_r} + \hat{\Theta}^T \Gamma_\Theta^{-1} \hat{\Theta}) \tag{4.34}$$

Where $\Gamma_x = \Gamma_x^T > 0 \in \mathbb{R}^2 \mathrm{x} \mathbb{R}^2$,$\Gamma_r = \Gamma_r^T > 0 \in \mathbb{R}^1 \mathrm{x} \mathbb{R}^1$,$\Gamma_\Theta = \Gamma_\Theta^T > 0 \in \mathbb{R}^2 \mathrm{x} \mathbb{R}^2$
Differentiating V, along trajectories of 4.33 , gives

$$\begin{aligned}
\dot{V} &= \dot{e^T} Pe + e^T \dot{e} + 2tr(\hat{k_x}^T \Gamma_x^{-1} \dot{\hat{K}_x} + \hat{k_r}^T \Gamma_r^{-1} \dot{\hat{K}_r} + \hat{\Theta}^T \Gamma_\Theta^{-1} \dot{\hat{\Theta}}) \\
&= (A_m e - B\hat{k_x} x - B\hat{k_r} r + B\hat{\Theta}^T \phi(x))^T Pe \\
&+ e^T P(A_m e - B\hat{k_x}^T x - B\hat{k_r} r + B\hat{\Theta}^T \phi(x)) \\
&+ 2tr(\hat{k_x}^T \Gamma_x^{-1} \dot{\hat{K}_x}^T + \hat{k_r}^T \Gamma_r^{-1} \dot{\hat{K}_r} + \hat{\Theta}^T \Gamma_\Theta^{-1} \dot{\hat{\Theta}}) \\
&- 2e^T Pd(t)
\end{aligned} \tag{4.35}$$

After substituting equation 4.13 and 4.33 into equation 4.35 and applying the vector trace identity we get the following equation.

$$\begin{aligned}\dot{V} = &-e^T Qe + 2tr(\hat{k_x^T}\left[\Gamma_x^{-1}\dot{\hat{K}}_x - xe^T PB\right]) \\ &+ 2tr(\hat{k_r^T}\left[\Gamma_r^{-1}\dot{\hat{K}}_r - re^T PB\right]) \\ &+ 2tr(\hat{\Theta^T}\left[\Gamma_\Theta^{-1}\dot{\hat{\Theta}} + \phi(x)e^T PB\right]) \\ &- 2e^T Pd(t)\end{aligned} \tag{4.36}$$

Suppose that we use the same adaptive update laws as the above subsections, that is,

$$\begin{aligned}\dot{\hat{k_x}} &= \Gamma_x x(t)e^T PB \\ \dot{\hat{k_r}} &= \Gamma_r r(t)e^T PB \\ \dot{\hat{\Theta}} &= -\Gamma_\Theta \phi(x)e^T PB\end{aligned} \tag{4.37}$$

Then

$$\dot{V} = -e^T Qe - 2e^T Pd(t) \tag{4.38}$$

Now determine the upper bound of 4.38

$$\dot{V} \leq -\lambda_{min}(Q)||e||^2 + 2||e||\lambda_{max}(P)\bar{d} \tag{4.39}$$

- Case 1

$$||e|| \geq \frac{2\lambda_{max}(P)}{\lambda_{min}(Q)}\bar{d}$$

In these case $\dot{V}\leq 0$ (Negative semi-definite) ,and also all $V(t)$, $e(t)$, $\hat{k_x}$, $\hat{k_r}$ and $\hat{\Theta}$ are bounded

- Case 2

$$||e|| \leq \frac{2\lambda_{max}(P)}{\lambda_{min}(Q)}\bar{d}$$

In these case $\dot{V} \leq$ some positive number we can not say $V(t)$, $\hat{k_x}$, $\hat{k_r}$ and $\hat{\Theta}$ are bounded. The Lyapunov method does not guarantee the boundedness of the estimation error. As a consequence, the parameter, estimation error can grow unbounded but the tracking error norm remains finite at all times. This phenomenon is called "**Parameter drift**". This argument shows that the conventional MRAC law 4.37 is not robust to bounded disturbances, no matter how small the disturbances are.

4.4.1 Modifications Technique For Robustness

There are many techniques to improve the robustness of MRAC. The techniques are called robust modification techniques. There are two general methods to increase the robustness of MRAC.

1. **Limiting adaptive parameters**

   The projection methods and dead zone are the two frequently used robust modification techniques that limit adaptive parameters. If the tracking error norm decreases beyond a certain value then the dead-zone modification hinders the adaptation process [5]. This method prevents parameter drift caused by noise in adaptive systems. The use of the projection method is quite common in various adaptive control systems. This robustfication technique requires the knowledge of upper bounds on disturbance. A convex set can be established once the bounds have been set. As long as the adaptive parameters stay inside the convex set, this projection technique permits the standard model-reference adaptive control adaption process to continue. The projection approach modifies the adaptation mechanism to bring the adaptive parameters back inside the set when they cross the convex set's boundary.

2. **Adding damping methods in the rules of adaptation**.

   The σ and e modifications are well-known robust modification techniques that add damping mechanisms to limit adaptive parameters, resulting in robustness. In this research, these two techniques are discussed, and the Lyapunov direct stability analysis is provided. The optimal control modification is another modern robust modification technique that also adds damping mechanisms to adaptive update laws. The optimal control modification is developed based on the optimal control theory. The main idea behind optimal control modification is to explicitly seek bounded tracking instead of asymptotic tracking when designing model-reference adaptive control. The formulation of bounded tracking involves minimizing the norm of the tracking error, which is bounded by an unknown lower limit. A trade-off between robustness and bounded tracking performance can be achieved.

4.4.1.1 σ-Modification

The σ robust modification technique was proposed ed by Ioannu and Kokotovic [30]. A number of modification techniques were proposed in the 1980s, among them the σ modification is the simplest modification technique that improve the robustness of uncertain plants. In the σ -modification approach, prior knowledge of the upper bound of disturbance ($\bar{d}$) is not necessary..

The update law with the σ-modification is given as

$$\begin{aligned} \dot{k_x} &= \Gamma_x(x(t)e^T PB - \sigma_x k_x) \\ \dot{k_r} &= \Gamma_r(r(t)e^T PB - \sigma_r k_r) \\ \dot{\Theta} &= -\Gamma_\Theta(\phi(x)e^T PB + \sigma_\Theta \Theta) \end{aligned} \tag{4.40}$$

where σ_x,σ_r and σ_Θ are >0 is the modification parameter. These modification parameters must chosen properly. The larger value of σ_x, σ_r, and σ_Θ increase the tracking errors, but it offers better robustness. There is always a trade-off between robustness and asymptotic tracking. Necessarily σ-modification term adds a constant damping term in the updated law, which provides a technique to bound the adaptive parameters k_x, k_r and Θ. The σ-modification is easy to apply and effective. This modification procedure is commonly employed to guarantee MRAC's robustness. The ideal asymptotic tracking quality of MRAC was no longer retained by the σ-modification procedure.

Lyapunov Stability Analysis

Lyapunov function chosen to be

$$V(e, \hat{k_x}, \hat{k_r}, \hat{\Theta}) = e^T pe + tr(\hat{k_x}^T \Gamma_x^{-1} \hat{K_x} + \hat{k_r}^T \Gamma_r^{-1} \hat{K_r} + \hat{\Theta}^T \Gamma_\Theta^{-1} \hat{\Theta}) \tag{4.41}$$

The derivative tracking error equation is obtained as:

$$\dot{e(t)} = \dot{x_m}(t) - \dot{x(t)} = A_m e - B\hat{k_x}^T x - B\hat{k_r} r + B\hat{\Theta}^T \phi(x) - d(t) \tag{4.42}$$

Differentiating $V(e, \hat{k_x}, \hat{k_r}, \hat{\Theta})$ then substitute equation 4.40 yields

$$\begin{aligned}\dot{V} &= \dot{e^T}Pe + e^T\dot{e} + 2tr(\hat{k_x}^T\Gamma_x^{-1}\dot{\hat{K}_x} + \hat{k_r}^T\Gamma_r^{-1}\dot{\hat{K}_r} + \hat{\Theta}^T\Gamma_\Theta^{-1}\dot{\hat{\Theta}}) \\ &= e^T(A_m^TP + PA_m)e - 2e^TPB\hat{k_x}^Tx \\ &- 2e^TPB\hat{k_r}r + 2e^TPB\hat{\Theta}^T\phi(x) \\ &+ 2tr(\hat{k_x}^T\Gamma_x^{-1}\dot{\hat{K}_x}) + 2tr(\hat{k_r}^T\Gamma_r^{-1}\dot{\hat{K}_r}) + 2tr(\hat{\Theta}^T\Gamma_\Theta^{-1}\dot{\hat{\Theta}}) \\ &- 2e^TPd(t) \end{aligned} \tag{4.43}$$

$$\begin{aligned}\dot{V} &= -e^TQe - 2e^TPB\hat{k_x}^Tx - 2e^TPB\hat{k_r}r + 2e^TPB\hat{\Theta}^T\phi(x) \\ &+ 2tr(\hat{k_x}^T\Gamma_x^{-1}(\Gamma_x(x(t)e^TPB - \sigma_xk_x)) + 2tr(\hat{k_r}^T\Gamma_r^{-1}(\Gamma_r(r(t)e^TPB - \sigma_rk_r)) \\ &+ 2tr(\hat{\Theta}^T\Gamma_\Theta^{-1}(\Gamma_\Theta(\phi(x)e^TPB + \sigma_\Theta\Theta)) - 2e^TPd(t)\end{aligned}$$

$$\begin{aligned}\dot{V} &= -e^TQe \\ &- 2tr(\hat{k_x}^T\sigma_xk_x) - 2tr(\hat{k_r}^T\sigma_rk_r) - 2tr(\hat{\Theta}^T\sigma_\Theta\Theta) - 2e^TPd(t)\end{aligned} \tag{4.44}$$

Substitute equation 4.9 into 4.44

$$\begin{aligned}\dot{V} &= -e^TQe \\ &- 2\sigma_xtr(\hat{k_x}^T\hat{k_x} + \hat{k_x}^Tk_x^*) - 2\sigma_rtr(\hat{k_r}^T\hat{k_x} + \hat{k_r}^Tk_x^*) - 2\sigma_\Theta tr(\hat{\Theta}^T\hat{\Theta} + \hat{\Theta}^T\Theta^*) - 2e^TPd(t)\end{aligned} \tag{4.45}$$

Frobenius norm of a matrix is given as

$$||A||_F^2 \triangleq \sum\sum a_{ij}^2 = trace(A^TA)$$

Further, using the Cauchy-Schwartz inequality

$$|| < A, B >_F || \leq ||A||_F||B||_F \tag{4.46}$$

$$trace(A^TB) \leq |A||_F||B||_F \tag{4.47}$$

By using the above relation express the upper bound of equation 4.45 in Frobenius norm of a matrix form .

The upper bound of $\dot{V}$ is computed as

$$\dot{V} \leq -\lambda_{min}(Q)||e||^2 + 2\lambda_{max}(P)|e||\bar{d} - 2\sigma_x||\hat{k_x}||^2 + 2\sigma_x||\hat{k_x}||k_{x0} \tag{4.48}$$
$$- 2\sigma_r||\hat{k_r}||^2 + 2\sigma_r||\hat{k_r}||k_{r0} - 2\sigma_\Theta||\hat{\Theta}||^2 + 2\sigma_\Theta||\hat{\Theta}||\Theta_0$$

Where k_{x0}=$||k_x^*||$, k_{r0}=$||k_r^*||$, Θ_0=$||\Theta^*||$

We must show that $\dot{V} > 0$ inside a compact set but $\dot{V} < 0$ outside of it in order to demonstrate that the solution is bounded. Completing square of the equation 4.48

$$\dot{V} \leq -\lambda_{min}(Q)\left[||e|| - \frac{\lambda_{max}(P)\bar{d}}{\lambda_{min}(Q)}\right]^2 + \frac{\lambda_{max}^2(P)\bar{d}^2}{\lambda_{min}(Q)} \tag{4.49}$$
$$- 2\sigma_x\left[||\hat{k_x}|| - \frac{k_{x0}}{2}\right]^2 + \frac{\sigma_x k_{x0}^2}{2} - 2\sigma_r\left[||\hat{k_r}|| - \frac{k_{r0}}{2}\right]^2 + \frac{\sigma_r k_{r0}^2}{2}$$
$$- 2\sigma_\Theta\left[||\hat{\Theta}|| - \frac{\Theta_0}{2}\right]^2 + \frac{\sigma_\Theta \Theta_0^2}{2}$$

Thus $\dot{V} \leq 0$

$$|e|| \geq \frac{\lambda_{max}(P)\bar{d}}{\lambda_{min}(Q)} + \sqrt{\frac{\lambda_{max}^2(P)\bar{d}^2}{\lambda_{min}^2(Q)} + \frac{\sigma_\Theta\Theta_0^2}{2\lambda_{min}(Q)} + \frac{\sigma_x k_{x0}^2}{2\lambda_{min}(Q)} + \frac{\sigma_r k_{r0}^2}{2\lambda_{min}(Q)}} \tag{4.50}$$

$$|\hat{k_x}|| \geq \frac{k_{x0}}{2} + \sqrt{\frac{\lambda_{max}^2(P)\bar{d}^2}{2\lambda_{min}^2(Q)\sigma_x} + \frac{\sigma_\Theta\Theta_0^2}{4\sigma_x} + \frac{k_{x0}^2}{4} + \frac{\sigma_r k_{r0}^2}{4\sigma_x}} \tag{4.51}$$

$$|\hat{k_r}|| \geq \frac{k_{r0}}{2} + \sqrt{\frac{\lambda_{max}^2(P)\bar{d}^2}{2\lambda_{min}^2(Q)\sigma_r} + \frac{\sigma_\Theta\Theta_0^2}{4\sigma_r} + \frac{k_{r0}^2}{4} + \frac{\sigma_x k_{r0}^2}{4\sigma_r}} \tag{4.52}$$

$$|\hat{\Theta}|| \geq \frac{\Theta_0}{2} + \sqrt{\frac{\lambda_{max}^2(P)\bar{d}^2}{2\lambda_{min}^2(Q)\sigma_\Theta} + \frac{\Theta_0^2}{4} + \frac{\sigma_x k_{x0}^2}{4\sigma_\Theta} + \frac{\sigma_r k_{r0}^2}{4\sigma_\Theta}} \tag{4.53}$$

$\dot{V} \leq 0$ outside a compact set $\mathscr{L}$

$$\mathscr{L} = \Bigg((\|e\|, \|\hat{k_x}\|, \|\hat{k_r}\|, \|\hat{\Theta}\|) : \lambda_{min}(Q)\left[||e|| - \frac{\lambda_{max}(P)\bar{d}}{\lambda_{min}(Q)}\right]^2$$
$$+ 2\sigma_x\left[||\hat{k_x}|| - \frac{k_{x0}}{2}\right]^2 + 2\sigma_r\left[||\hat{k_r}|| - \frac{k_{r0}}{2}\right]^2$$
$$+ 2\sigma_\Theta\left[||\hat{\Theta}|| - \frac{\Theta_0}{2}\right]^2 \leq \frac{\lambda_{max}^2(P)\bar{d}^2}{\lambda_{min}(Q)} + \frac{\sigma_x k_{x0}^2}{2} + \frac{\sigma_r k_{r0}^2}{2} + \frac{\sigma_\Theta \Theta 0}{2} \Bigg)$$

Therefore, the solution exhibits uniform ultimate boundedness with the ultimate bounds. We can state that the σ-modification term causes an increase in the bound on the tracking error. This is due to the trade-off between asymptotic tracking performance and robustness. Also, we observe that if σ_x=0, σ_r=0 and σ_Θ=0, then the conventional MRAC is restorted

and $\|\hat{k_x}\|$, $\|\hat{k_r}\|$,and$\|\hat{\Theta}\|$ is bounded if $\bar{d}$ is not presented.

4.4.1.2 *e*- Modification

The *e*-modification is also another famous robust modification method, proposed by Narendra and Annaswammy [41]. There are performance-related problems with applying the σ-modification. This technique is proposed to improve a limitation of asymptotic tracking with the σ modification in that it can achieve asymptotic tracking rather than σ under specific conditions while improving robustness. When the error is small, one of the adaptive update law dynamics in equation 4.40 can be approximately expressed as $\dot{\hat{k}_x}$=$-\Gamma_x\sigma_x\hat{k_x}$. Even if the tracking error becomes small, the damping term does not have a tendency to return to the origin, because it does not depend on the error. Furthermore, the disturbance is absent from the plant equation 4.5, and if the reference command $r(t)$ is persistently exciting , the parameter estimation error $\Delta k_x(t)$ do not converge to the origin. Therefore to handle this undesirable effect *e*-modification was proposed. *e*-modification reduces the damping term proportional to the norm of the tracking error as shown in equation 4.54. In the ideal scenario with Model-Reference Adaptive Control (MRAC), as the tracking error gets closer to zero, the damping term decreases, which restores the asymptotic tracking property of MRAC. However, bounded tracking is achieved by *e* modification as demonstrated by the Lyapunov stability study. It is no longer possible to maintain MRAC's ideal asymptotic tracking property in all circumstances. Therefore, more robustness cannot generally improve asymptotic tracking performance. This is due to a trade-off between tracking performance and robustness of *e*-modification.
The update laws are expressed as

$$\begin{aligned}
\dot{\hat{k_x}} &= \Gamma_x(x(t)e^TPB - \mu_x\|e^TPB\|k_x) \\
\dot{\hat{k_r}} &= \Gamma_r(r(t)e^TPB - \mu_r\|e^TPB\|k_r) \\
\dot{\hat{\Theta}} &= -\Gamma_\Theta(\phi(x)e^TPB + \mu_\Theta\|e^TPB\|\Theta)
\end{aligned} \tag{4.54}$$

Where μ_x, μ_r and μ_Θ> 0 is the modification parameter.
The significance of using an error-dependent damping is that it goes to zero, as the tracking error decreases. As we can see from equation 4.54, the *e*-modification adds a tracking error-dependent damping $\|e^TPB\|$ to the adaptive laws.

Lyapunov Stability Analysis

select Lyapunov function 4.41 and use error dynamics 4.33

$$V(e,\hat{k_x},\hat{k_r},\hat{\Theta}) = e^T pe + trace(\hat{k_x}^T\Gamma_x^{-1}\hat{K}_x + \hat{k_r}^T\Gamma_r^{-1}\hat{K_r} + \hat{\Theta}^T\Gamma_\Theta^{-1}\hat{\Theta})$$

$$\dot{e(t)} = \dot{x_m}(t) - \dot{x(t)} = A_m e - B\hat{k_x}^T x - B\hat{k_r} r + B\hat{\Theta}^T\phi(x) - d(t)$$

Now differentiate $\dot{V}$ along error dynamics trajectory 4.33 and substitute equation 4.54 yields

$$\begin{aligned}\dot{V} &= -e^TQe \\ &\quad - 2tr(\hat{k_x}^T\mu_x\|e^TPB\|k_x) - 2tr(\hat{k_r}^T\mu_r\|e^TPB\|k_r) \\ &\quad - 2tr(\hat{\Theta}^T\mu_\Theta\|e^TPB\|\Theta) - 2e^TPd(t)\end{aligned} \tag{4.55}$$

$$\begin{aligned}\dot{V} &= -e^TQe \\ &\quad - 2\mu_x\|e^TPB\|tr(\hat{k_x}^Tk_x) - 2\mu_r\|e^TPB\|tr(\hat{k_r}^Tk_r) \\ &\quad - 2\mu_\Theta\|e^TPB\|tr(\hat{\Theta}^T\Theta) - 2e^TPd(t)\end{aligned} \tag{4.56}$$

Substitute equation 4.9 into 4.56

$$\begin{aligned}\dot{V} &= -e^TQe \\ &\quad - 2\mu_x\|e^TPB\|tr(\hat{k_x}^T\hat{k_x}) + \hat{k_x}^Tk_x^*) - 2\mu_r\|e^TPB\|tr(\hat{k_r}^T\hat{k_r}) + \hat{k_r}^Tk_r^*) \\ &\quad - 2\mu_\Theta\|e^TPB\|tr(\hat{\Theta}^T\hat{\Theta} + \hat{\Theta}^T\Theta^*) - 2e^TPd(t)\end{aligned} \tag{4.57}$$

By using the Frobenius norm of a matrix we can determine the upper bound of $\dot{V}$

$$\begin{aligned}\dot{V} &\le -\lambda_{min}(Q)||e||^2 + 2\lambda_{max}(P)|e||\bar{d} - 2\mu_x\|e\|\|PB\|\|\hat{k_x}||^2 + 2\mu_x\|e\|\|PB\|\|\hat{k_x}||k_{x0} \\ &\quad - 2\mu_r\|e\|\|PB\|\|\hat{k_r}||^2 + 2\mu_r\|e\|\|PB\|\|\hat{k_r}||k_{r0} \\ &\quad - 2\mu_\Theta\|e\|\|PB\|\|\hat{\Theta}||^2 + 2\mu_\Theta\|e\|\|PB\|\|\hat{\Theta}||\Theta_0\end{aligned} \tag{4.58}$$

Where k_{x0}=$||k_x^*||$, k_{r0}=$||k_r^*||$, Θ_0=$||\Theta^*||$

To determine the maximum lower bound of $\|e\|$ the objective is to maximize the bound on $\dot{V}$ by taking partial derivatives with respect to $\dot{V}$ with respect to $\|\hat{k_x}\|$, $\|\hat{k_r}\|$ and $\|\hat{k_x}\|$ and setting it equal to zero yields

$$\begin{aligned}&- 4\mu_x\|e\|\|PB\|\|\hat{k_x}\| + 2\mu_x\|e\|\|PB\|k_{x0} - 4\mu_r\|e\|\|PB\|\|\hat{k_r}\| + 2\mu_r\|e\|\|PB\|k_{r0} \\ &- 4\mu_\Theta\|e\|\|PB\|\|\hat{\Theta}\| + 2\mu_\Theta\|e\|\|PB\|\Theta_0 = 0\end{aligned}$$

Solving for $\hat{k_x}$, $\hat{k_r}$ and $\hat{\Theta}$ that maximize $\dot{V}$ gives $\hat{k_x}=\frac{k_{x0}^2}{2}$, $\hat{k_r}=\frac{k_{r0}^2}{2}$,$\hat{\Theta}=\frac{\Theta_0^2}{2}$
Then

$$\dot{V} \leq -\lambda_{min}(Q)||e||^2 + 2\lambda_{max}(P)|e||\bar{d} + \frac{\mu_x\|e\|\|PB\|k_{x0}^2}{2} + \frac{\mu_r\|e\|\|PB\|k_{r0}^2}{2} + \frac{\mu_\Theta\|e\|\|PB\|\Theta_0^2}{2}$$

$\dot{V}\leq 0$ if

$$\|e\| \geq \frac{4\lambda_{max}(P)|\bar{d} + \mu_x\|PB\|k_{x0}^2 + \mu_r\|PB\|k_{r0}^2 + \mu_\Theta\|PB\|\Theta_0^2}{2\lambda_{min}(Q)} = p$$

And also $\dot{V}$ is bounded by

$$\begin{aligned}\dot{V} \leq\ & 2\lambda_{max}(P)|e||\bar{d} - 2\mu_x\|e\|\|PB\|\|\hat{k_x}||^2 + 2\mu_x\|e\|\|PB\|\|\hat{k_x}||k_{x0} \\ & - 2\mu_r\|e\|\|PB\|\|\hat{k_r}||^2 + 2\mu_r\|e\|\|PB\|\|\hat{k_r}||k_{r0} \\ & - 2\mu_\Theta\|e\|\|PB\|\|\hat{\Theta}||^2 + 2\mu_\Theta\|e\|\|PB\|\|\hat{\Theta}||\Theta_0\end{aligned}$$

$$\|\hat{k_x}\| \geq \frac{k_{x0}}{2} + \sqrt{\frac{k_{x0}^2}{4} + \frac{k_{r0}^2}{4} + \frac{\Theta_0^2}{4} + \frac{\lambda_{max}(P)\bar{d}}{\mu_x\|PB\|}} = \alpha$$

$$\|\hat{k_r}\| \geq \frac{k_{x0}}{2} + \sqrt{\frac{k_{x0}^2}{4} + \frac{k_{r0}^2}{4} + \frac{\Theta_0^2}{4} + \frac{\lambda_{max}(P)\bar{d}}{\mu_r\|PB\|}} = \beta$$

$$\|\hat{\Theta}\| \geq \frac{k_{x0}}{2} + \sqrt{\frac{k_{x0}^2}{4} + \frac{k_{r0}^2}{4} + \frac{\Theta_0^2}{4} + \frac{\lambda_{max}(P)\bar{d}}{\mu_\Theta\|PB\|}} = \gamma$$

Therefore $\dot{V}\leq 0$ outside a compact set $\mathscr{L}$

$$\mathscr{L} = \left\{(\|e\|, \|\hat{k_x}\|, \|\hat{k_r}\|, \|\hat{\Theta}\|) : \|e\| < p, \|\hat{k_x}\| < \alpha, \|\hat{k_r}\| < \beta, \|\hat{\Theta}\| < \gamma\right\}$$

Therefore $\|e\|, \|\hat{k_x}\|, \|\hat{k_r}\|, \|\hat{\Theta}\|$ are bounded.

4.4.1.3 Optimal Control Modification

In fact, robust adaptive control ensures robustness by making trade-offs that compromise the ideal asymptotic tracking property of Model Reference Adaptive Control (MRAC). The optimal control modification method is another robust modification method that bounds adaptive parameters and addresses adaptive control in the context of optimal control. This modification method is designed to minimize the tracking error norm by not allowing the tendency of the tracking error to the origin, and the robustness of the controller increase. The tracking error is bounded away from the origin by an unknown lower bound Δ. The

optimal control modification is derived from optimal control theory, serving as an adaptive optimal control approach.

The adaptive control update law is given by

$$\begin{aligned}\dot{\hat{k}_x} &= \Gamma_x x(e^T P + v_x x(t)^T k_x B^T P A_m^{-1})B \\ \dot{\hat{k}_r} &= \Gamma_r r(t)(e^T P + v_r r(t)^T k_r B^T P A_m^{-1})B \\ \dot{\hat{\Theta}} &= -\Gamma_\Theta \phi(x)(e^T PB - v_\Theta \phi(x)^T \Theta B^T P A_m^{-1})B \end{aligned} \tag{4.59}$$

where $v_x, v_y, v_\Theta > 0$ is the modification parameter. If the tracking performance is more desired in a control design than robustness, then a smaller value of v should be chosen. If robustness is more desired in a control design than tracking performance, then v could be selected to be a large value

Derivation of optimal control

In this section drive the update law for $\Theta(t)$. By using the same procedure We can also drive the updated law for $k(t)_x$ and $k(t)_r$. The optimal control modification minimizes the $\mathscr{L}_2$ of the tracking error with the cost function [42].

$$J = \lim_{t_f \to \infty} \frac{1}{2} \int_0^{t_f} (e - \Delta)^T Q (e - \Delta)\, dt \tag{4.60}$$

Δ represent a lower bound of tracking error. The error dynamics is given at equation 4.33.

$$\dot{e(t)} = \dot{x_m(t)} - \dot{x(t)} = A_m e + B\hat{\Theta}^T \phi(x) - d(t)$$

Now define the Hamiltonian function(it is a function of tracking error and estimation error)given as

$$H(e, \hat{\theta}) = \frac{1}{2}(e - \Delta)^T Q (e - \Delta) + \lambda^T (A_m e + B\hat{\Theta}^T \phi(x) - d(t)) \tag{4.61}$$

Here, consider $\lambda(t) \in \mathbb{R}$ as adjoint vector.

Differentiate the λ

$$\dot{\lambda} = -\nabla H_e^T = -Q(e - \Delta) - A_m^T \lambda \tag{4.62}$$

The transversality condition $\lambda(t_f \to \infty)$=0. Now, $\hat{\Theta(t)}$ is Considered as a control variable, the necessary condition is given as

$$\nabla H_{\hat{\Theta}}^T = \phi(x)\lambda^T B \tag{4.63}$$

Adaptive update can expressed by the gradient update law as

$$\dot{\hat{\Theta}} = -\Gamma_\Theta \nabla H_{\hat{\Theta}}^T = -\Gamma_\Theta \phi(x)\lambda^T B \tag{4.64}$$

The above equation 4.64 is dependent upon the adjoint vector λ. To substitute λ, use the sweep method.

Assume the adjoint equation.

$$\lambda = Pe + S\Theta^T \phi(x) \tag{4.65}$$

Substitute equation 4.65 into equation 4.62 yields

$$\dot{P}e + P(A_m e + B(\Theta - \Theta^*)^T\phi(x) - d(t)) + \dot{S}\Theta^T\phi(x) + S\frac{d}{dt}(\Theta^T\phi(x)) = -Q(e-\Delta) - A_m^T(Pe + S\Theta^T\phi(x))$$

Collecting the equation containing $e(t)$

$$\dot{P} + PA_m + A_m^T P + Q = 0 \tag{4.66}$$

When collecting $\Theta^T\phi(x)$ yields

$$\dot{S} + A_m^T S + PB = 0 \tag{4.67}$$

Collecting the remaining term resultst in

$$Q\Delta + PB\Theta^*\phi(x) + Pd - S\frac{d}{dt}(\Theta^T\phi(x)) = 0 \tag{4.68}$$

Equation 4.68 illustrates how the parametric uncertainty Θ^* and the disturbance d affect the tracking error lower bound Δ. The lower bound will exist and be finite because of finite disturbance and uncertainty. Therefore, the error bounded away from the origin by Δ.

At t=0 equation 4.66 and 4.67 tends to their constant solution which are expressed as

$$PA_m + A_m^T P + Q = 0 \tag{4.69}$$

$$A_m^T S + PB = 0 \tag{4.70}$$

Equation 4.69 is the known Lyapunov equation in MARC. The solution to equation 4.70 is given by

$$S = -A_m^T PB \tag{4.71}$$

The adjoint equation is obtained as

$$\lambda = Pe - A_m^T PB\Theta^T \phi(x) \tag{4.72}$$

Substitute equation 4.71 into 4.64 yields optimal modification update law

$$\dot{\hat{\Theta}} = -\Gamma_\Theta \phi(x)(e^T PB - \phi(x)^T \Theta B^T P A_m^{-1})B \tag{4.73}$$

The first term is conventional MRAC and the second expression represents the damping term. To make the optimal control adaptive law more flexible a modification term v_θ is introduced as a modification term.

Now S is given by

$$S = -v_\theta A_m^T PB \tag{4.74}$$

The final expression of the optimal control modification is provided by:

$$\dot{\hat{\Theta}} = -\Gamma_\Theta \phi(x)(e^T PB - v_\Theta \phi(x)^T \Theta B^T P A_m^{-1})B \tag{4.75}$$

We use a similar procedure to drive adaptive law for $\hat{k_x}$ and $\hat{k_r}$.

Lyapunov Stability Analysis

Proof select a Lyapunov function 4.41

$$V(e, \hat{k_x}, \hat{k_r}, \hat{\Theta}) = e^T pe + trace(\hat{k_x}^T \Gamma_x^{-1} \hat{K_x} + \hat{k_r}^T \Gamma_r^{-1} \hat{K_r} + \hat{\Theta}^T \Gamma_\Theta^{-1} \hat{\Theta})$$

The tracking error dynamics is obtained as 4.33:

$$\dot{e(t)} = \dot{x_m(t)} - \dot{x(t)} = A_m e - B\hat{k_x}^T x - B\hat{k_r} r + B\hat{\Theta}^T \phi(x) - d(t)$$

Differentiating $V(e, \hat{k_x}, \hat{k_r}, \hat{\Theta})$ along error dynamics then substitute 4.59 yields

$$\dot{V} = -e^T Qe - 2e^T PB\hat{k_x}^T x - 2e^T PB\hat{k_r} r + 2e^T PB\hat{\Theta}^T \phi(x)$$
$$+ 2tr(\hat{k_x}^T \Gamma_x^{-1}(\Gamma_x x(e^T P + v_x x(t)^T k_x B^T P A_m^{-1})B)$$
$$+ 2tr(\hat{k_r}^T \Gamma_r^{-1}(\Gamma_r r(t)(e^T P + v_r r(t)^T k_r B^T P A_m^{-1})B)$$
$$+ 2tr(\hat{\Theta}^T \Gamma_\Theta^{-1}(-\Gamma_\Theta \phi(x)(e^T PB - v_\Theta \phi(x)^T \Theta B^T P A_m^{-1})B) - 2e^T Pd(t)$$

Applying the vector trace identity

$$trace(a^T b) = ba^T$$

$$\dot{V} = -e^T Qe - 2e^T Pd(t) + 2v_x x(t)^T k_x B^T P A_m^{-1} B\hat{k_x^T} x$$
$$+ 2v_r r(t)^T k_r B^T P A_m^{-1} B\hat{k_r^T} r + 2v_\Theta \phi(x)^T \Theta B^T P A_m^{-1} B\hat{\Theta^T} \phi(x) \tag{4.76}$$

Now substitute equation 4.9 into 4.76

$$\dot{V} = -e^T Qe - 2e^T Pd(t) + 2v_x x(t)^T \hat{k_x} B^T P A_m^{-1} B\hat{k_x^T} x + 2v_x x(t)^T k_x^* B^T P A_m^{-1} B\hat{k_x^T} x$$
$$+ 2v_r r(t)^T \hat{k_r} B^T P A_m^{-1} B\hat{k_r^T} r + 2v_r r(t)^T k_r^* B^T P A_m^{-1} B\hat{k_r^T} r + 2v_\Theta \phi(x)^T \hat{\Theta} B^T P A_m^{-1} B\hat{\Theta^T} \phi(x)$$
$$+ 2v_\Theta \phi(x)^T \Theta^* B^T P A_m^{-1} B\hat{\Theta^T} \phi(x)$$

But

$$2v_x x(t)^T \hat{k_x} B^T P A_m^{-1} B\hat{k_x^T} x = -v_x x(t)^T \hat{k_x} B^T A_m^{-T} Q A_m^{-1} B\hat{k_x^T} x$$

$$2v_r r(t)^T \hat{k_r} B^T P A_m^{-1} B\hat{k_r^T} r = -v_r r(t)^T \hat{k_r} B^T A_m^{-T} Q A_m^{-1} B\hat{k_r^T} r$$

$$2v_\Theta \phi(x)^T \hat{\Theta} B^T P A_m^{-1} B\hat{\Theta^T} \phi(x) = -v_\Theta \phi(x)^T \hat{\Theta} B^T A_m^{-T} Q A_m^{-1} B\hat{\Theta^T} \phi(x)$$

Then $\dot{V}$ bounded by

$$\dot{V} \leq -\lambda_{min}(Q)||e||^2 + 2\lambda_{max}(P)|e||\bar{d} - v_x \lambda_{min}(B^T A_m^{-T} Q A_m^{-1} B)\|x\|^2 \|\hat{k_x}|^2$$
$$+ 2v_x \|B^T P A_m^{-1} B\|\|x\|^2 \|\hat{k_x}\| k_{x0} - v_r \lambda_{min}(B^T A_m^{-T} Q A_m^{-1} B)\|r\|^2 \|\hat{k_r}|^2$$
$$+ 2v_r \|B^T P A_m^{-1} B\|\|r\|^2 \|\hat{k_r}\| k_{r0} - v_\Theta \lambda_{min}(B^T A_m^{-T} Q A_m^{-1} B)\|\phi\|^2 \|\hat{\Theta}\|^2$$
$$+ 2v_\Theta \|B^T P A_m^{-1} B\|\|\phi\|^2 \Theta_0 \tag{4.77}$$

Now completing square the above equation then find the lower limit of $\|e\|, \|\hat{k_x}\|, \|\hat{k_r}\|, \|\hat{\Theta}\|$

$$\|e\| \geq \frac{\lambda_{max(P)\bar{d}}}{\lambda_{min}(Q)} + \sqrt{\frac{\lambda^2_{max}(P)\bar{d}^2}{\lambda^2_{min}(Q)} + \frac{v_x\|B^TPA_m^{-1}B\|\|\hat{k_x}\|k^2_{x0}}{\lambda_{min}(Q)\lambda_{min}(B^TA_m^{-T}QA_m^{-1}B)} + \frac{v_r\|B^TPA_m^{-1}B\|\|\hat{k_r}\|k^2_{r0}}{\lambda_{min}(Q)\lambda_{min}(B^TA_m^{-T}QA_m^{-1}B)} + \frac{v_\Theta\|B^TPA_m^{-1}B\|\|\phi\|^2\Theta_0^2}{\lambda_{min}(Q)\lambda_{min}(B^TA_m^{-T}QA_m^{-1}B)}}$$

$$= p$$

$$\|\hat{k_x}\| \geq \frac{\|B^TPA_m^{-1}B\|k_{x0}}{\lambda_{min}(B^TA_m^{-T}QA_m^{-1}B)} + \sqrt{\frac{\lambda^2_{max}(P)\bar{d}^2}{\lambda_{min}(Q)\lambda_{min}(B^TA_m^{-T}QA_m^{-1}B)} + \frac{v_x\|B^TPA_m^{-1}B\|\|\hat{k_x}\|k^2_{x0}}{\lambda_{min}(B^TA_m^{-T}QA_m^{-1}B)} + \frac{v_r\|B^TPA_m^{-1}B\|\|\hat{k_r}\|k^2_{r0}}{\lambda_{min}(B^TA_m^{-T}QA_m^{-1}B)} + \frac{v_\Theta\|B^TPA_m^{-1}B\|\|\phi\|^2\Theta_0^2}{\lambda_{min}(B^TA_m^{-T}QA_m^{-1}B)}}$$

$$= \alpha$$

$$\|\hat{k_r}\| \geq \frac{\|B^TPA_m^{-1}B\|k_{r0}}{\lambda_{min}(B^TA_m^{-T}QA_m^{-1}B)} + \sqrt{\frac{\lambda^2_{max}(P)\bar{d}^2}{\lambda_{min}(Q)\lambda_{min}(B^TA_m^{-T}QA_m^{-1}B)} + \frac{v_x\|B^TPA_m^{-1}B\|\|\hat{k_x}\|k^2_{x0}}{\lambda_{min}(B^TA_m^{-T}QA_m^{-1}B)} + \frac{v_r\|B^TPA_m^{-1}B\|\|\hat{k_r}\|k^2_{r0}}{\lambda_{min}(B^TA_m^{-T}QA_m^{-1}B)} + \frac{v_\Theta\|B^TPA_m^{-1}B\|\|\phi\|^2\Theta_0^2}{\lambda_{min}(B^TA_m^{-T}QA_m^{-1}B)}}$$

$$= \beta$$

$$\|\hat{\Theta}\| \geq \frac{\|B^TPA_m^{-1}B\|\Theta_0}{\lambda_{min}(B^TA_m^{-T}QA_m^{-1}B)} + \sqrt{\frac{\lambda^2_{max}(P)\bar{d}^2}{\lambda_{min}(Q)\lambda_{min}(B^TA_m^{-T}QA_m^{-1}B)} + \frac{v_x\|B^TPA_m^{-1}B\|\|\hat{k_x}\|k^2_{x0}}{\lambda_{min}(B^TA_m^{-T}QA_m^{-1}B)} + \frac{v_r\|B^TPA_m^{-1}B\|\|\hat{k_r}\|k^2_{r0}}{\lambda_{min}(B^TA_m^{-T}QA_m^{-1}B)} + \frac{v_\Theta\|B^TPA_m^{-1}B\|\|\phi\|^2\Theta_0^2}{\lambda_{min}(B^TA_m^{-T}QA_m^{-1}B)}}$$

$$= \gamma$$

keep in mind that p , α ,β and γ are the lower bound they are dependent on $\|x\|$, $\|r\|$ and $\|\phi\|$. Thus, we additionally require $\|x\|$, $\|r\|$, and $\|\phi\|$ to be bounded in order to demonstrate boundedness.

If $\|x\| \leq x_0$, $\|r\| \leq r_0$ and $\|\phi\| \leq \phi_0$ then the solution is uniformly ultimately bounded

Chapter 5

Simulation Results and Discussion

5.1 Introduction

In this chapter, the simulation results of different scenarios are represented, in chapter 4 controllers are designed like conventional MRAC in nominal scenarios, σ-modification MRAC, e-modification MRAC, and optimal control-modification MRAC. Also, the performance of the proposed controller is analyzed for different trajectories. Three different trajectories are prepared which include helical, pre-defined way-points(area coverage), and infinity. The model of the FWUAV is developed in Matlab/Simulink with disturbance and without disturbance. After developing the proposed control system, we can simulate and observe the behavior of the system. The simulation results are presented in the form of graphs, which help us to analyze the performance of the controller.

For each trajectory, a comparative analysis is made between three modified MRACs in terms of asymptotic tracking performance and used control efforts. Simulation results are presented and discussed to evaluate the effectiveness of each developed controller for position and orientation control of the flight system at different trajectories. The performance of the proposed controller is evaluated for external disturbance and parametric variation.

Control surface constraints and trust constraints are given at table5.1

Aileron deflection [deg]	±34
Elevator deflection [deg]	±60
Rudder deflection[deg]	±60
Trust[N]	270

Table 5.1: Constraints on control input [43]

5.2 Rejecting Plant Dynamics $d(t)$

5.2.1 Helical Trajectory Tracking

In this simulation reject plant dynamics $d(t)$ because we consider it as uncertainty due to disturbance. The adaptation rate must be chosen carefully to achieve sufficient robustness while achieving the desired level of tracking performance. The input trajectories along x is x_r=$20\cos(t)$, along y is x_r=$20\sin(t)$ along z is z_r=$2+t$ and ϕ_r=0.2 rad. After several try-and-error design iterations, the adaptation rates have chosen to be

Adaptive gain	Value	Adaptive gain	Value
Γ_x	10	Γ_ϕ	100
Γ_{xr}	10	$\Gamma_{\phi r}$	100
		$\Gamma_{\phi\Theta}$	10
Γ_y	10	Γ_θ	100
Γ_{yr}	10	$\Gamma_{\theta r}$	100
		$\Gamma_{\theta\Theta}$	10
Γ_z	10	Γ_ψ	1000
Γ_{zr}	10	$\Gamma_{\psi r}$	1000
		$\Gamma_{\psi\Theta}$	10

Table 5.2: Adaptation rates
Γ_x, Γ_y, Γ_z, Γ_ϕ, Γ_θ,Γ_ψ,$\Gamma_{\phi\Theta}$,$\Gamma_{\theta\Theta}$ and $\Gamma_{\psi\Theta} \in \mathbb{R}^2\text{x}\mathbb{R}^2$ the diagonal element values are given

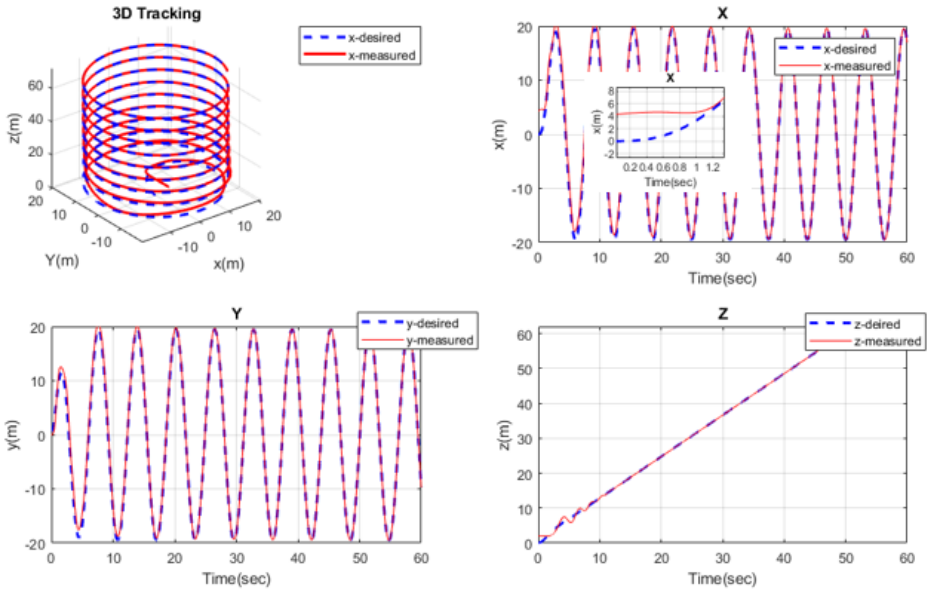

Figure 5.1: Position tracking for helical trajectories

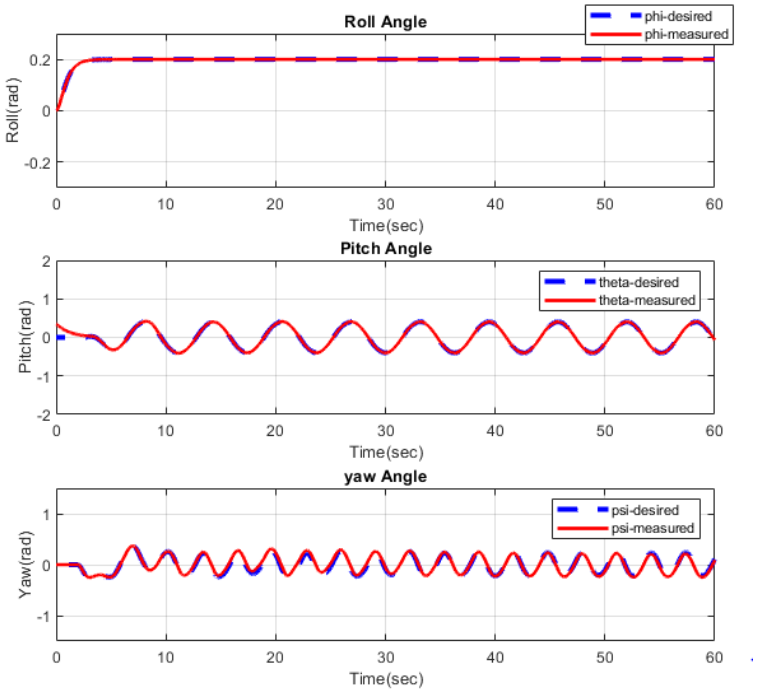

Figure 5.2: Attitude tracking for helical trajectories

In this thesis the throttle input represents the PWM voltage ratio, we can also represent it in percentile

$$\delta_t\% = \delta_t(ratio) * 100\% \tag{5.1}$$

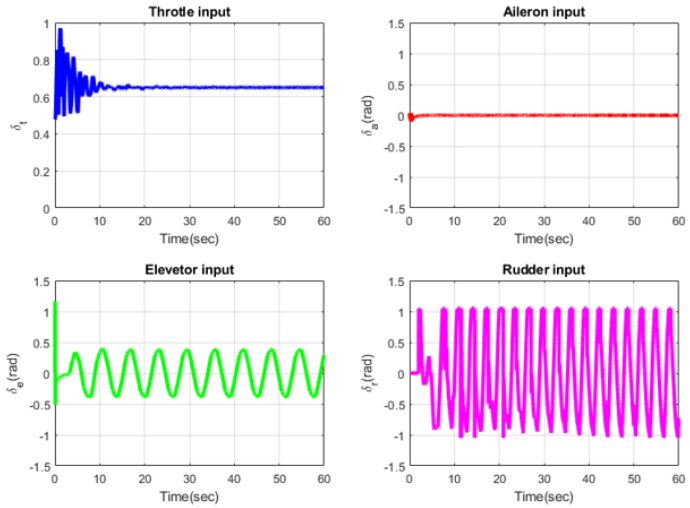

Figure 5.3: Control signal for helical trajectories

After analyzing the simulation results, it is evident that the tracking performance of the position and attitude is good. Additionally, we did not observe any divergence in the adaptive parameters, this is due to the absence of $d(t)$. However, if we include $d(t)$ in plant dynamics the adaptive parameter diverges as shown in the figure 5.4.

5.3 Considering Part Of Plant Dynamics $d(t)$ (Considered as Uncertainty)

In the case of Off-nominal Scenarios, we consider matched and unmatched uncertainty, Unmatched uncertainty can often lead to parametric drift. It's important to minimize any potential sources of uncertainty in order to maintain stability and consistency in our systems. When we include $d(t)$ for helical trajectory, it causes parameter drift. As we can observe from the figure provided in figure 5.4, it is evident that the presence of unmatched uncertainty causes the $x-$ position and pith angle controllers adaptive parameters divergence. The adaptive parameters diverge to infinity as time elapses. It is important to address such uncertainties to prevent any undesirable outcome. To prevent parameter drift, it's important to make the conventional MRAC more robust.

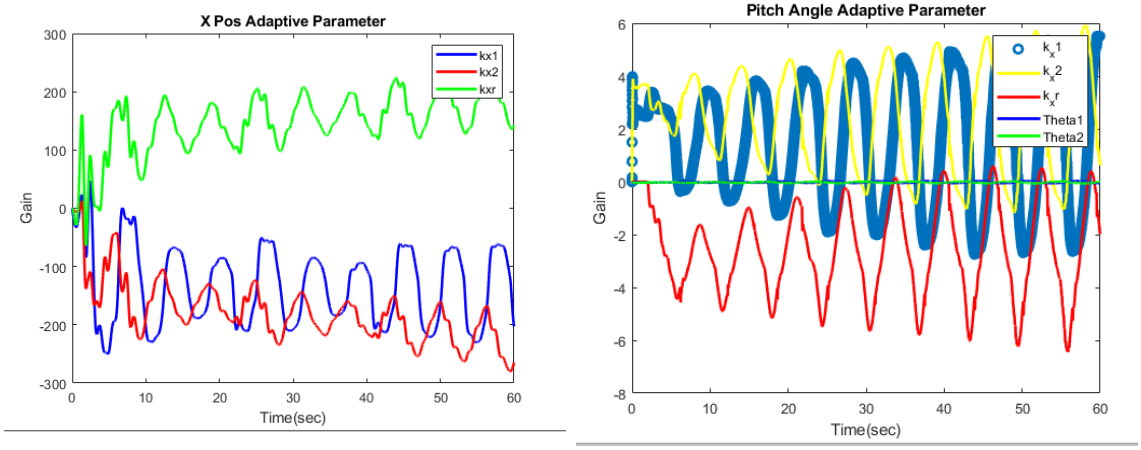

(a) x position adaptive parameter

(b) Pitch angle adaptive parameter

Figure 5.4: Divergence of adaptive parameters in the presence of plant dynamics(unmatched uncertainty $d(t)$)

5.3.1 σ-Modification for Helical Trajectories

The value of the $\sigma-$ modification parameters values are given below in table 5.3. As the value of the modification parameter increases, the tracking error becomes larger but has better robustness to unmatched uncertainty in return. This is a consequence of the trade-off between tracking performance and robustness. MATLAB/SIMULINK software is used to choose the modification parameter through try-and-error.

Modification parameter	value	Modification parameter	value
σ_x	0.3	σ_ϕ	0.02
σ_{rx}	0.3	$\sigma_{\phi r}$	0.02
		$\sigma_{\phi\Theta}$	0.01
σ_y	0.3	σ_θ	0.03
σ_{ry}	0.3	$\sigma_{\theta r}$	0.03
		$\sigma_{\theta\Theta}$	0.06
σ_z	0.1	σ_ψ	0.01
σ_{rz}	0.1	$\sigma_{\psi r}$	0.01
		$\sigma_{\psi\Theta}$	0.01

Table 5.3: σ modification parameter

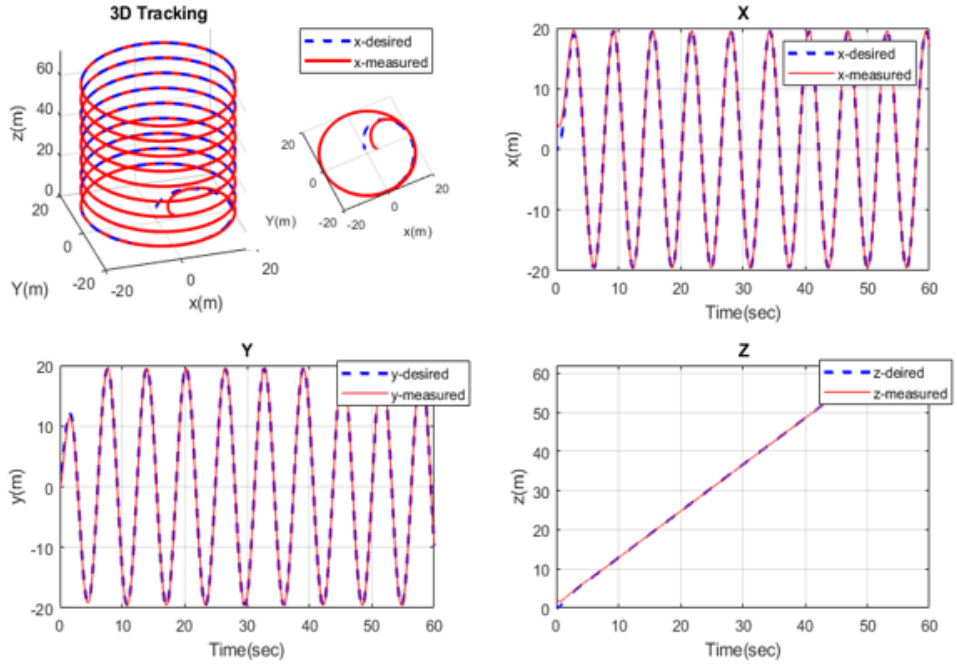

Figure 5.5: $\sigma-$ modification MRAC position tracking

From figure 5.8 we analyze that the x-position controller adaptive parameters and pitch angle adaptive parameters are bounded due to σ-modification. In essence, σ modification adds damping to the ideal adaptive law due to this modification, there is no parametric divergence. In Chapter Four stability analysis is proved that how σ-modification makes the system stable or how adaptive parameters are bounded. All the adaptive parameters for position x, y,z and for attitude ϕ, θ, ψ are bounded. Because of this, the overall system is stable.

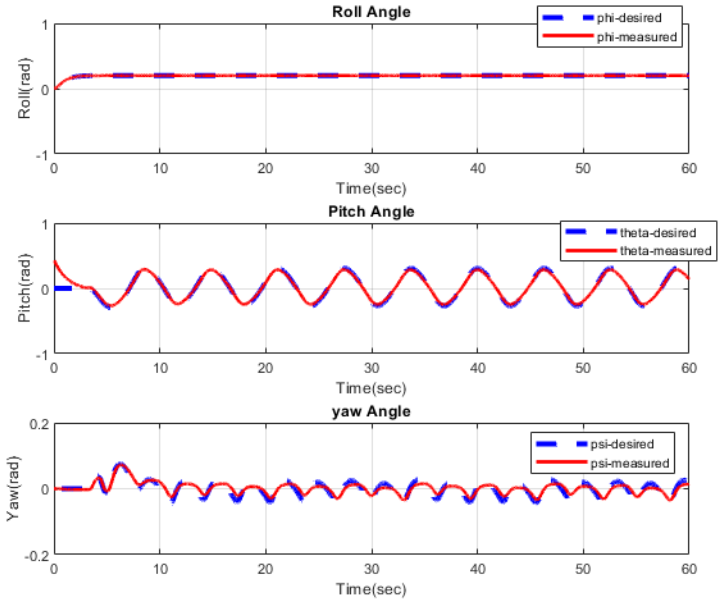

Figure 5.6: $\sigma-$modification attitude tracking

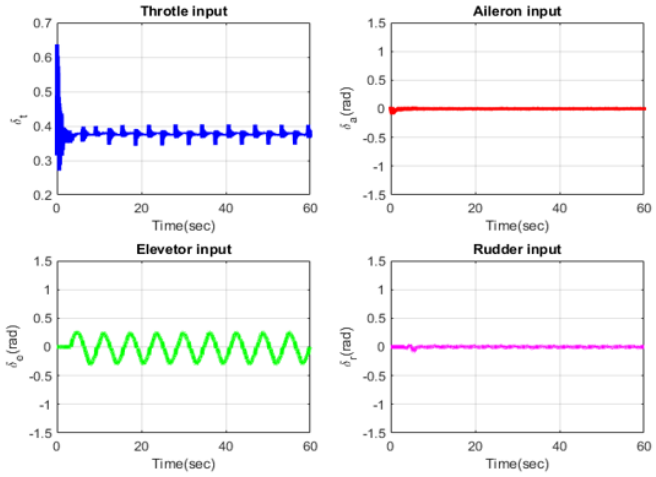

Figure 5.7: $\sigma-$ modification control signal

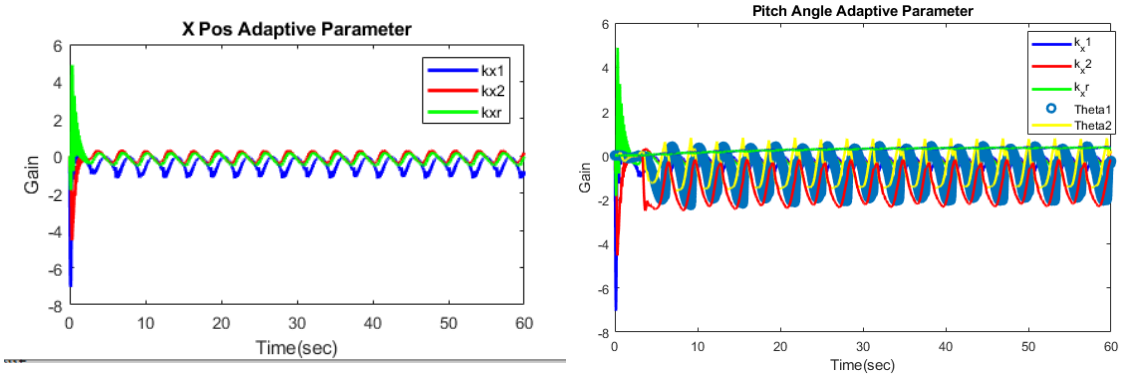

(a) X position adaptive parameter

(b) Pitch angle adaptive parameter

Figure 5.8: $\sigma-$ modification convergence of adaptive parameters in the presence of unmatched uncertainty($d(t)$)

5.3.2 e-Modification for Helical Trajectory

There is always a trade-off between asymptotic tracking and the robustness of MRAC. e-modification improves tracking performance compared with σ-modification. Similar to sigma modification, e-modification bounds adaptive parameters, but it causes significant chattering. The modification parameters and their corresponding values are given in table 5.4.

Modification parameter	value	Modification parameter	value
μ_x	0.3	μ_ϕ	0.02
μ_{rx}	0.3	$\mu_{\phi r}$	0.02
		$\mu_{\phi\Theta}$	0.01
μ_y	0.3	μ_θ	0.03
μ_{ry}	0.3	$\mu_{\theta r}$	0.03
		$\mu_{\theta\Theta}$	0.06
μ_z	0.1	μ_ψ	0.01
μ_{rz}	0.1	$\mu_{\psi r}$	0.01
		$\mu_{\psi\Theta}$	0.01

Table 5.4: $e-$ modification parameter

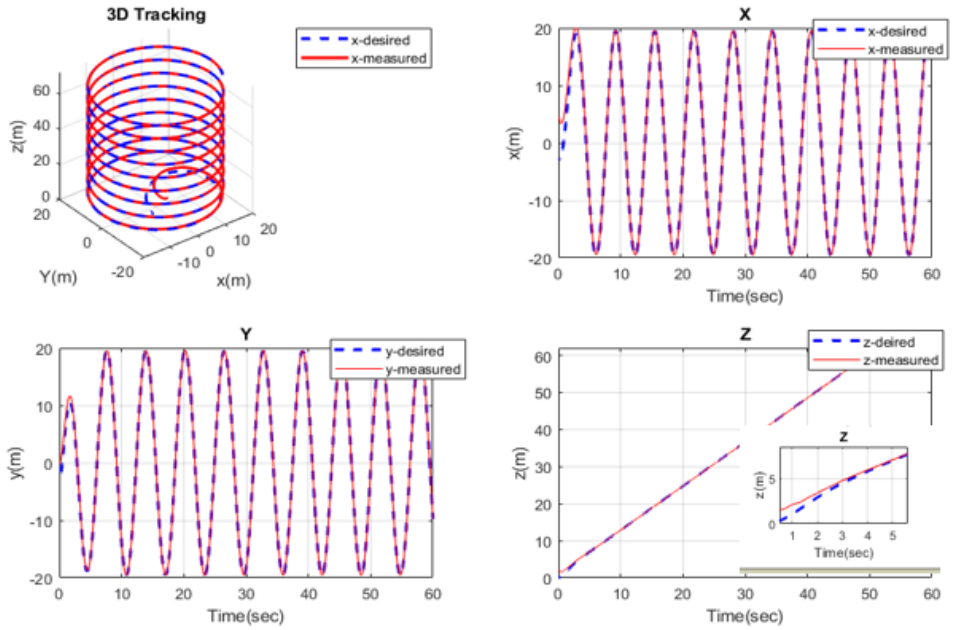

Figure 5.9: e-modification position tracking

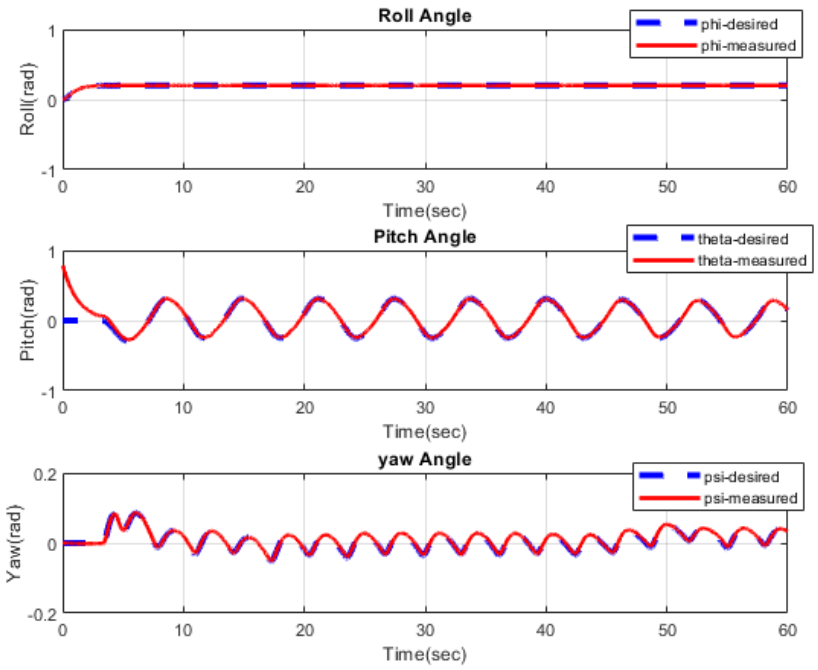

Figure 5.10: e-modification attitude tracking

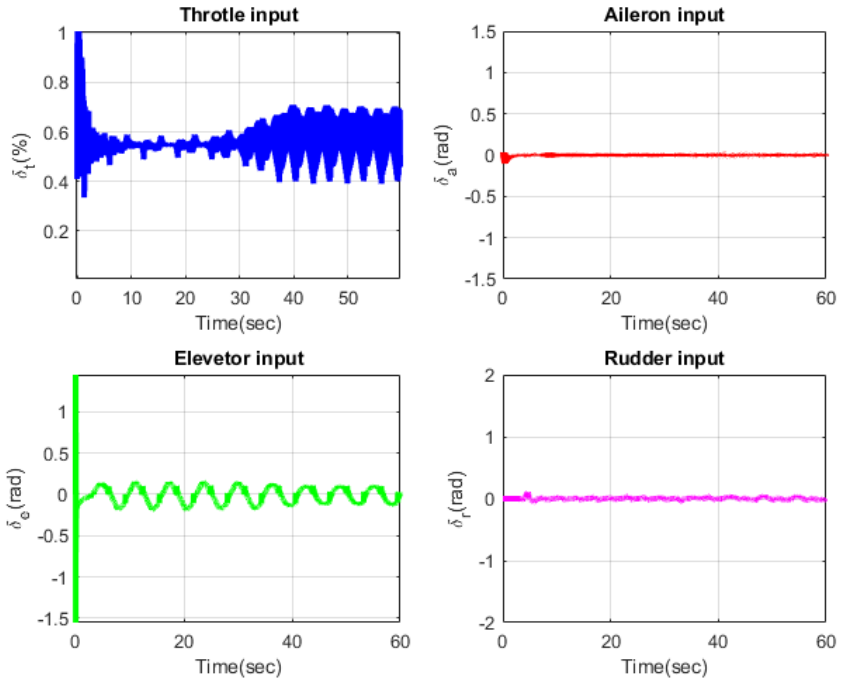

Figure 5.11: e-modification control input

Look at $e-$ modification MRAC in figure 5.11 throttle input command has a high chattering effect. This is one of the drawbacks of $e-$ modification and performance indices in table 5.5 show that $e-$ modification has better tracking performance compared with $\sigma-$ modification.

Asymptotic tracking performance for helical trajectories in terms of $ITAE$

	States	$ITAE$		States	$ITAE$
	x	53.59		x	34.34
	y	29.13		y	14.9
	z	4.253		z	4.141
$\sigma-$modification	ϕ	0.03612	$e-$modification	ϕ	0.0253
	θ	28.53		θ	2.286
	ψ	33.63		ψ	2.475

Table 5.5: Performance indices for asymptotic tracking

5.3.3 e-Modification for Pre-defined Way-points(Area Coverage)

In table 5.6, the way-points are listed. The path can be generated by using these way-points to cover an area. This can be done by using a path-planning algorithm. In this thesis work, we use pre-defined way-points. A navigation speed of 20 m/s is taken to prepare the flight timetable. After the preparation of the flight timetable, generate a third-order polynomial function that has four coefficients, and to smooth the sharp turn consider the four *seconds* banking of fixed-wing UAV.

$x(m)$	$y(m)$	$z(m)$	$Time(sec)$
0	0	2	0
200	0	200	14
400	0	200	24
400	200	200	34
200	200	200	44
200	400	200	54
400	400	200	64
400	600	200	74
0	600	200	94
0	0	200	124
0	0	0	134

Table 5.6: way-points

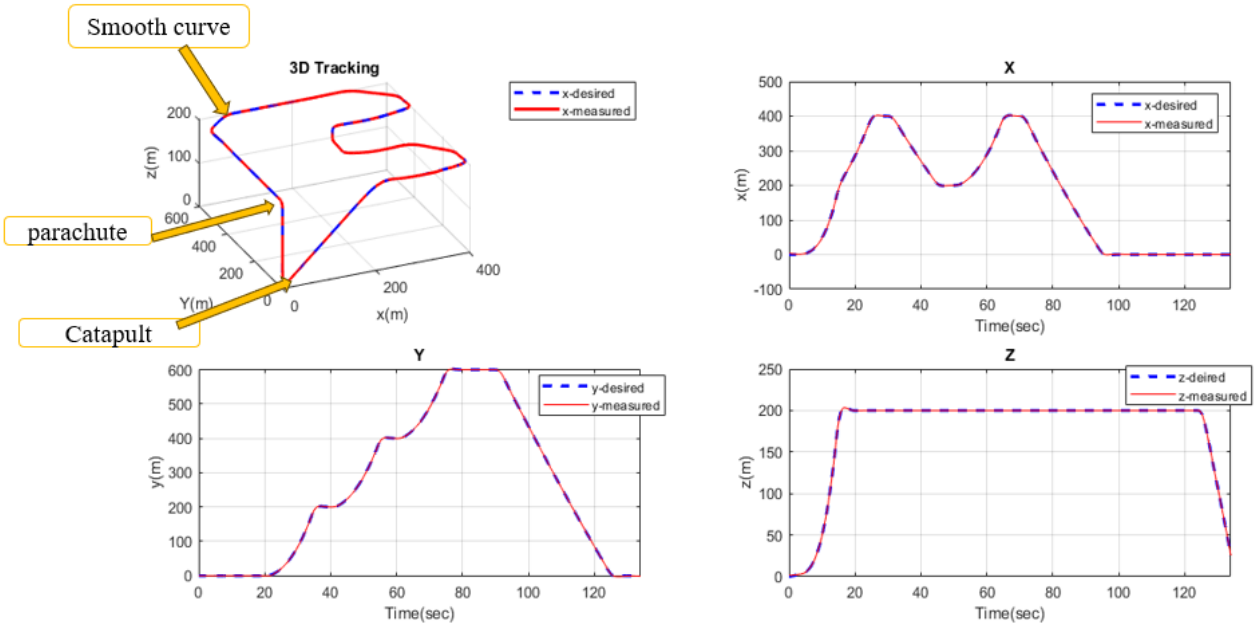

Figure 5.12: $e-$modification MRAC position tracking

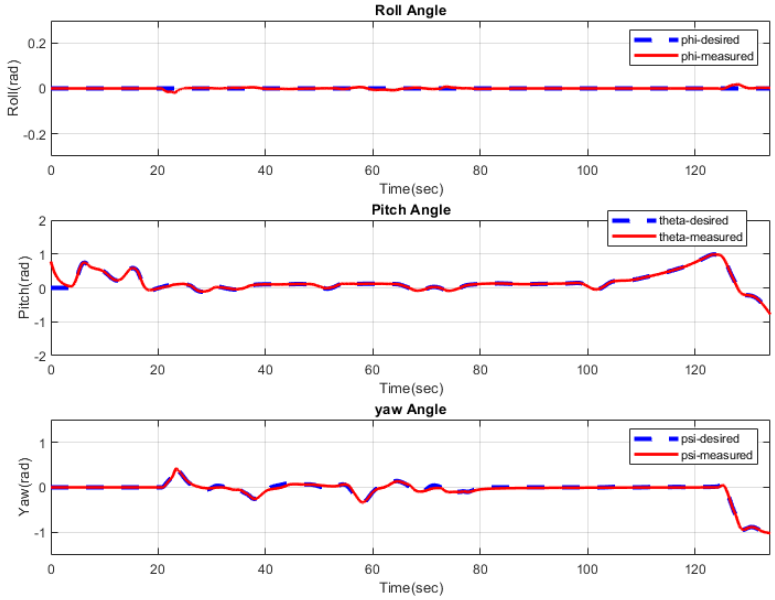

Figure 5.13: $e-$modification MRAC attitude tracking

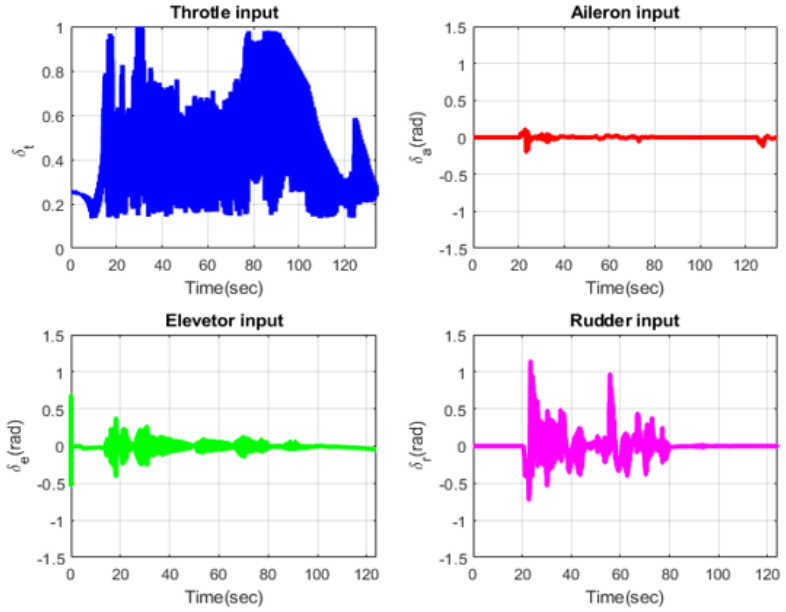

Figure 5.14: $e-$modification MRAC control effort

As shown in the figure all the states track the given trajectories. However, the throttle control effort has a high chattering effect, this is a drawback of $e-$ modification MRAC. In table 5.8 asymptotic tracking performance is compared for both optimal modification and $e-$ modification in terms of $ITAE$.

5.3.4 Optimal Control Modification for Pre-defined Way-points

The same pre-defined way-points are used and the modification parameters are listed below in table 5.7. The modification parameters are carefully chosen to achieve good tracking performance and robustness, through try-and-error. When the modification parameters are chosen we consider tracking performance and robustness issues. There is always a trade-off between asymptotic tracking and robustness.

Modification parameter	value	Modification parameter	value
v_x	0.01	v_ϕ	0.06
v_{rx}	0.01	$v_{\phi r}$	0.001
		$v_{\phi\Theta}$	0.06
v_y	0.01	v_θ	0.3
v_{ry}	0.01	$v_{\theta r}$	0.3
		$v_{\theta\Theta}$	0.0001
v_z	0.01	v_ψ	0.01
v_{rz}	0.01	$v_{\psi r}$	0.01
		$v_{\psi\Theta}$	0.01

Table 5.7: optimal control modification parameters

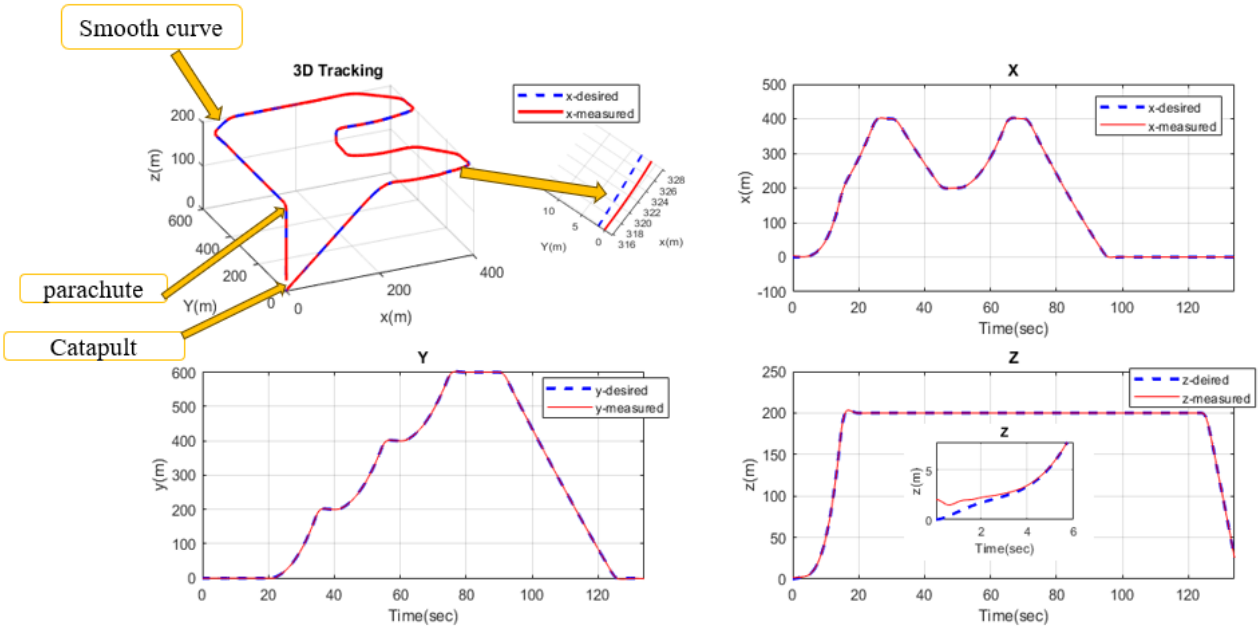

Figure 5.15: optimal control modification MRAC position tracking

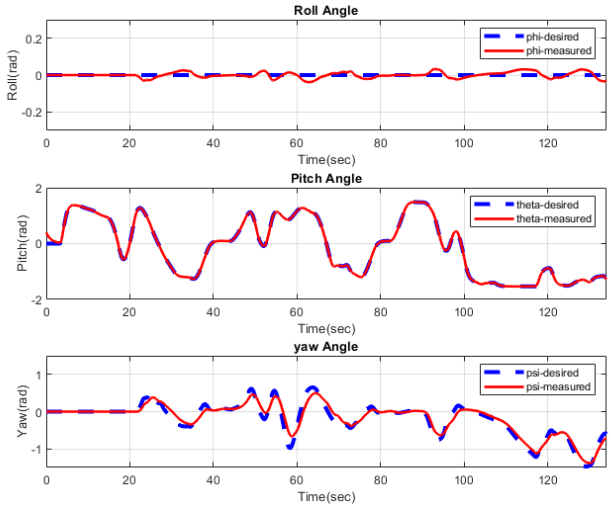

Figure 5.16: Optimal control modification MRAC Attitude tracking

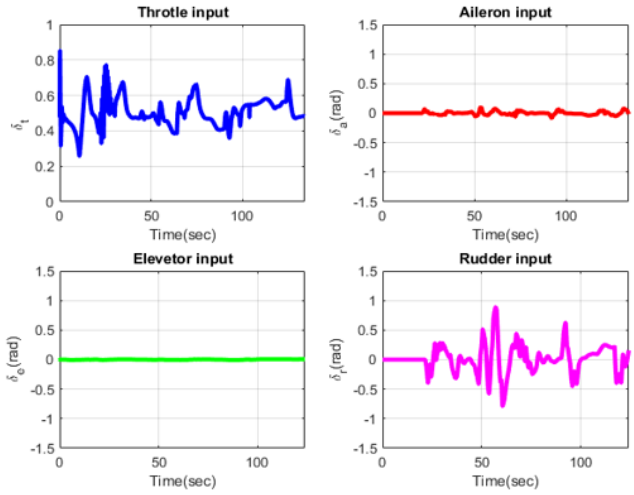

Figure 5.17: Control effort

Asymptotic tracking performance for pre-defined way-points in terms of $ITAE$

From the performance indices for z, ϕ, θ, and ψ $e-$ modification has better asymptotic

	States	$ITAE$		States	$ITAE$
	x	834.7		x	966.5
	y	195.3		y	589.5
	z	121		z	0.1146
Optimal control	ϕ	153.2	$e-$modification	ϕ	16.01
	θ	12.14		θ	11.61
	ψ	1077		ψ	114.9

Table 5.8: Performance indices for asymptotic tracking

tracking performance than optimal control modification.

5.3.5 $\sigma-$Modification For Infinity Trajectory

In this section, the infinity trajectory tracking performance of $\sigma-$modification is demonstrated. The infinity trajectory is prepared to cover $80m$ along x, $80m$ along y, and the altitude is $30m$ along z and ϕ_r set to be 0.2 rad. As shown in figure 5.18 the position tracks the reference model, but it has a tracking error. To achieve position trajectory tracking and attitude tracking the controller consumes a control effort presented in figure 5.20

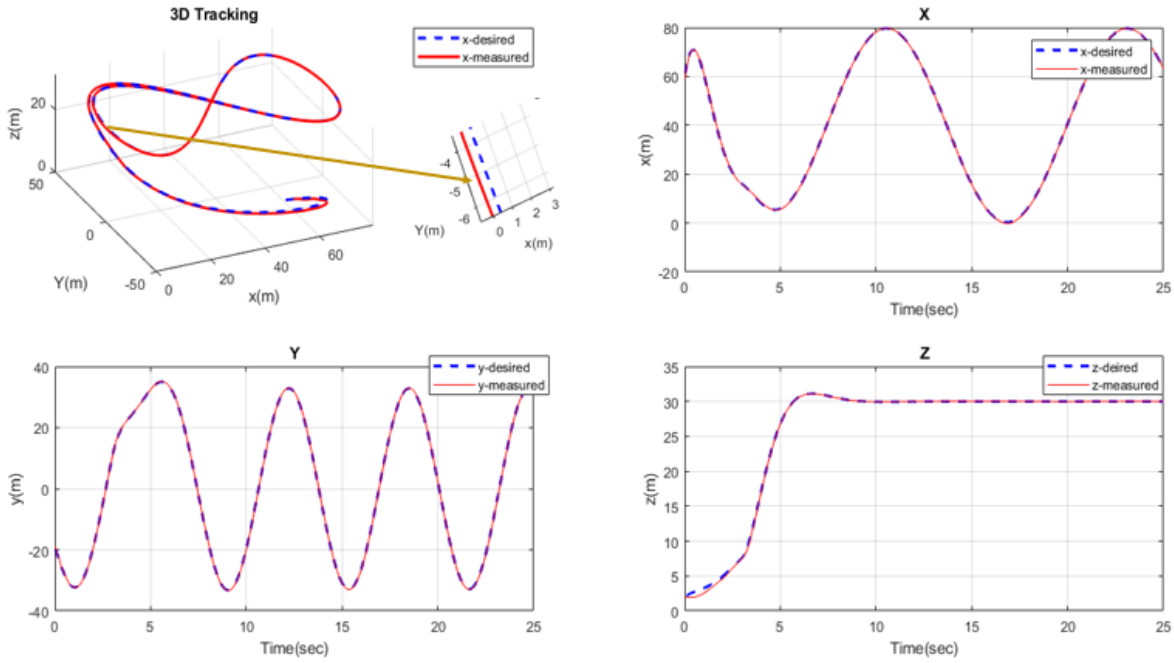

Figure 5.18: Infinity trajectory position tracking forσmodification

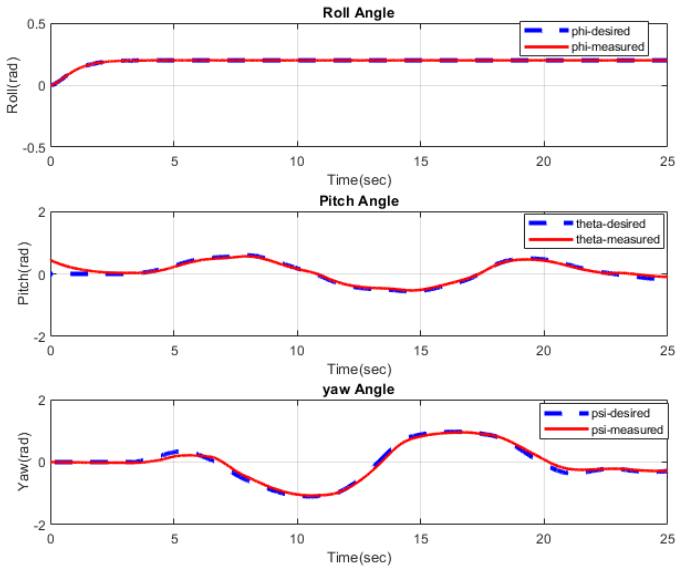

Figure 5.19: Infinity trajectory attitude tracking for σ modification

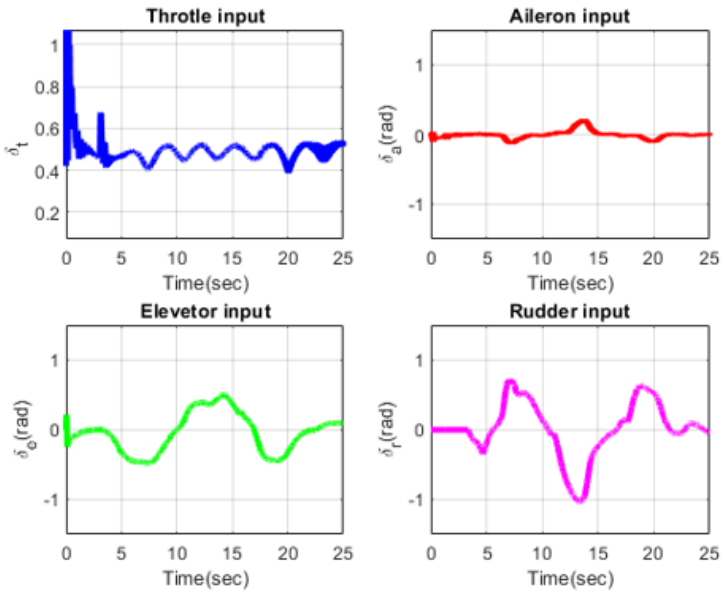

Figure 5.20: Infinity trajectory tracking control effort for σ modification

5.3.6 Optimal Control Modification For Infinity Trajectory

Here infinity trajectory is used to demonstrate the trajectory-tracking performance of optimal control modification. From figure 5.21 we analyze that optimal control modification has good tracking performance, but it has steady-state tracking error. The attitude tracks the reference trajectories in a good way 5.22. When we compare the throttle control effort between optimal control modification and $\sigma-$ modification for infinity trajectory, $\sigma-$ modification requires less effort.

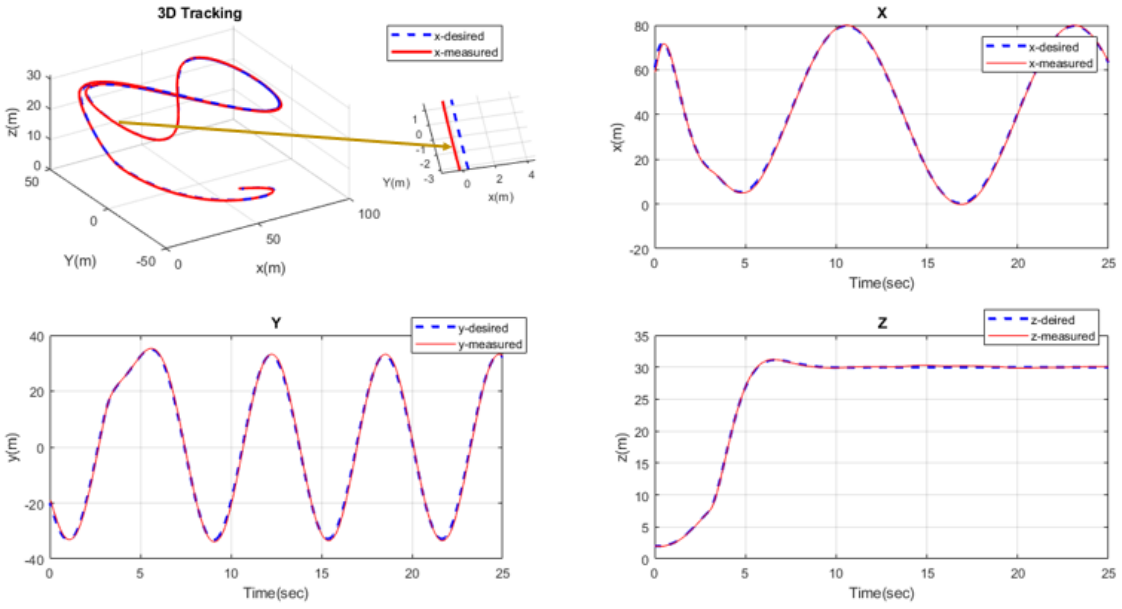

Figure 5.21: Infinity trajectory position tracking for optimal control modification

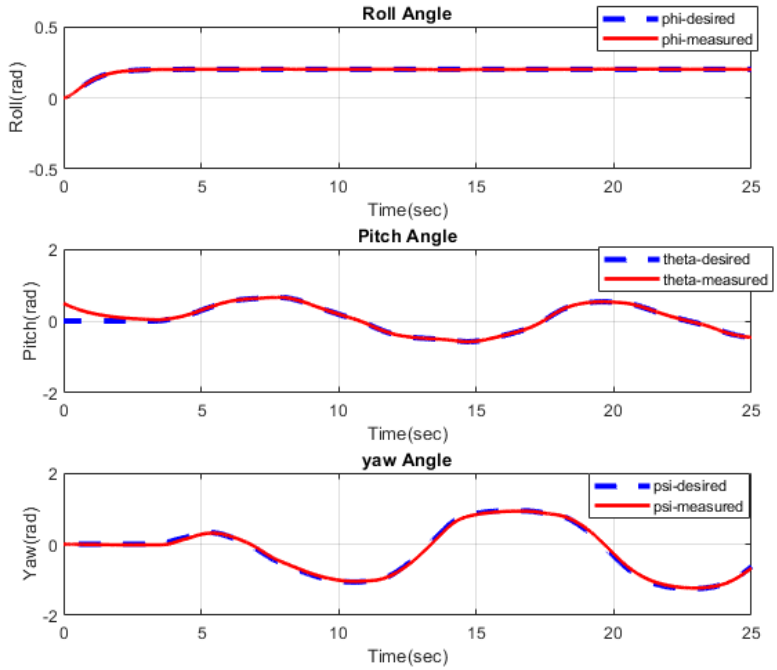

Figure 5.22: Infinity trajectory attitude tracking for optimal control modification

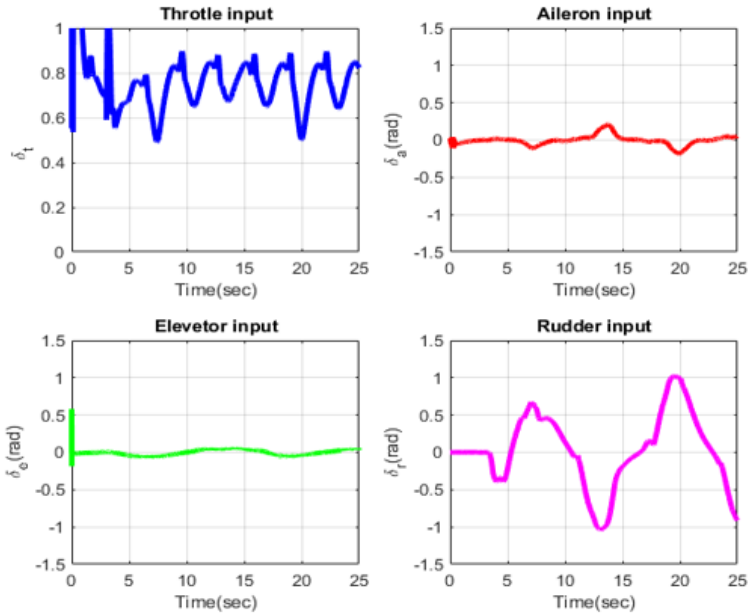

Figure 5.23: Infinity trajectory control signal for optimal control modification

5.3.7 Disturbance Rejection and Uncertainty Tolerance

Now in this section, the robustness of MRAC is demonstrated for external disturbance and parametric variation. Here Integral Time Absolute Error (ITAE) is used as performance indices to compare the controller performance for external disturbance and parametric uncertainty. The waypoints-based predefined trajectory for optimal control modification is chosen to test the robustness of MRAC. Two different scenarios are listed below.

5.3.7.1 Scenario-1: Disturbed Environment(Wind Gust)

In order to show the robustness of modified MRAC for external disturbance in tracking paths use a wind gust disturbance. Now apply a wind gust that exerts a constant force of -10 N along x,y, and z direction at t = 25 sec to 30 sec, t = 60 sec to 65 sec and t = 95 sec to 100 sec respectively. The response of the disturbed system is presented in figure 5.24. It is clear from figure 5.25 that during the time the disturbance occurs, the overall control command is adapted in a way that the overall systems' stability is not compromised. From the simulation result, we observe that the proposed adaptive controller can achieve good tracking performance in the presence of disturbance.

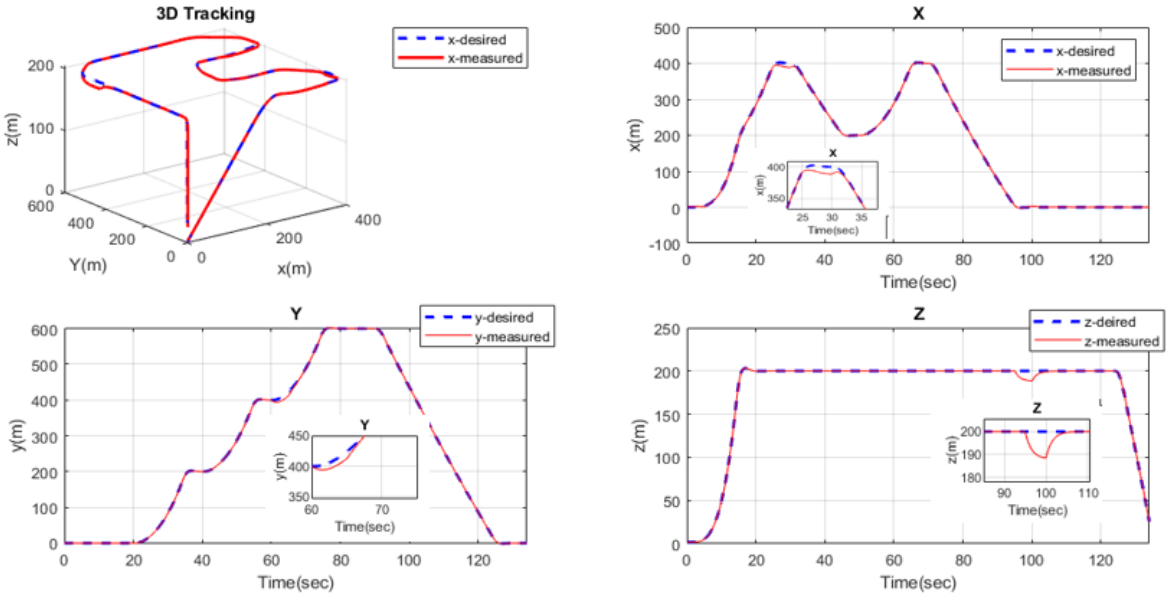

Figure 5.24: 3D position tracking in the presence of disturbance

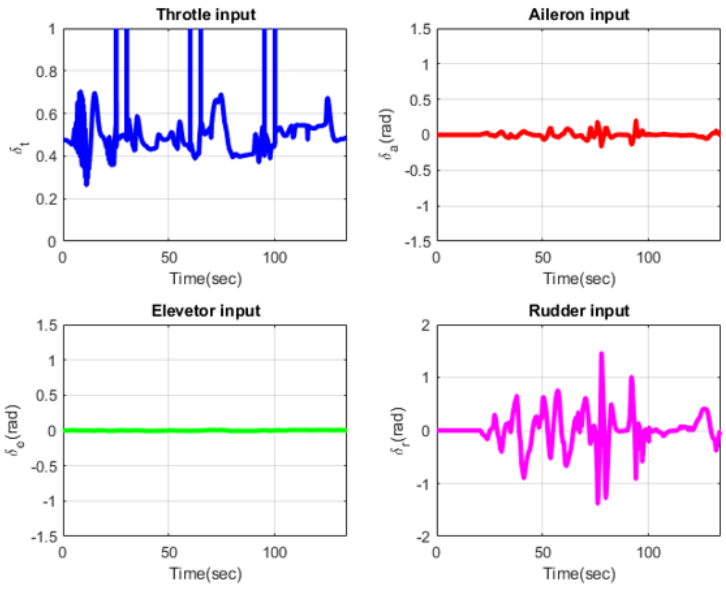

Figure 5.25: Control effort is affected by wind gust

5.3.7.2 Scenario-2: Parametric Uncertainties

Parametric uncertainties are imposed due to inertia and aerodynamic coefficients to analyze uncertainty tolerance. The aerodynamic coefficients are assumed to be two times their nominal design values. Looking at the dynamics of the FWUAVs, it can be seen that uncertainty of these parameters causes control effectiveness issues, in the control input matrix in equation 4.28, 4.29, 4.30 there are aerodynamic coefficients and the inertial tensor is assumed to be uncertain having two times the design time value. Furthermore, a comparative analysis is made.

Imposed Uncertainty	Values
Uncertainty due to inertia	2*nominal inertia
Uncertainty due to aerodynamic coefficients	2*nominal coefficients

Table 5.9: Imposed Uncertainty

Parametric uncertainty also affects attitude tracking. The attitude dynamics in equation3.109, 3.111 and 3.113 contain aerodynamic coefficients of forces and moments due to this reason attitude tracking is also affected by parametric uncertainty as we can see from figure 5.26. Figure 5.17 and 5.27 represent the Optimal control modification MRAC control effort in the nominal scenario and parametric uncertainty condition. It is clear the imposed uncertainty affects a control input. However, the proposed controller stabilizes the plant. In table 5.10 the performance indices are given for position trajectory tracking, and the parametric variation and external disturbance affect the the proposed controller.

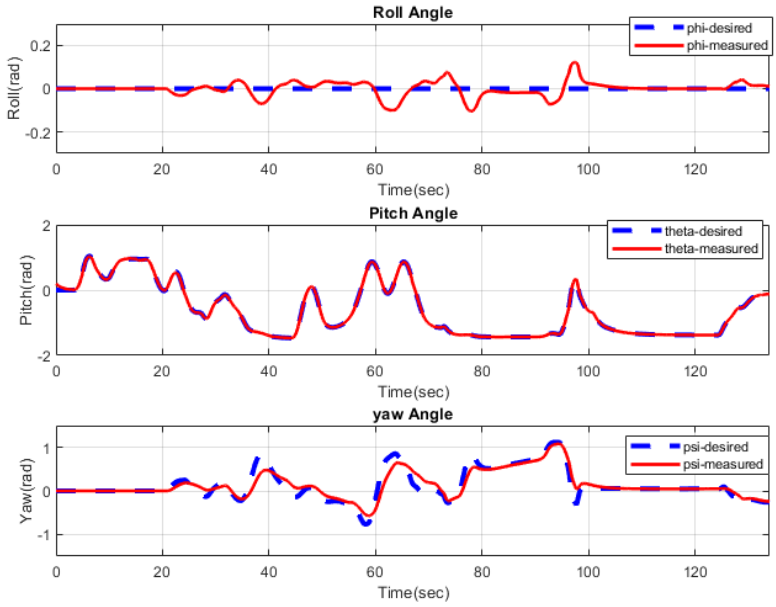

Figure 5.26: Attitude tracking if affected by imposed uncertainty

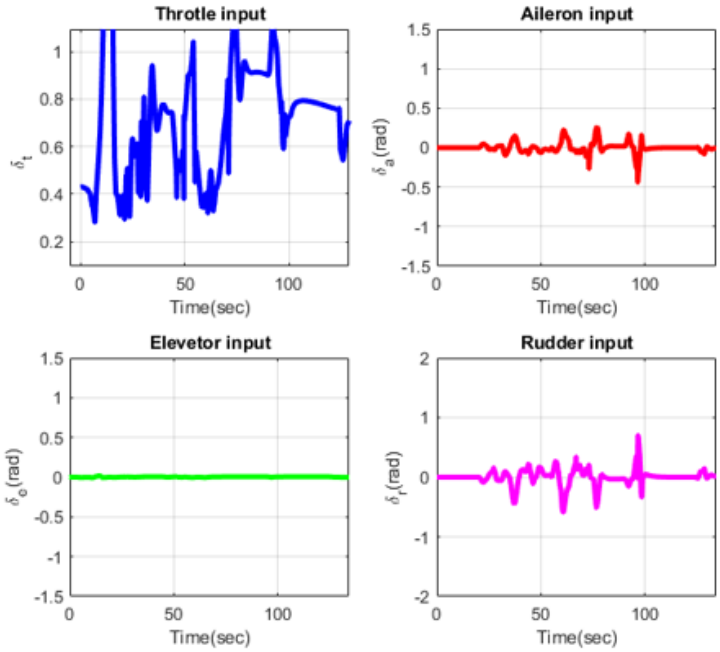

Figure 5.27: Control effort is affected by imposed uncertainty

Operating condition	Adaptive controller
Nominal Scenario	$ITAE$=1151
Operating in a wind gust	$ITAE$=14183
Imposing uncertainty	$ITAE$=4520.1

Table 5.10: Performance indices for position trajectory tracking

According to the simulation result, the pros and cons of different modification techniques are summarized below

Modification	pros	cons
σ	It is simple, economic and consumes less control effort for smooth trajectories like helical and infinity trajectory	Consumes more control effort for square wave trajectory and achieve bounded tracking
e	Good in asymptotic tracking	It uses high control effort and has chattering effect
optimal control	Uses less control effort for square wave trajectory	Result in bounded tracking.

Table 5.11: Pros and Cons of modification technique

Square wave trajectory represents a pre-defined waypoints-based trajectory for areal coverage.

Chapter 6

Conclusion and Recommendations

6.1 Conclusion

This thesis has two parts modelling and controller design part. The mathematical model of fixed-wing UAV is highly non-linear, coupled, and complex, to simplify the control process, it is necessary to decouple the mathematical models before starting controller design. Decoupling processing mainly extracts the dominant state quantity in the control process and treats the remaining state quantity as unmatched uncertainty. Then, the Conventional Model Reference Adaptive controller is developed to control position(x,y,z) and attitude(ϕ,θ,ψ). However, it has a stability problem when unmatched uncertainty is considered. To overcome this problem robustification is necessary. This thesis work uses, $\sigma-$modification, $e-$modification, and optimal control modification techniques as a robustification method.

The performance of the developed Robust Model Reference Adaptive Controller is tested for different trajectories. As we can see from the simulation result for helical trajectory $e-$ modification MRAC tracks the given trajectories more asymptotically compared with σ modification MRAC. However, it requires more control effort. On the other hand for a pre-defined waypoint(area coverage) or a trajectory that has sharp turns an optimal control modification MRAC requires less control effort compared with $e-$modified MARC. For infinity or smooth curve trajectory, $\sigma-$ modification MRAC requires less control effort. Optimal control modification and $\sigma-$ modification result in bounded tracking rather than asymptotic tracking.

Furthermore, the performance of the Robust Model Reference Adaptive Controller is tested by imposing parametric uncertainty and external disturbance(wind gust) along x, y, and z directions. However, fully Robust MRAC is found to be able to cope.

6.2 Recommendation For Future Work

In considering the implications of this research, there are key areas that could be explored further:

- It is important to possess a path-planning algorithm that can effectively and efficiently calculate the optimal, safest, and quickest route to the final destination. This ensures that FWUAV arrives at's desired destination in a timely and secure manner. Path planning takes into account obstacles such as buildings, trees, mountains, and other UAVs. By planning a route that avoids these obstacles, the risk of collisions is minimized, ensuring the safety of the UAV.
- Implement the hardware and the proposed controller of fixed-wing UAV.

Bibliography

[1] Yeonsik Kang and J Karl Hedrick. "linear tracking for a fixed-wing uav using nonlinear model predictive control". *IEEE Transactions on Control Systems Technology*, 17(5):1202–1210, 2009.

[2] H Philip Whitaker, Joseph Yamron, and Allen Kezer. *"Design of model-reference adaptive control systems for aircraft"*. Massachusetts Institute of Technology, Instrumentation Laboratory, 1958.

[3] Ri E Kalman. "design of a self-optimizing control system". *Transactions of the American Society of Mechanical Engineers*, 80(2):468–477, 1958.

[4] Dennis R Jenkins. *"Hypersonics before the shuttle: A concise history of the X-15 research airplane"*. National Aeronautics and Space Admin., NASA Office of Policy and Plans, NASA . . . , 2000.

[5] Nhan T. Nguyen. "model-reference adaptive control". *Springer*, AG 2018.

[6] Petros "Ioannou and Simone" Baldi. *Robust Adaptive Control*, pages 1–22. 12 2010.

[7] Ruiyong Zhai, Zhaoying Zhou, Wendong Zhang, Shengbo Sang, and Pengwei Li. "control and navigation system for a fixed-wing unmanned aerial vehicle". *Aip Advances*, 4(3), 2014.

[8] Pakorn Poksawat, Liuping Wang, and Abdulghani Mohamed. "gain scheduled attitude control of fixed-wing uav with automatic controller tuning". *IEEE Transactions on Control Systems Technology*, 26(4):1192–1203, 2017.

[9] Heri Purnawan, Eko Budi Purwanto, et al. "design of linear quadratic regulator (lqr) control system for flight stability of lsu-05". In *Journal of Physics: Conference Series*, volume 890, page 012056. IOP Publishing, 2017.

[10] Kedir Mustefa. "designing a sliding mode controller for fixed-wing unmanned aerial vehicle for medical supply mission". *MSc. Thesis*, Nov 2021.

[11] Wenya Zhou, Kuilong Yin, Rui Wang, Yue-E Wang, et al. "design of attitude control system for uav based on feedback linearization and adaptive control". *Mathematical Problems in Engineering*, 2014, 2014.

[12] Yufei Guo, Leru Luo, Changchun Bao, et al. "design of a fixed-wing uav controller combined fuzzy adaptive method and sliding mode control". *Mathematical Problems in Engineering*, 2022, 2022.

[13] Changchun Bao, Yufei Guo, Leru Luo, and Guanqun Su. "design of a fixed-wing uav controller based on adaptive backstepping sliding mode control method". *IEEE Access*, 9:157825–157841, 2021.

[14] Tadeo Espinoza, AE Dzul, Rogelio Lozano, and Pavel Parada. "backstepping-sliding mode controllers applied to a fixed-wing uav". *Journal of Intelligent & Robotic Systems*, 73:67–79, 2014.

[15] Zewei Zheng, Zhenghao Jin, Liang Sun, and Ming Zhu. "adaptive sliding mode relative motion control for autonomous carrier landing of fixed-wing unmanned aerial vehicles". *IEEE access*, 5:5556–5565, 2017.

[16] Herman Castañeda, Oscar S Salas-Peña, and Jesús de León-Morales. "extended observer based on adaptive second order sliding mode control for a fixed wing uav". *ISA transactions*, 66:226–232, 2017.

[17] Lamia Melkou, Mustapha Hamerlain, and Amar Rezoug. "fixed-wing uav attitude and altitude control via adaptive second-order sliding mode". *Arabian Journal for Science and Engineering*, 43:6837–6848, 2018.

[18] Xiaoqi Qiu, Mingen Zhang, Wuxing Jing, and Changsheng Gao. "dynamics and adaptive sliding mode control of a mass-actuated fixed-wing uav". *International journal of aeronautical and space sciences*, 22:886–897, 2021.

[19] Marc L Steinberg and Anthony B Page. "nonlinear adaptive flight control with genetic algorithm design optimization". *International Journal of Robust and Nonlinear Control*, 9(14):1097–1115, 1999.

[20] Jiao Chen, Jiangyun Wang, and Weihong Wang. "robust adaptive control for nonlinear aircraft system with uncertainties". *Applied Sciences*, 10(12):4270, 2020.

[21] C Rohrs, Lena Valavani, Michael Athans, and Gunter Stein. "robustness of continuous-time adaptive control algorithms in the presence of unmodeled dynamics". *IEEE Transactions on Automatic Control*, 30(9):881–889, 1985.

[22] Richard Harry Barnard and David R Philpott. *"Aircraft flight: a description of the physical principles of aircraft flight"*. Pearson education, 2010.

[23] WF Phillips. "incompressible flow over finite wings". *Mechanics of Flight, 2nd ed., Wiley, Hoboken, NJ*, pages 46–94, 2010.

[24] Lavretsky Eugene, Wise Kevin, and D Howe. "robust and adaptive control with aerospace applications". *Springer*, 2013.

[25] Herbert Goldstein, Charles Poole, and John Safko. "classical mechanics", 2002.

[26] STEFANO FARI. "guidance and control for a fixed-wing uav". 2017.

[27] Randal W Beard and Timothy W McLain. *"Small unmanned aircraft: Theory and practice"*. Princeton University Press, 2012.

[28] V. Dobrokhodov. "kinematics and dynamics of fixed-wing uavs", 2015.

[29] Rick Cory and Russ Tedrake. "experiments in fixed-wing uav perching". In *AIAA Guidance, Navigation and Control Conference and Exhibit*, page 7256, 2008.

[30] Annaswamy A.M. Narendra, K.S. "a new adaptive law for robust adaptive control without persistency of excitation". *IEEE Trans.Automat Contr.*, Feb. 1987.

[31] MV Cook. "flight dynamics principles, 1997".

[32] Purdue University. "modeling a servo motor system".

[33] Mihret Kochito. "mrac design for a surveillance uav for the detection of water hyacinth". *MSc Thesis*, 2021.

[34] Nhan T. Nguyen. "model-reference adaptive control". *Springer*, pages 2–3, AG 2018.

[35] John Bosworth and Peggy Williams-Hayes. "flight test results from the nf-15b intelligent flight control system (ifcs) project with adaptation to a simulated stabilator failure". In *AIAA Infotech@ Aerospace 2007 Conference and Exhibit*, page 2818, 2007.

[36] Nhan T. Nguyen. "model-reference adaptive control". *Springer*, pages 83–118, AG 2018.

[37] Priyank Jain and M. J. Nigam. "design of a model reference adaptive controller using modified mit rule for a second order system.". *Advance in Electronic and Electric Engineering 3(4): pages=477–484,, year=2013,.*

[38] Muluken Menebo. "neural network based model reference adaptive control of quadrotor uav for precision agriculture". *MSc Thesis*, 2022.

[39] Nhan T. Nguyen. "model-reference adaptive control". *Springer*, pages 95–96, AG 2018.

[40] Lavretsky Eugene, Wise Kevin, and D Howe. "robust and adaptive control with aerospace applications". *Springer*, page 221, 2013.

[41] Kokotovic Ioannou, P. "instability analysis and improvement of robustness of adaptive control". *Automatic*, 11984.

[42] Nhan T Nguyen. "optimal control modification for robust adaptive control with large adaptive gain". *Systems & Control Letters*, 61(4):485–494, 2012.

[43] Satoshi Kohno and Kenji Uchiyama. Design of robust controller of fixed-wing uav for transition flight. In *2014 International Conference on Unmanned Aircraft Systems (ICUAS)*, pages 1111–1116. IEEE, 2014.

Appendix A

Differentiation of a Vector, Aerodynamic Coefficients and Parametric Uncertain matrix

A.1 Differentiation of a Vector

To derive the mathematical model of FWUAVs, it is mandatory to differentiate vectors in different reference frames that are moving with respect to one another. Assume that there are two coordinate system, f^i and f^b as shown in the figure A.1 f^i represent inertial frame

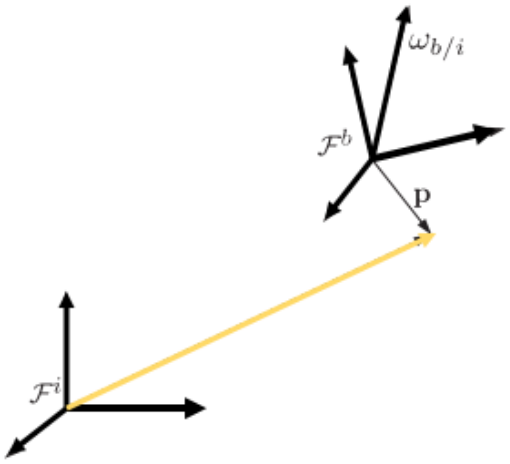

Figure A.1: Vector differentiation

and f^b represent body frame of FWUAVs. If vector P moves in moving frame f^b and also f^b is rotating with respect to an inertial frame. Our aim is to drive the time derivative of P from the inertial frame f^i. Let the angular speed of body frame f^b in inertial frame f^i be $\omega_{b/i}$

Vector P in terms of unit vector component expressed as

$$P = P_x i^b + P_y j^b + P_z k^b \tag{A.1}$$

Now differentiate equation A.1 with respect to the inertial frame f^i

$$\frac{d}{dt_i}P = \dot{P}_x i^b + \dot{P}_y j^b + \dot{P}_z k^b + P_x \frac{d}{dt_i} i^b + P_y \frac{d}{dt_i} j^b + P_z \frac{d}{dt_i} k^b \tag{A.2}$$

$\frac{d}{dt_i}$ represent the differentiation of P with respect to inertial frame f^i. The first three term of equation A.2represents the change in P with respect to the rotating frame f^b. We denote this term by

$$\frac{d}{dt_b}P = \dot{P}_x i^b + \dot{P}_y j^b + \dot{P}_z k^b \tag{A.3}$$

The next three term represents of equation A.2 the change in vector P due to the rotation in body frame f^b with respect to inertial frame f^i. The unit vector i^b, j^b and k^b are fixed in the f^b frame, their time derivatives can be calculated as shown in [9] as

$$\dot{i^b} = \omega_{b/i} \times i^b$$
$$\dot{j^b} = \omega_{b/i} \times j^b$$
$$\dot{k^b} = \omega_{b/i} \times k^b$$

Now substitute the above expression yeilds

$$P_x \frac{d}{dt_i} i^b + P_y \frac{d}{dt_i} j^b + P_z \frac{d}{dt_i} k^b = p_x(\omega_{b/i} \times i^b) + p_y(\omega_{b/i} \times j^b) + p_z(\omega_{b/i} \times k^b) \tag{A.4}$$

Combining equation A.2, A.3 and A.4 to obtain the following relation.

$$\frac{d}{dt_i}P = \frac{d}{dt_b}P + \omega_{b/i} \times P \tag{A.5}$$

A.2 Aerodynamic Coefficients

C_{m_α}, C_{l_β}, C_{n_β}, C_{m_q}, C_{l_q}, and C_{n_r} are aerodynamic coefficients and known as stability derivatives. C_{m_α} is called longitudinal static stability derivative. To make fixed wing UAV statically stable C_{m_α} must be negative. C_{l_β} is referred to as the roll static stability derivative. For the fixed wing UAV statically stable, C_{l_β} must be less than zero. To make fixed wing statically stable C_{n_β} must be positive. C_{n_β} is called the yaw static stability derivative. The

pitch damping derivative is denoted by C_{m_q}, the roll damping derivative by C_{l_q}, and the yaw damping derivative by C_{n_r}. Typically, all of these damping derivatives have a numerical value of zero.

The aerodynamic coefficient $C_{m_{\delta e}}$, $C_{l_{\delta a}}$, and $C_{n_{\delta r}}$ are called the primary control derivatives. $C_{l_{\delta r}}$ and $C_{n_{\delta a}}$ are called cross-control derivatives

$$C_{p_0} = \frac{J_{zz}}{\Gamma} C_{l_0} + \frac{J_{xz}}{\Gamma} C_{n_0}$$

$$C_{p_\beta} = \frac{J_{zz}}{\Gamma} C_{l_\beta} + \frac{J_{xz}}{\Gamma} C_{n_\beta}$$

$$C_{p_p} = \frac{J_{zz}}{\Gamma} C_{l_p} + \frac{J_{xz}}{\Gamma} C_{n_p}$$

$$C_{p_r} = \frac{J_{zz}}{\Gamma} C_{l_r} + \frac{J_{xz}}{\Gamma} C_{n_r}$$

$$C_{p_{\delta a}} = \frac{J_{zz}}{\Gamma} C_{l_{\delta a}} + \frac{J_{xz}}{\Gamma} C_{n_{\delta a}}$$

$$C_{p_{\delta r}} = \frac{J_{zz}}{\Gamma} C_{l_{\delta r}} + \frac{J_{xz}}{\Gamma} C_{n_{\delta r}}$$

$$C_{r_0} = \frac{J_{xz}}{\Gamma} C_{l_0} + \frac{J_{xx}}{\Gamma} C_{n_0}$$

$$C_{r_\beta} = \frac{J_{xz}}{\Gamma} C_{l_\beta} + \frac{J_{xx}}{\Gamma} C_{n_\beta}$$

$$C_{r_p} = \frac{J_{xz}}{\Gamma} C_{l_p} + \frac{J_{xx}}{\Gamma} C_{n_p}$$

$$C_{r_r} = \frac{J_{xz}}{\Gamma} C_{l_r} + \frac{J_{xx}}{\Gamma} C_{n_r}$$

$$C_{r_{\delta a}} = \frac{J_{xz}}{\Gamma} C_{l_{\delta a}} + \frac{J_{xx}}{\Gamma} C_{n_{\delta a}}$$

$$C_{r_{\delta r}} = \frac{J_{xz}}{\Gamma} C_{l_{\delta r}} + \frac{J_{xx}}{\Gamma} C_{n_{\delta r}}$$

The inertia parameter specified by Γ_1..... Γ_8 expressed in chapter four.

A.3 Aerodynamic Coefficients and Parameters

parameter	value	Long.coff	value	Lat.coff	value
m	$13.5Kg$	C_{L_0}	0.28	C_{Y_0}	0
J_x	$0.8244kg\text{-}m^2$	C_{D_0}	0.03	C_{l_0}	0
J_y	$1.135kg\text{-}m^2$	C_{M_0}	-0.02338	C_{n_0}	0
J_z	$1.759kg\text{-}m^2$	C_{L_α}	3.45	C_{Y_β}	-0.98
J_{xz}	$0.1204kg\text{-}m^2$	C_{D_α}	0.3	C_{l_β}	-0.12
S	$0.55m^2$	C_{M_α}	-0.38	C_{n_β}	0.25
b	$2.8956m$	C_{L_q}	0	C_{Y_p}	0
c	$0.18994m$	C_{D_q}	0	C_{l_p}	-0.26
S_{prop}	$0.2027m^2$	C_{M_q}	-3.6	C_{n_p}	0.022
ρ	$1.2682kg/m^3$	$C_{L_\delta e}$	-0.36	C_{Y_r}	0
K_{motor}	80	$C_{D_{\delta e}}$	0	C_{l_r}	0.14
K_{T_p}	0	$C_{M_{\delta e}}$	-0.50	C_{n_r}	-0.35
K_ω	0	C_{prop}	1	$C_{Y_{\delta a}}$	0
		C_{D_p}	0.0437	$C_{l_{\delta r}}$	0.105
				$C_{l_{\delta a}}$	0.08
				$C_{n_{\delta a}}$	0.06
				$C_{Y_{\delta r}}$	-0.17
		$C_{n_{\delta r}}$	-0.032		

Table A.1: Aerodynamic coefficients and parameters for the Aerosonde UAV [27]

A.4 Parametric Uncertainty Matrix

States affected by parametric uncertainly	ϕ	θ	ψ
Parametric uncertain matrix	$[0\ 0.5]^T$	$[0.1\ 0.5]^T$	$[0\ 0.5]^T$

Table A.2: parametric uncertainty matrix

Appendix B

Simulink Model and Equation of Trajectory

B.1 Complete Simulink Model

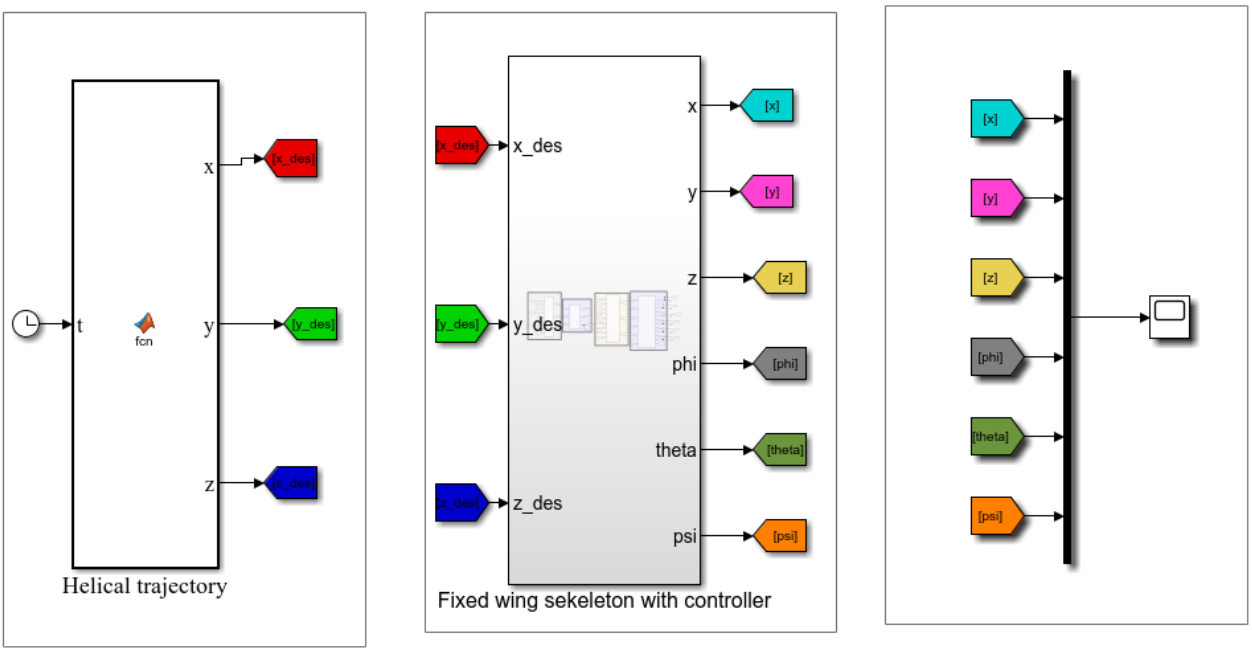

Figure B.1: Complete simulink model

B.2 Position Controller Simulink Model

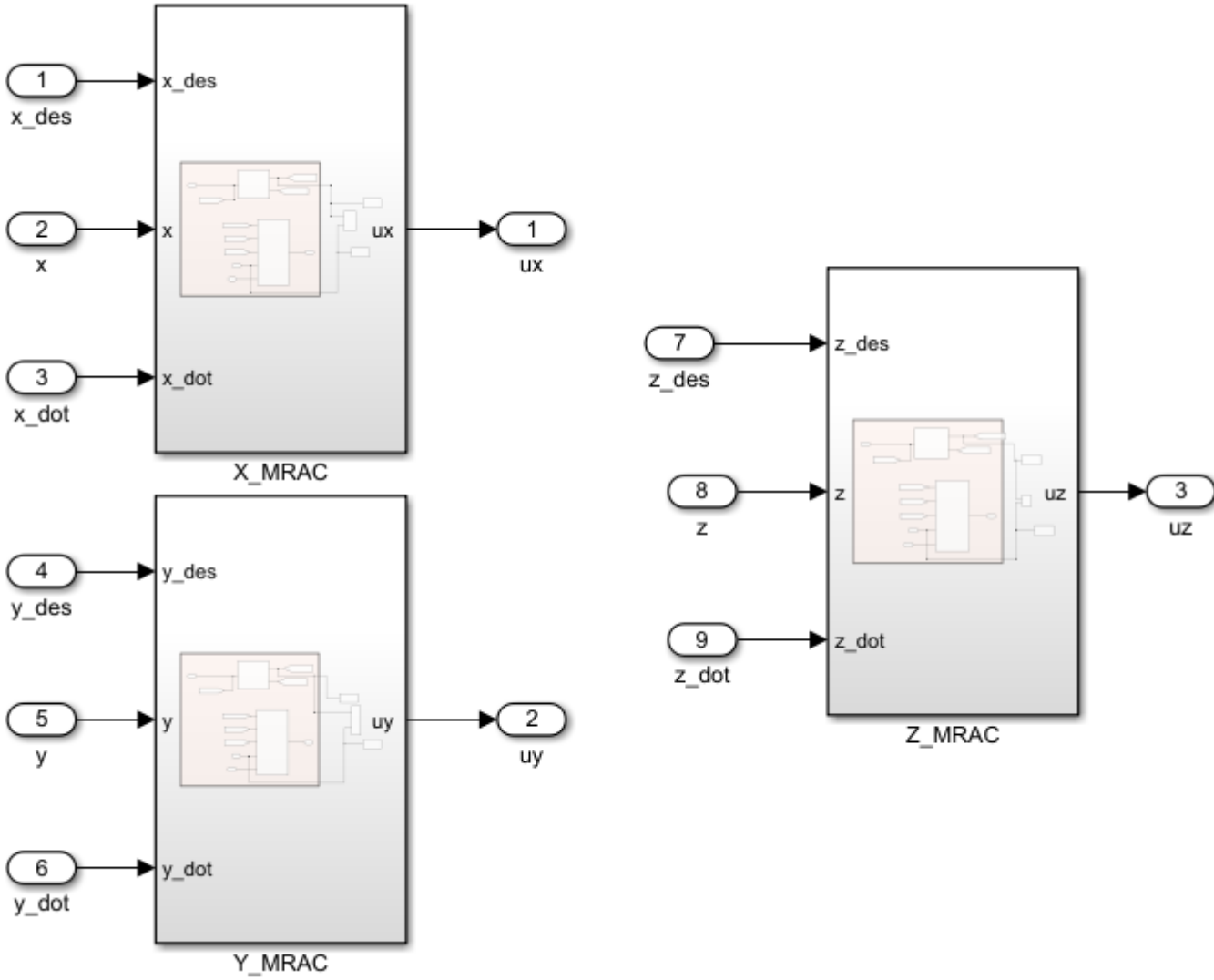

Figure B.2: Position MRAC

B.3 Conversion Block

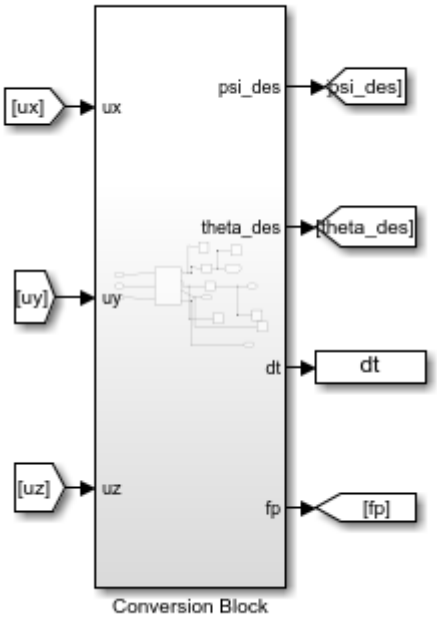

Figure B.3: Conversion Block

B.4 Attitude Controller Block

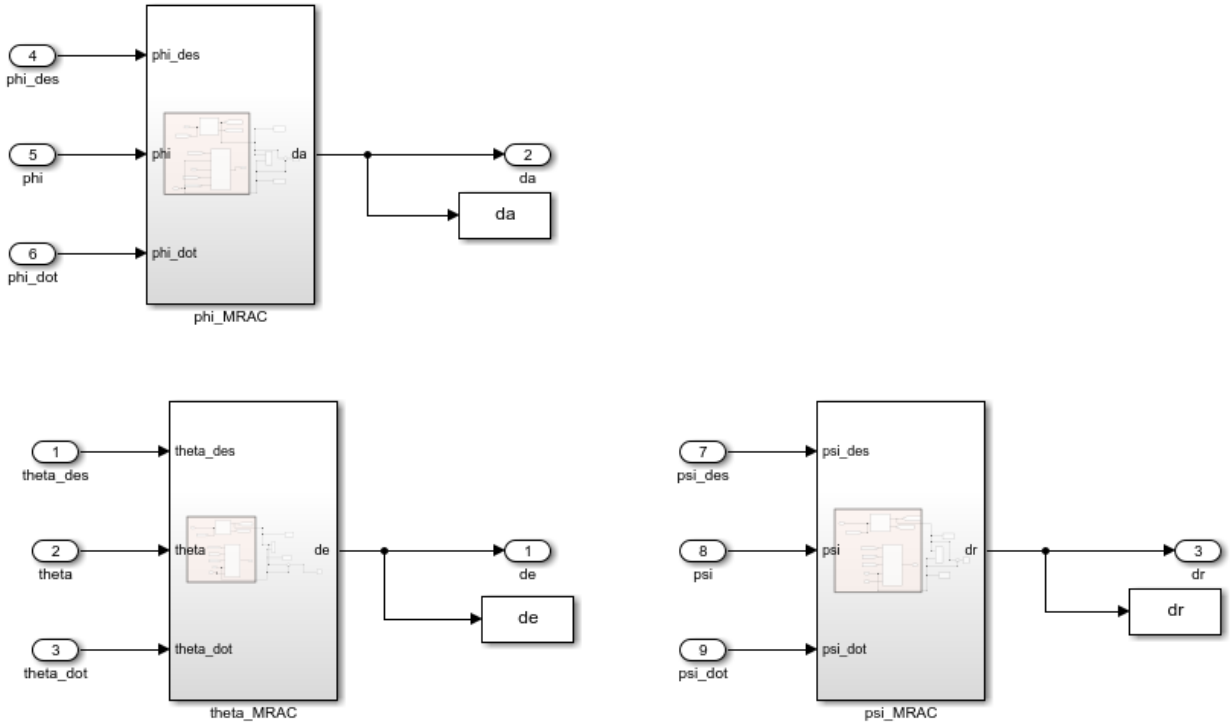

Figure B.4: Attitude MRAC

B.5 Pre-defined way-points trajectory

function [x,y,z] = fcn(t)

if t<=14

x=-0.082042979591837*t^2 + 0.078746510204082 $* t^3$;

$y = 0$;

$z = 2 - 0.080818489795918 * t^2 + 0.077930183673469 * t^3$;

$elseif\ t >= 14 \&\& t < 20$

$x = 22.784099770644527 + 11.120656842105266 * t - 0.004546920226351 * t^2 + 0.008169788922830 * t^3$;

$y = 0$;

$z = 200$;

$elseif\ t >= 20 \&\& t < 24$

$x = 22.784099770644527 + 11.120656842105266 * t - 0.004546920226351 * t^2 + 0.008169788922830 * t^3$;

$y = 1.0e+02 * (1.234093224812482 - 0.105820105820106 * t - 0.000035846253944 * t^2 + 0.000112080924146 * t^3);$

$z = 200;$

$elseif\ t >= 24 \&\& t < 30$

$x = 400;$

$y = 1.0e+02 * (1.234093224812482 - 0.105820105820106 * t - 0.000035846253944 * t^2 + 0.000112080924146 * t^3);$

$z = 200;$

$elseif\ t >= 30 \&\& t < 34$

$x = 1.0e+02 * (8.974910633748706 - 0.173745173745174 * t + 0.000087719716892 * t^2 + 0.000005870253089 * t^3);$

$y = 1.0e+02 * (1.234093224812482 - 0.105820105820106 * t - 0.000035846253944 * t^2 + 0.000112080924146 * t^3);$

$z = 200;$

$elseif\ t >= 34 \&\& t < 40$

$x = 1.0e+02 * (8.974910633748706 - 0.173745173745174 * t + 0.000087719716892 * t^2 + 0.000005870253089 * t^3);$

$y = 200;$

$z = 200;$

$elseif\ t >= 40 \&\& t < 44$

$x = 1.0e+02 * (8.974910633748706 - 0.173745173745174 * t + 0.000087719716892 * t^2 + 0.000005870253089 * t^3);$

$y = 1.0e+02 * (8.033520696367233 - 0.243161094224924 * t - 0.000010976667605 * t^2 + 0.000057976339700 * t^3);$

$z = 200;$

$elseif\ t >= 44 \&\& t < 50$

$x = 200;$

$y = 1.0e+02 * (8.033520696367233 - 0.243161094224924 * t - 0.000010976667605 * t^2 + 0.000057976339700 * t^3);$

$z = 200;$

$elseif\ t >= 50 \&\& t < 54$

$x = 1.0e+03 * (1.185131660319630 - 0.031328320802005 * t - 0.000000731699378 * t^2 + 0.000004664909026 * t^3);$

$y = 1.0e+02 * (8.033520696367233 - 0.243161094224924 * t - 0.000010976667605 * t^2 +$

$0.000057976339700 * t^3$);

$z = 200$;

$elseif\ t >= 54\&\&t < 60$

$x = 1.0e+03 * (1.185131660319630 - 0.031328320802005 * t - 0.000000731699378 * t^2 + 0.000004664909026 * t^3)$;

$y = 400$;

$z = 200$;

$elseif\ t >= 60\&\&t < 64x = 1.0e+03 * (1.185131660319630 - 0.031328320802005 * t - 0.000000731699378 * t^2 + 0.000004664909026 * t^3)$;

$y = 1.0e+03 * (1.861886853485376 - 0.038379530916844 * t - 0.000000522039766 * t^2 + 0.000003901686781 * t^3)$;

$z = 200$;

$elseif\ t >= 64\&\&t < 70$

$x = 400$;

$y = 1.0e+03 * (1.861886853485376 - 0.038379530916844 * t - 0.000000522039766 * t^2 + 0.000003901686781 * t^3)$;

$z = 200$;

$elseif\ t >= 70\&\&t < 74$

$x = 1.0e+03 * (1.999738516817156 - 0.024898373983740 * t + 0.000001956566651 * t^2 + 0.000000389389170 * t^3)$;

$y = 1.0e+03 * (1.861886853485376 - 0.038379530916844 * t - 0.000000522039766 * t^2 + 0.000003901686781 * t^3)$;

$z = 200$;

$elseif\ t >= 74\&\&t < 90$

$x = 1.0e+03 * (1.999738516817156 - 0.024898373983740 * t + 0.000001956566651 * t^2 + 0.000000389389170 * t^3)$;

$y = 600$;

$z = 200$;

$elseif\ t >= 90\&\&t < 94$

$x = 1.0e+03 * (1.999738516817156 - 0.024898373983740 * t + 0.000001956566651 * t^2 + 0.000000389389170 * t^3)$;

$y = 1.0e+03 * (2.502390290390015 - 0.022264980758659 * t + 0.000001185376532 * t^2 + 0.000000126003331 * t^3)$;

$z = 200$;

$elseif\ t >= 94\&\&t < 124$

$x = 0;$

$y = 1.0e+03 * (2.502390290390015 - 0.022264980758659 * t + 0.000001185376532 * t^2 + 0.000000126003331 * t^3);$

$z = 200;$

$else$

$x = 0;$

$y = 0;$

$z = 1.0e+02 * (9.600976574322560 + 0.000006053146627 * t^2 - 0.000004035431085 * t^3);$

end